

Exploring Nonstatistical Dynamic Effects in Exothermic Organic Reactions

Jamie Johnson

A thesis submitted in partial fulfilment of the requirements
for the degree of Doctor of Philosophy

Cardiff University School Of Chemistry

January 2014

Education is an admirable thing, but it is well to remember from time to time that nothing that is worth knowing can be taught.

Oscar Wilde

DECLARATION

This work has not been submitted in substance for any other degree or award at this or any other university or place of learning, nor is being submitted concurrently in candidature for any degree or other award.

Signed (candidate) Date

STATEMENT 1

This thesis is being submitted in partial fulfilment of the requirements for the degree of PhD

Signed (candidate) Date

STATEMENT 2

This thesis is the result of my own independent work/investigation, except where otherwise stated.

Other sources are acknowledged by explicit references. The views expressed are my own.

Signed (candidate) Date

STATEMENT 3

I hereby give consent for my thesis, if accepted, to be available for photocopying and for inter-library loan, and for the title and summary to be made available to outside organisations.

Signed (candidate) Date

ABSTRACT

Two organic systems have been selected for the study of nonstatistical dynamic effects using a combination of computational and lab based techniques. Chapters one and two provide an introduction to nonstatistical dynamics and computational methodology respectively.

The computational element of this work focuses on the thermal rearrangements of spiropentane, and is presented in chapters three and four. The rearrangement involves two singlet biradical intermediates, and the suitability of the rearrangement to the study of nonstatistical dynamics is explored. While evidence of nonstatistical effects has been found in previous experimental work on the system, the study presented here involves molecular dynamics simulations to uncover further details about the nature and mechanism of the rearrangements. The work also involved an evaluation of the use of various density functional methods for studying the system and a benchmarking exercise to choose a suitable computational methodology for the dynamics. The results of two sets of simulations are presented, and evidence of nonstatistical effects from both is discussed.

Chapters five and six concern the synthesis of a novel peroxide that was designed specifically for this work, which undergoes thermal dissociation to form a radical pair. The properties of the molecule are discussed, and various attempts at its synthesis are described. An explanation of how the compound could be used for lab-based nonstatistical dynamics studies is also presented, involving an isotopic labelling study. Unfortunately, while several synthetic routes were proposed, the synthesis was ultimately unsuccessful and so could not be used to search for nonstatistical dynamic effects.

ACKNOWLEDGEMENTS

I would like to begin by thanking my supervisor Barry Carpenter, for giving me the opportunity to undertake this research and for all his time, attention and guidance. I have never met anyone so talented but modest. His contribution to the scientific community is immeasurable and it has been a privilege to be a part of his group. I will always be grateful that I was able to join such a dynamic (pardon the pun) crowd and to learn in-depth about things that I consider to be of real, fundamental importance. I would also like to thank my mentor, Thomas Wirth, for advice and conversation along the way.

The POC has been a wonderful place to work, and the supportive and encouraging atmosphere has contributed massively to my being able to complete this project. I would like to thank Dr Niek Buurma for acting as my examiner and for his infectious enthusiasm. Also for challenging but incredibly useful conversation. Of those now departed, I would like to say a special thank you to Drs Julia Rehbein, Rob Richardson and Larry Goldman, without who I would never have gotten started. I blame Rob for most of the times I was in the lab way beyond home time. Larry welcomed me to the group, showed me the ropes, and kept me laughing with his inexhaustible supply of terrible puns. Julia's continued support and friendship throughout my time here has been invaluable and her patience and diligence in teaching me some things I should already have known was never overlooked. I really appreciate the friendship and kindness of everyone else in the POC, including Azz, Ed, Josie, Mihaela, Stefania, Andy, Ismail, Mazin, Hiwa, Alicja and Zuzka. Azz in particular made me laugh a lot, and never let me get out of date with the latest technology.

Elsewhere in the department I would like to thank everyone who keeps the place running: the guys in stores, the office, the workshops and of course the technicians. Without all their hard work and expertise this work would have been impossible. Special thanks also goes to Andy Thomas at ARCCA, Cardiff's research computing facility.

Finally I would like to say thank you to my friends and family for all their love and support throughout my time at university.

TABLE OF CONTENTS

Declaration	i
Abstract	ii
Acknowledgements	iii
Table of Contents	v
List of Figures	viii
List of Tables	x
List of Graphs	xi
1 Introduction to Nonstatistical Dynamics	1
1.1 Overview of Reaction Dynamics	1
1.2 Potential Energy Surfaces	1
1.3 Established Kinetic Theories	4
1.3.1 Transition State Theory (TST)	4
1.3.2 Rice-Ramsperger-Kassel-Marcus (RRKM) Theory	8
1.4 Phase Space and The Transition State Hypothesis	8
1.5 Nonstatistical Effects	10
1.5.2 Examples of Nonstatistical Dynamics – The Acetone Radical Cation	11
1.5.3 Examples of Nonstatistical Dynamics – Vinylcyclopropane	13
2 Computational Methodology	16
2.1 Introduction to Computational Methodology	16
2.2 Molecular Mechanics	16
2.3 Electronic Structure Methods	17
2.3.1 Hartree-Fock Methods	20
2.3.2 Post Hartree-Fock Methods	23
2.3.3 Multi-Determinant Methods	24
2.3.4 Perturbation Methods	25
2.3.5 Multi-Reference Methods	27
2.4 Density Functional Methods	28
2.4.1 Traditional Density Functional Methods	28
2.4.2 Hybrid Density Functional Methods	30
2.5 Simulation Techniques	31

2.5.1	Monte Carlo Methods	31
2.5.2	Molecular Dynamics Methods	32
2.6	Summary and Aims	34
3	Nonstatistical Dynamics in the Thermal Rearrangement of Spiropentane	35
3.1	Introduction	35
3.2	The Thermal Rearrangements of Spiropentane	39
3.2.1	Labelling Studies	40
3.2.2	Pressure Dependence and Product Ratios	42
3.2.3	Stereomutation Pathways	44
3.2.4	Previous Computational Studies	45
3.3	DFT Benchmarking	45
3.4	Molecular Dynamics Results	53
3.4.1	Unimolecular Dynamics	53
3.4.2	Bimolecular Dynamics	64
3.5	Summary and Conclusions	66
4	Experimental Section for Chapter 3	68
4.1	Geometry Optimisation Details	68
4.1.1	Sample Gaussian Input - Geometry Optimization	69
4.1.2	Optimised Geometries and Energies - Section 3.3	70
4.1.3	Sample Gaussian Input - TS4	77
4.1.4	Optimised Geometry and Energy for TS4	79
4.2	Molecular Dynamics Details for Section 3.4.1	80
4.2.1	Sample Gaussian Input - BOMD	81
4.2.2	Sample Gaussian Input - Initial Condition Sampling for GAMESS	84
4.2.3	Sample GAMESS US Input - DRC	85
4.3	Molecular Dynamics Details for Section 3.4.2	89
5	Nonstatistical Dynamics in the Thermal Dissociation Of A Dewar Benzene Functionalised Peroxide	90
5.1	Introduction	90

5.1.1	Thermal Decomposition of Benzoyl Peroxide	90
5.1.2	The Reactivity of Dewar Benzene	91
5.2	Synthetic Work	95
5.2.1	Dewar Benzene Synthesis	95
5.2.2	Formation of the Peroxide Bond	101
5.3	Summary and Conclusions	102
6	Experimental Section for Chapter 5	103
6.1	General Experimental Procedures	103
6.2	Instrumentation	103
6.3	Experimental Procedures	104
7	Works Cited	112
Appendix A		117
	Sample Gaussian Output - BOMD	117
Appendix B		140
	Sample GAMESS US Output - DRC	140

LIST OF FIGURES

Figure 1.1: Reaction Coordinate Diagram for a Two Step Reaction.....	2
Figure 1.2: PES With Two Symmetrical Pathways.....	3
Figure 1.3: Reaction Coordinate Diagram for a One Step Reaction.....	5
Figure 1.4: An Illustration of Phase Space.....	9
Figure 1.5: A Multistep Reaction.....	10
Figure 1.6: Summary of the McLafferty Rearrangement.....	11
Figure 1.7: The Thermal Rearrangement of Vinylcyclopropane.....	13
Figure 2.1: A Slater determinant.....	21
Figure 2.2: Illustration of Excited Slater Determinants.....	25
Figure 3.1: Biradical Electronic Configurations.....	36
Figure 3.2: The Fragmentation of Cyclobutane.....	37
Figure 3.3: Thermal Rearrangements of Spiropentane.....	39
Figure 3.4: Mechanistic Pathways for the Rearrangement of SP to MCB.....	40
Figure 3.5: Labelling Study of SP to MCB Rearrangement.....	41
Figure 3.6: Formation and Fragmentation of HBC.....	41
Figure 3.7: Proposed Addition Pathways.....	43
Figure 3.8: Proposed Insertion Pathways.....	43
Figure 3.9: Possible Stereomutation Pathways of Spiropentane.....	44
Figure 3.10: Summary of Enthalpies combined by Carpenter.....	45
Figure 3.11: Summary of structures optimised using PBE1PBE/3-21G, with locations of B1 and B2 taken from Carpenter's paper.....	54
Figure 3.12: TS2 Geometries from a) B1B95 b))3LYP and c) PBE1PBE using the 3-21G Basis Set.....	59
Figure 3.13: Summary of stereochemical outcomes for complete trajectories, showing branching ratios in red and the statistical uncertainties in the branching ratios in blue.....	59
Figure 3.14: Summary of stereochemical outcomes forward trajectories, showing branching ratios in red and the statistical uncertainties in the branching ratios in blue.....	60
Figure 3.15: Possible rearrangement pathways via B1.....	60
Figure 3.16 Summary of results from forward trajectories.....	62
Figure 3.17: Initial structure of B1.....	63
Figure 3.18: TS4, starting point for dynamics.....	64
Figure 5.1: Thermal Decomposition of Benzoyl Peroxide.....	90

Figure 5.2: A Functional Group Isomer of Benzoyl Peroxide.....	92
Figure 5.3: Proposed Thermal Decomposition of Dewar Benzene Functionalised Peroxide	93
Figure 5.4: Proposed Labelling Study to Determine Rate of Decarboxylation	94
Figure 5.5: Proposed Synthesis of 24	95
Figure 5.6: Synthesis of cyclobutadieneiron tricarbonyl 30.....	96
Figure 5.7: First Preparation of Alkyne Trapping Agent.....	96
Figure 5.8: Successful Trapping of Cyclobutadiene using 37	97
Figure 5.9: Successful Trapping of Cyclobutadiene using 39	97
Figure 5.10: NMR spectra of 40 taken at a) 12hrs, b) 36hrs and c) 84hrs.....	98
Figure 5.11: Attempted monoesterification of acetylenedicarboxylic acid using a PTC99	
Figure 5.12: Alternative route to monomethyl ester from methyl propiolate.....	100
Figure 5.13: Coupling of mCPBA and benzoyl chloride.....	101
Figure 5.14: Peroxybenzoic acid synthesis.....	101
Figure 5.15. Anhydride synthesis	102

LIST OF TABLES

Table 3.1: Product Distributions from Doering and Frey Experiments (by Percentage)	42
Table 3.2: DFT Benchmarking Results by RMS Analysis	50
Table 3.3: Results of Comparative MD tests after 200 trajectories	55
Table 3.4: Summary of correlated product distributions	57
Table 3.5: Summary of trajectory results following collision	64
Table 5.1: Summary of Half-Lives for Dewar Benzene Derivatives	92

LIST OF GRAPHS

Graph 3.1: Results of DFT Benchmarking	51
Graph 3.2: Formation of MCB isomers as function of time	58
Graph 3.3: Comparison of MCB isomers 11a/11b and 11c/11d as function of time	61

1 INTRODUCTION TO NONSTATISTICAL DYNAMICS

1.1 Overview of Reaction Dynamics

To thoroughly address and explore nonstatistical dynamic effects, it is prudent to first establish what reaction dynamics really refers to, and what we would expect from a reaction that exhibits ‘normal’, statistical dynamics.

The simplest cases to consider are those of isolated, gas-phase systems, where interactions with solvents and other particles outside of the boundaries may be disregarded. By developing an understanding of such fundamental processes, it becomes possible to model the probable outcomes of more complex reactions. Dynamics deals with how and why reactions occur on a microscopic level, and takes into consideration atomic changes such as inter-atomic distances and bond vibrations. These atomic level properties underlie the bulk properties of a reacting system, and determine its kinetic profile.

1.2 Potential Energy Surfaces

Reaction co-ordinate diagrams, which commonly plot the reaction coordinate against potential energy (PE) or Gibbs energy, are an incredibly useful tool for examining kinetic profiles, and can also be used to show important details about the thermochemistry of a reaction. They provide us with a way of mapping out how small changes in the molecular structure of a system affect its overall energy. It is conventional to depict a potential energy surface in two dimensions, plotting energy against the reaction coordinate of interest. In reality, for a many-bodied system, this is a vast oversimplification. The hypersurface for such a system would have $3N-5$ dimensions: the familiar $3N-6$ dimensions relating to various degrees of freedom and one additional dimension relating to energy. This method of simplification can prove problematic when dealing with highly reactive species, where more than one reaction co-ordinate may need to be considered to give a true picture.

We can identify the ‘most important’ points on a PE diagram quite easily i.e. those corresponding to reactants, transition states, intermediates or products. They occur at

points where the partial first derivatives of energy in all directions are zero, and so appear as stationary points on the curve. Further detail can be obtained by taking the second derivatives of energy at these points. For a reactant, intermediate or product all the partial second derivatives will be positive as movement in any direction will involve moving towards a higher energy, and thus these species appear as minima on a surface. Transition states are a little more complex.

As a point of definition, whilst it is commonplace to see the term ‘transition state’ used interchangeably with ‘activated complex,’ it is important to note that there is a subtle difference between the two. Strictly speaking, a transition state is a property of a system that describes a precise configuration of atoms corresponding to a maximum on a potential energy surface. An activated complex is a collection of structures which exist around the maximum, but which may have transient structures very close to that of the transition state. For the purposes of this work the two will be treated with synonymy.

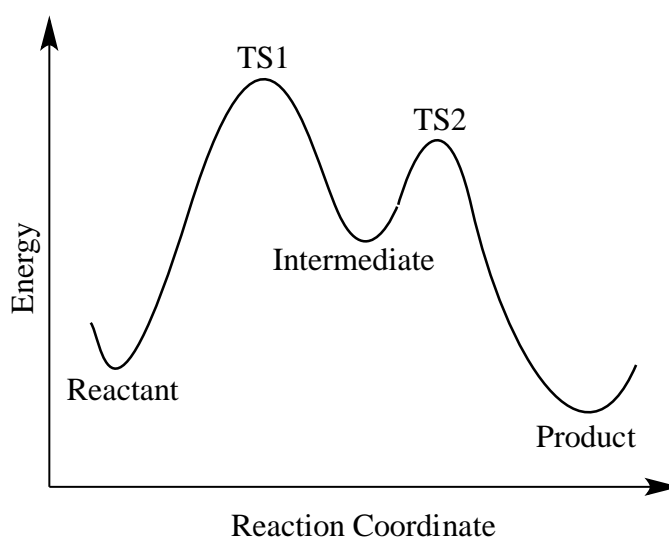


Figure 1.1: Reaction Coordinate Diagram for a Two Step Reaction

On a traditional two-dimensional energy diagram such as that in Figure 1.1 above for a two-step reaction, transition states appear as maxima, as they are the highest energy species that can be reached when considering only the reaction coordinate. Thus, movement in any direction from the transition state along the reaction coordinate will mean moving to a lower energy. In other words it is actually a minimum in all directions except one, relating to the reaction co-ordinate in question, and when dealing

with a multi-dimensional surface transition states are a unique feature and appear as saddle points. Because of this downward curvature, calculation of the vibrational frequencies for transition states gives rise to one normal mode with an imaginary vibrational frequency. Identification of this frequency is very important for determining the accurate location of a transition state computationally. While a transition state may not be the highest energy point on a surface (a global maximum) it represents an energy barrier that a molecule must surmount on its journey from reactant to product. Generally, following the steepest path of descent from a transition state should lead directly to a minimum for the reactant or product; this path is known as the intrinsic reaction co-ordinate (IRC). This interpretation comes with a caveat, though.

Figure 1.2 below shows a potential energy surface with a transition state leading to two possible products. The local minimum on the surface appertains to an intermediate. With essentially symmetrical TSs between the intermediate and each product, TST would dictate that if both products were energetically equivalent, they should be formed with near equal probability.

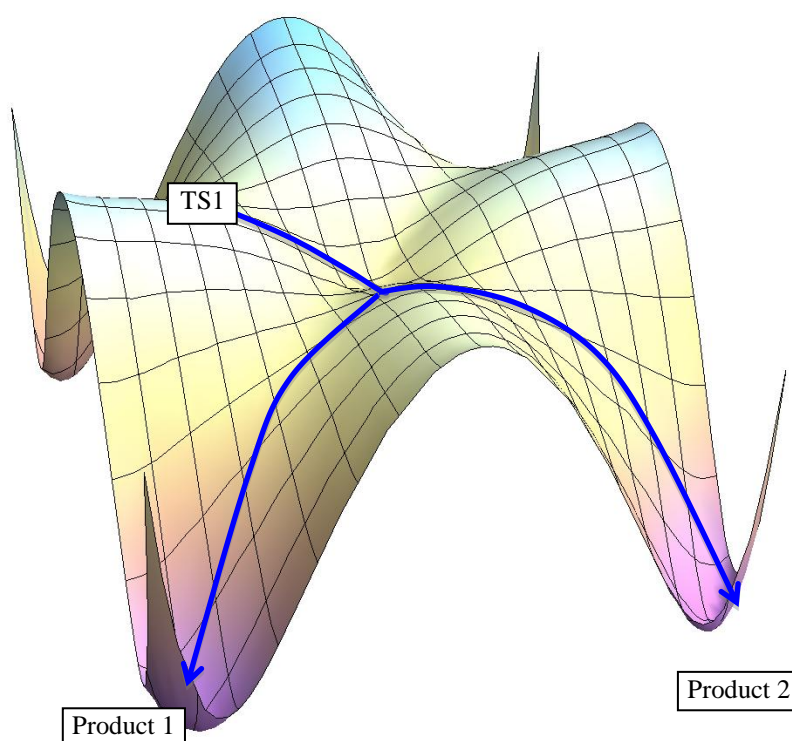


Figure 1.2: PES With Two Symmetrical Pathways

However, viewing the PES in three dimensions allows us to see that the two potential products are actually subtly different. Product 2 is collinear with the path of the trajectory over TS1, whereas product 1 would require a significant change in geometry before formation. Therefore, they may not be formed in equal ratios as TST would predict. It will become apparent from subsequent discussion that there are several features of energy hypersurfaces that can enable us to elucidate mechanistic detail otherwise precluded by a traditional two-dimensional view such as in Figure 1.2, which only shows one reaction co-ordinate. Bifurcation points, for example, involve trajectories along multiple reaction co-ordinates. Such features make it difficult to predict, using TST alone, a product ratio from a given reaction. The supposition that both products from TS1 are formed in equal quantities is one which is increasingly brought into question, particularly in cases where the species reaching the intermediate minima are believed to possess a ‘molecular memory’ of the TS they came from, and this is what gives rise to the study of nonstatistical dynamics (Section 1.5).

1.3 Established Kinetic Theories

Over the years many different kinetic theories have been published with the common goal of enabling us to predict, with a reasonable degree of accuracy, the rate of chemical reactions. Not only this, but some take us part way towards being able to explain these rates in terms of mechanism. Many of the most commonly used models have evolved over time to take into account an expanding wealth of empirical evidence, and as one would expect, these are the models which have proved most successful. While an in-depth discussion of reaction kinetics is beyond the scope of this work, the following section provides an outline of two of the most prevalent kinetic models in use today: transition state theory¹ and Rice-Ramsperger-Kassel-Marcus (RRKM) theory.^{2,3,4,5}

1.3.1 Transition State Theory (TST)

To determine the rate of a reaction, we first need to find an adequate way to describe the macroscopic properties of the system whilst still giving reasonable definition to individual molecular states. We use a statistical model called an ensemble to make a connection between the dynamics of an individual reacting species (microscopic properties) and the overall ‘look’ of the system as a whole (macroscopic properties). The ensembles give us an average view of what is happening in a reaction and allow us

to estimate the probability of finding a molecule in a particular state within a system. Thus, the choice of which ensemble to base our kinetic model on depends on what we are willing to assume about the macroscopic properties of the reaction in question.

Transition state theory (TST) is arguably the most well known of all the kinetic theories, and enables the evaluation of rate with regard to the thermochemical properties of a reactant and the corresponding activated complex, or transition state. It is based on a canonical ensemble, also known as the NVT ensemble. The canonical ensemble defines a system enclosed in a heat bath with which it is in thermal equilibrium. The system has a fixed number of atoms, N , fixed volume, V , and fixed temperature, T . The final parameter is of most interest to us: it tells us that the calculation of rate using this model relies on there being a well-defined temperature for the reaction in question. In TST, once a temperature is fixed, the energies of the molecules are distributed according to the Boltzmann distribution.

There are two primary routes to deriving TST, both of which enable us to evaluate the equilibrium constant. One takes us down the path of partition functions and the other, which will be presented here, links it to familiar thermodynamic principles. The most important detail of this with respect to the present work is the no re-crossing assumption: every instance of reaching the transition state should result in the irreversible formation of product. Thus, TST gives us an upper-bound estimate of rate.

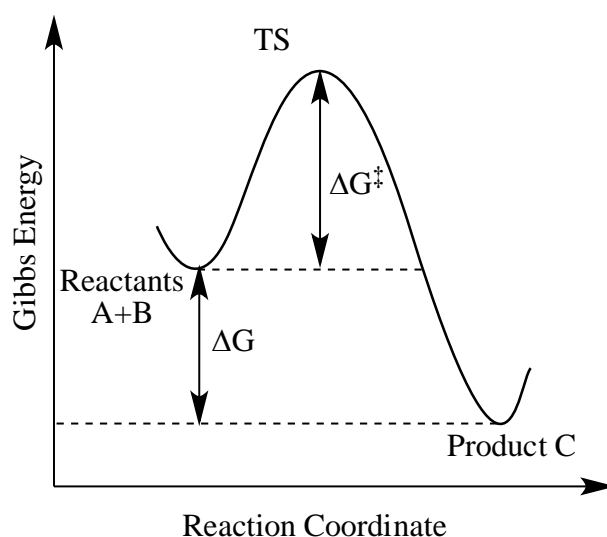


Figure 1.3: Reaction Coordinate Diagram for a One Step Reaction

Figure 1.3 depicts a simple reaction coordinate diagram for an exothermic reaction between reactants A and B to form C, with a single transition state, AB^\ddagger , and no intermediates. In order to calculate a rate constant, we first have to assume a quasi-equilibrium between the reactants and the transition state. It is not a true equilibrium, as increasing the concentration of the transition state would not shift the equilibrium towards product – instead, we can almost treat the equilibria between reactants and TS and reactants and products as being separate. Knowledge of these equilibria allows us to construct the following expressions for the rate of product formation:

$$\frac{d[C]}{dt} = k^\ddagger [AB^\ddagger]$$

Equation 1.1

$$\frac{d[C]}{dt} = k[A][B]$$

Equation 1.2

Combination of these two equations gives us an expression which shows the equilibrium between the reactants and the activated complex:

$$[AB^\ddagger] = K^\ddagger [A][B]$$

Equation 1.3

We then need to consider what actually happens to the reactants as they surmount the energy barrier and pass over the transition state, and to consider the rate at which this occurs. Passage over the barrier is related to one particular vibrational mode: a small movement is enough to move the complex over the barrier and *en route* to product. Thus we can link the rate of passage to the frequency of this vibration, ν , with a vibrational energy that is related to $k_B T$.

$$E_{\text{vib}} = k_B T = h\nu$$

Equation 1.4

$$\nu = \frac{k_B T}{h}$$

Equation 1.5

$$\text{rate} = [\text{AB}^\ddagger]v$$

Equation 1.6

Combining equations 1.3 and 1.6 above we obtain the an expression of rate (Equation 1.7) which can be converted to an expression of the second order rate constant, k , for the transformation of A and B to C (Equation 1.8).

$$\text{rate} = \frac{k_b T}{h} K^\ddagger [\text{A}][\text{B}]$$

Equation 1.7

$$k = \frac{k_b T}{h} K^\ddagger$$

Equation 1.8

To relate this rate constant to the reaction in question, we need to find a way to calculate the equilibrium constant. This can be approached in two ways, again either by consideration of thermodynamics or partition functions, but for this study a solely thermodynamic treatment will suffice. The following relationships (Equations 1.9 and 1.10) are well known and can be used to formulate the expression for the equilibrium constant in Equation 1.11, assuming that the change in Gibbs energy is for one mole of product.

$$RT \ln K = -\Delta G^0$$

Equation 1.9

$$\Delta G^0 = \Delta H^0 - T\Delta S^0$$

Equation 1.10

$$K^\ddagger = e^{-\Delta G^\ddagger / RT}$$

Equation 1.11

Finally, combination of equations 1.8 and 1.11 give us a familiar form of the Eyring equation.

$$k = \frac{k_b T}{h} e^{-\Delta G^\ddagger / RT}$$

Equation 1.12

Thus, the Eyring equation gives us a means by which to relate the thermodynamic properties of a system to an estimate of reaction rate. The presupposition that there is a quasi-equilibrium between the reactant and TS is an important one when considering nonstatistical effects. In fact, it is an implicit invocation of the statistical approximation, which will be discussed in Section 1.4.

1.3.2 Rice-Ramsperger-Kassel-Marcus (RRKM) Theory

RRKM theory can predict reaction rates by comparing the vibrational and rotational properties of the reactant and activated complex if the initial energy of the molecule is known.

It was first formulated by Rice and Ramsperger in the late 1920s and was later extended by Kassel and Marcus. As described above, TST is based on a canonical statistical ensemble where a Boltzmann distribution of energies between the molecules is assumed with the constraint of a fixed temperature for the system. In contrast, RRKM theory is based on the microcanonical (NVU) ensemble. Analogous to the canonical ensemble, the number of atoms and volume must remain constant. However, rather than a fixed temperature, it assumes a fully isolated system where each molecule will have the same (fixed) total energy.

The equivalence of these two ensembles with respect to rate calculation has been studied and it has been shown that the results obtained from each method should be concordant if the microcanonical result is averaged over a Boltzmann distribution.⁶

1.4 Phase Space and The Transition State Hypothesis

The phase space of a system is a theoretical ‘space’ with $6N-12$ dimensions, which incorporates all potential velocities and geometries of a molecule as it proceeds along a hypersurface. The $6N-12$ dimensions arise because we are not only considering the traditional degrees of freedom for each atom, but also velocities in the x, y and z directions for each. The trajectory of a given molecule over the surface must be a path that exists within this space.

The development of both kinetic theories discussed here was based on an emerging Transition State Hypothesis.⁷ Its basis is an approximation whereby the transition state's location within phase space made it equivalent to a plane, dissecting the phase space into a reactant space and a product space. This is illustrated in Figure 1.4, which is a simple representation of the phase space for a generic microcanonical ensemble of molecules such as that used in the formulation of RRKM theory. The plane itself is located in the region where the molecules potential energy is highest and so excess energy (velocity) is lowest, preventing the molecules from exploring such a large area of the phase space. This gives rise to the 'bottleneck' that can be seen. TST was designed in part to optimise the location of this plane.

In order for a molecule to pass over a transition state barrier, it not only needs to be of sufficiently high energy, but needs to have this energy localised within the correct vibrational modes i.e. those related to the specific bond dissociation required to form the transition structure. Pictorially, reflected in the 'shape' of the phase space, one can envisage that when dealing with trajectories moving almost at random within a large reactant space, once they reach the ideal conditions to traverse into the product space they should be highly unlikely to recross.

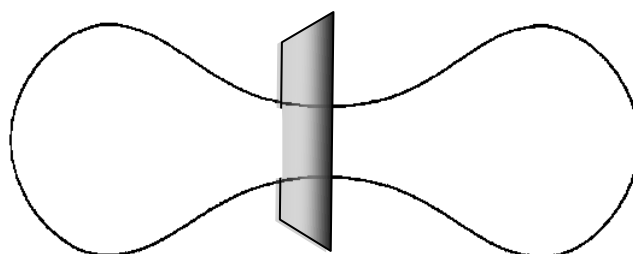


Figure 1.4: An Illustration of Phase Space

Once it is established that when a system reaches the transition state it will unequivocally form products, it is only necessary to know the equilibrium concentration of the transition state and the rate at which the system passes through this state to form products to predict reaction rate. By assuming that there is an equilibrium (more accurately, a quasi-equilibrium) between the activated complex and the reactants, it is possible to obtain the concentration of the transition state, which can then be multiplied

by a term describing the frequency with which the system crosses over the transition state to obtain an estimate of rate.

1.5 Nonstatistical Effects

The non-recrossing assumption is vital to the validity of using models such as RRKM and TST to predict reaction rate. However, this assumption should be treated with caution as will be shown throughout this work.

So far only single step reactions have been considered. However, there are further consequences for the use of statistical models when studying multi-step reactions such as that depicted using the reaction coordinate diagram at Figure 1.5. As alluded to above, molecules move around essentially at random within the reactant phase space unless in a specific energetic configuration which allows them to pass over the transition state barrier – in this case TS1. By the time the structure resembles that of the intermediate, it is presumed that the energy which was localised in the vibrational modes relating to the reaction co-ordinate has redistributed itself to a statistical configuration as determined by the microcanonical ensemble.⁸ This process is referred to as intramolecular vibrational energy redistribution (IVR) and is assumed to follow first order kinetics with a ‘rate constant’ of 10^{12}s^{-1} .⁹ The statistical approximation, in its simplest form, postulates that the rate of IVR in a reaction should be significantly quicker than that of any further reaction.

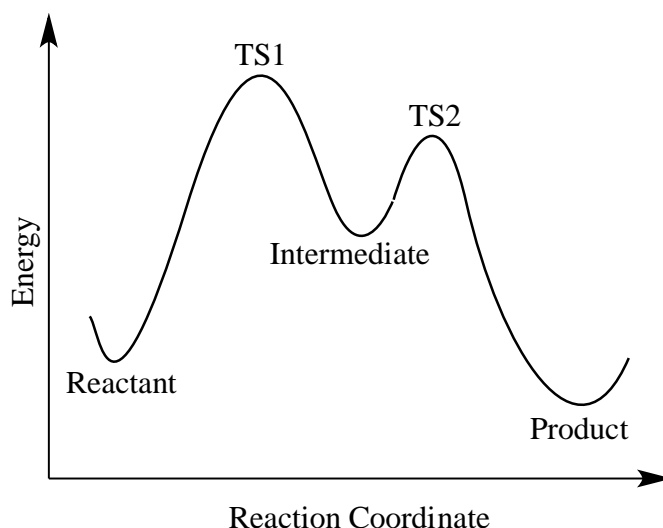


Figure 1.5: A Multistep Reaction

In cases where this may not be the case, for example reactions where the intermediate has a lifetime shorter than a picosecond, it may be that IVR is incomplete before the second step of the reaction. In other words, the molecule would have a nonstatistical distribution of energy throughout its vibrational modes. If the vibrational modes which are excited on passing over TS1 are similar to those which need to be excited to pass over TS2, then it is plausible that the second step of the reaction may occur much more quickly than one would predict if treating each step as discrete, rendering it difficult to predict an equilibrium concentration of the intermediate or product ratios.

In cases where an intermediate can form several different products, there are additional considerations to be made. If the transition states for each possible reaction are degenerate, then the products should be formed with equivalent rates and therefore exist with equal concentrations in the product mixture. However, if the intermediate being formed has a ‘molecular memory’ of a prior transition state, then it may pass over a second transition state with preference and thus give an unexpected product distribution. This will be discussed further in Section 1.5.2-1.5.3. The product distribution may be further affected by time. Any measure of product ratios before IVR is complete is potentially affected by the phenomena described above. Conversely, as reaction time increases and IVR has fully occurred, the product ratio is most likely to tend towards the statistical distribution one would ordinarily expect.

1.5.1 Examples of Nonstatistical Dynamics – The Acetone Radical Cation

One of the most commonly cited examples of nonstatistical behaviour is the McLafferty rearrangement.¹⁰ An example scheme for this is shown in Figure 1.6 below.

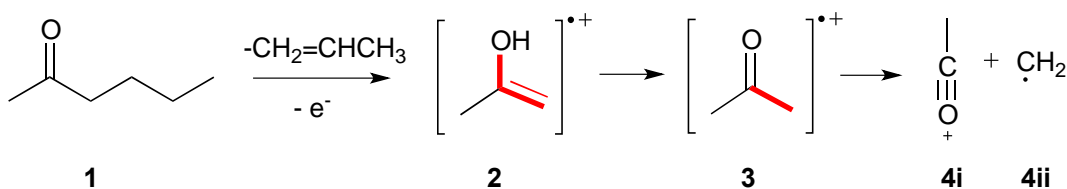


Figure 1.6: Summary of the McLafferty Rearrangement

The reaction was noted as taking place in the mass spectrometer. Prior to McLafferty’s work in 1970, it was believed that the commonly occurring **2** decomposed by simple cleavage of the methyl group. However, this study found that it was more probable for

the enolic intermediate to undergo tautomerisation via [1,3] hydrogen shift to the acetone radical cation **3**. Subsequently this fragments as shown.

Deuterium labelled versions of **1** were used, with labelling in the alpha positions. Given the symmetry present in the acetone radical cation, the product distribution of **4i** and **4ii** should have displayed a 1:1 ratio of labelling between the acylium ion and the methyl radical. However, the results showed that the final location of the deuterium label showed a bias relating to its initial position. If the label began on the methyl group of the enol, **2**, then it wound up preferentially on the acylium ion, **4i**. If it began on the vinyl group, it would preferentially feature in the methyl radical **4ii**. In both cases, the ratio of major to minor products was around 1.3:1. Furthermore, the methyl group in the enol would preferentially end up in the acylium ion, despite there being a symmetrical intermediate, **3**, en route. It was observed that both the tautomerisation and fragmentation steps could exhibit secondary isotope effects. In the first instance, the tautomerisation would lead to the same intermediate **3** regardless of whether the deuterium label was initially on the methyl or vinyl group of **2**, so should be irrelevant. In the latter case, the fragmentation occurs from **3** as a common intermediate and so both fragmentation pathways should be equally favourable. Additionally, later work was carried out on the system but using ^{13}C instead of ^2H labelling.¹¹ One would expect the secondary isotope effect for a $^{13}\text{C}/^{12}\text{C}$ substitution to be far less pronounced, due to the far smaller difference in mass between the two carbon isotopes when compared with the two hydrogen isotopes. However, the same asymmetry in the product distribution was found, with a similar preference for the methyl group ending up in the acylium ion.

It would appear that one explanation for the product ratios described above could lie in nonstatistical dynamics, specifically in the hypothesis that IVR is not always complete before an intermediate undergoes a secondary reaction. If excess vibrational energy was located in specific modes within the acetone radical cation, then it may not truly be a symmetrical intermediate.

A computational study was conducted in which molecular dynamics simulations (described in detail in Section 2.4) were used to explore the reaction and compare experimental results with those determined computationally.¹² Dynamics trajectories that began at the structure **3** resulted in either methyl group being lost with equal probability. However, in a second set of dynamics trajectories which were started at an optimised

structure for the transition state between **2** and **3**, there was a distinct preference for the newly formed methyl group (that highlighted in red in Figure 1.6) to be lost and to form the methyl radical.

In the original mechanism proposed by McLafferty, it was suggested that when **3** was formed, it would have specific localisation of energy related to the bending mode of the CCO bond highlighted (the newly formed methyl group), but only in that case. The other CCO bond was hypothesised to have no selective excitation. The dynamics results suggested that in a lot of cases, the methyl group dissociated before IVR could occur, meaning that this particular fragment of the molecule could remain selectively excited and could give rise to the higher incidence of dissociation for that methyl group.

Another interesting effect found in the computational work was that of product distribution dependence on time. Because the vibrational energy between the two CCO bonds would rapidly oscillate, after an initial period (around 50 fs) of the newly formed methyl radical being lost preferentially, the initial methyl group's bending mode would then become 'excited' and so for a period of time, this methyl group would be lost instead. In this manner, the preference could shift a number of times before IVR fully occurred. Overall, though, the initial effects were found to predominate and the newly formed methyl group was lost more frequently.

1.5.2 Examples of Nonstatistical Dynamics – Vinylcyclopropane

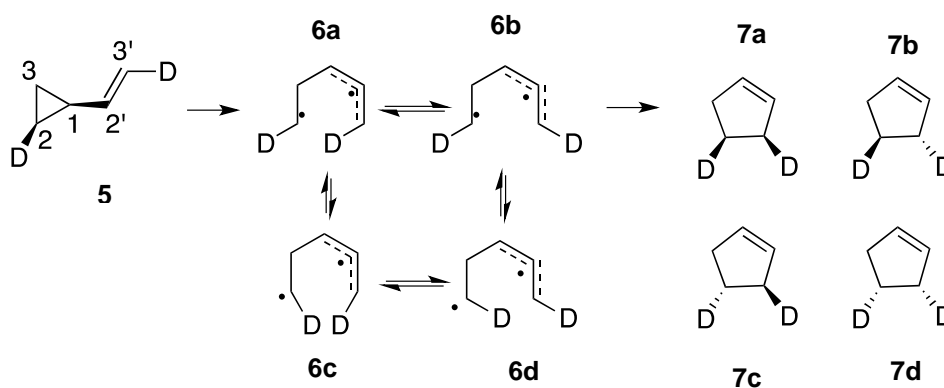


Figure 1.7: The Thermal Rearrangement of Vinylcyclopropane

Vinylcyclopropane **5** undergoes a thermal rearrangement to form cyclopentene (Figure 1.7).¹³ The reaction may go through either a stepwise or a concerted mechanism, but ultimately the C1-C2 bond breaks and a bond is formed between C2-C3'. The stereochemistry of the labelled methylene (which can be retained or inverted in the ring closure) and the method of ring closure (either suprafacial or antarafacial) give rise to the four distinct cyclopentenes **7a-d**.

In the concerted route, the ring closure would be pericyclic and the product ratio would be determined by the Woodward-Hoffman rules, which would stipulate that the two trans isomers **7b** and **7c** would be 'allowed' whereas the two cis isomers **7a** and **7d** would be 'forbidden.' It would follow that the latter would be formed with far lower probability. In a stepwise mechanism, the four biradicals can be conceived, which should be energetically degenerate. Given that the intermediates **6a-6d** are achiral, you would expect a racemic mixture of products with the concentrations of **7a** and **7d** being equal and the concentrations of **7b** and **7c** also equal.

The reported experimental product ratio is 23 : 13 : 40 : 24 for **7a** : **7b** : **7c** : **7d**.¹⁴ This is not consistent with the expected outcome of the stepwise mechanism, and gives a trans : cis ratio of 53 : 47, which is also non-concordant with the predicted ratio from a pericyclic reaction.

In order to further explore the system, a molecular dynamics study was carried out by Doubleday.¹⁵ The results supported a biradical intermediate, and were also in good agreement with the experimental values. Again, they hinted at a time dependence for the reaction. Reactions that occurred quickly appeared to show a high preference for forming a trans-deuterated product, and could be considered to be following a pericyclic mechanism. On the other hand, slower reactions resulted in roughly equal proportions of all possible products, which is more in line with the stepwise mechanism. One potential explanation for this is that the biradical mechanism predominates, but that some biradicals could be formed with selective excitation which would enable them immediately perform the 'allowed' ring closure. The other biradicals may spend some time sat on a biradical 'plateau' on the potential energy surface, during which time IVR can fully occur to form equal proportions of all biradicals and this, all four cyclopentenes.

The plateau on the PES for biradical systems is an important feature. It is a region where a number of reasonably large changes to the structure of the molecule can occur with almost complete preservation of potential energy. By its nature, it may allow almost barrierless exits to a number of products, and so can be problematic when using RRKM/TST theory to predict rate. In reactions where such a plateau may exist, there is likely to be difficulty in attempting to determine what kind of mechanism is being followed, and it may be almost impossible to predict product ratios without a clearer understanding of the dynamics of the reaction taking place. In such cases, methods such as molecular simulation, which have been touched on in this section, become vital tools to elucidate mechanism. In the section to follow there is a more comprehensive overview of these methods.

2 COMPUTATIONAL METHODOLOGY

2.1 Introduction to Computational Methodology

With the continual advent of new lab-based technologies, it has become commonplace to study many reactions experimentally that would previously have been practically impossible. Nonetheless, this study deals with thermal reactions, and in cases with very short lived and highly reactive intermediates it is still incredibly difficult to follow these reactions in the lab. Not only is this due to the very short-lived nature of the intermediates, but also their very small concentrations and similar structures when compared with reactants and products, rendering any sort of spectroscopic detection impractical. Where there is more than one intermediate, rapid interconversion between them can make any quantitative measure almost impossible too.

In such situations, using computational methods to model reactions and structures has proved highly useful. Many of the examples discussed in the previous chapter have involved the use of computational chemistry to uncover evidence of non-statistical dynamic effects.

In a very broad sense, computational chemistry can be split into two main fields: molecular mechanics and electronic structure methods.¹⁶ Whilst both methods can be used for similar types of calculation including geometry optimisation and calculation of vibrational energy levels for a species, they vary fundamentally in their approaches and applications.

2.2 Molecular Mechanics

Molecular mechanics, which is outside the scope of this project, is based on classical physics and is made up of a variety of different methods each dependent on its own *force field*. A force field has its own set of equations which determine how the energy of a molecule varies with the location of its atoms, and one or more *parameter sets* which define force constants and relate atomic characteristics to the energy of the molecule. However, molecular mechanics does not involve an independent consideration of electronic interactions and focuses instead on the interaction between

nuclei. Implicitly, the electronic characteristics of molecules are dealt with by considering the atom type, for example an atom of a particular element will be assigned subtly different properties if it features in one functional group rather than another. These calculations are generally relatively inexpensive, and less intensive computationally than those that do factor in electronic interactions. They are highly suited to the study of very large molecular systems and are used frequently in biological modelling of species such as DNA and its derivatives, proteins and carbohydrates. However, they tend to be limited to systems where electronic effects are not so pronounced, so they would be inaccurate in studies such as that presented here, which involves biradicals and a number of bond fissions and formations.

2.3 Electronic Structure Methods

The electronic structure methods to be employed in this project deviate in part from classical physics and are instead based on the laws of quantum mechanics. In other words, the energetic properties of a molecule can be calculated by solving the Schrödinger equation:

$$\hat{H}\psi(\vec{r})=E\psi(\vec{r})$$

Equation 2.1

Historically, there have been two major classes of electronic structure calculation: ab initio and semi-empirical. As the name would suggest, semi-empirical methods solve a form of the Schrödinger equation that contains some parameters from experimental data. These methods are also largely beyond the scope of this work.

Ab initio methods do not rely on any empirical data and instead make calculations based solely on quantum mechanics. These calculations tend to be the most costly and time consuming, but unlike semi-empirical or force field methods require very little prior knowledge of the system being studied. They are most suitable for systems with smaller molecules, where very accurate details of energy and electronic interaction are required. In order to calculate parameters for almost any type of system, ab initio

calculations include a number of mathematical approximations that will be discussed below.

The well known, time-independent Schrödinger equation (Equation 2.1) relates \hat{H} , the Hamiltonian, and E , the energy of the system by a wavefunction, ψ and a spatial function r . The wavefunction for a system is a complex number that describes mathematically an atom or molecule's wave-like behaviour with relation to space and time, and the product of the wavefunction with its complex conjugate, $|\Psi|^2$, is interpreted as the probability density for the particle. The Hamiltonian is an operator that is made up of kinetic and potential energy operators:

$$\hat{H} = \hat{T} + \hat{V}$$

Equation 2.2

The kinetic energy term, \hat{T} , is a summation of all the partial differentials of motion in the x, y and z directions, while the potential energy term, V , is a combination of electron-nucleus, electron-electron and nucleus-nucleus repulsion. This can be summarised in Equation 2.3:

$$\hat{H} = \hat{T}_N + \hat{T}_e + \hat{V}_{Ne} + \hat{V}_{ee} + \hat{V}_{NN}$$

Equation 2.3

Where \hat{T}_N and \hat{T}_e are the nuclear and electronic components of the kinetic energy respectively and \hat{V}_{Ne} , \hat{V}_{ee} and \hat{V}_{NN} are the various electron-nucleus components of the potential energy.

Solving the Schrödinger equation for different values of the Hamiltonian operator gives rise to energies for various stationary states of the molecule, the lowest of which tells us the ground state energy. Thus, by solving the Schrödinger equation, we are able to calculate the energy for various configurations of a molecule and this is the basis of most electronic structure calculations.

As alluded to previously, as the Schrödinger equation can only be solved with complete accuracy for systems with one electron such as a hydrogen atom or a He_2^+ ion, many

simplifications and assumptions are required to calculate energies for larger molecules; this is termed the many-body problem. One way to get around this, as described above, is to introduce an element of experimental data i.e. semi-empirical methods. However, where this is not possible we use a series of mathematical approximations as part of an ab initio methodology.

When we considered equation 2.3 we were implicitly invoking one of the most fundamental theories in quantum mechanics: the Born-Oppenheimer approximation. It separates the movement of electrons and nuclei in a system, and based on the observation that electronic motion is vastly greater than nuclear motion, allows us to consider electronic motion in the framework of a stationary nucleus. In other words, while positions of nuclei are relevant, their velocities are not, and the Schrödinger equation can be reduced to an electronic only form:

$$\hat{H}^{\text{elec}} \psi^{\text{elec}} = E^{\text{eff}} \psi^{\text{elec}}$$

Equation 2.4

In this equation, H^{elec} is the electronic Hamiltonian with the kinetic energy term for the nucleus removed, ψ^{elec} is the electronic wavefunction, and E^{eff} is the *effective nuclear potential* function which is calculated for particular nuclear co-ordinates and defines the potential energy surface for a system. Conversely, if you needed to calculate the nuclear motion of a system, the value for E^{eff} would replace the potential energy term when calculating the nuclear Hamiltonian. This would be necessary, for example, to calculate vibrational spectra where changes in nuclear motion would be vital to consider. Throughout the rest of this work, only the electronic Hamiltonian will be discussed and the term used synonymously with “the Hamiltonian.”

Before moving from defining the Hamiltonian to calculating energy, it is important to note a couple of limitations on the value of ψ which will become relevant in further discussion. Firstly, the wavefunction must be normalised so that a solution for its integral over space is equal to one i.e. it has unit probability of existing somewhere in space. This is achieved by multiplying ψ by a constant. Secondly, because electrons are

fermionic the wavefunction must be antisymmetric, meaning that if two electrons are interchanged the wavefunction will change from positive to negative or vice versa.

2.3.1 Hartree-Fock Methods

One of the more basic methodologies for ab initio calculation is Hartree-Fock (HF) theory.¹⁷ It is known as an *independent-particle model* because it deals with the motion of a particular electron as being independent of all the other electrons in a given system. In HF theory specifically, the interactions between all the other electrons are taken into account as an averaged factor.

In the HF model, each electron is described in terms of an orbital(Φ), and the total wavefunction for a molecule is formulated by a combination of these orbitals. This is called linear combination of atomic orbitals (LCAO) and is described in Equation 2.5 below:

$$\psi(\vec{r}) = \phi_1(\vec{r}_1) \cdot \phi_2(\vec{r}_2) \dots \phi_n(\vec{r}_n)$$

Equation 2.5

However, this combined wavefunction does not fulfil our requirement for a wavefunction to be antisymmetric, as exchanging two of the electrons would not result in the sign of the wavefunction changing. In HF theory, the way to overcome this is to build the molecular orbital using Slater determinants. Equation 2.5 above considers orbitals which each contain a single electron, but does not consider that electrons exist in one of two possible spin states. However, many calculations as we will see later consider electron shells containing two electrons. By using the determinant, we consider the various wavefunctions of the LCAO as a matrix, where each orbital is composed of pairs of electrons, and each pair of electrons is considered with the various achievable combinations of spin up and spin down. Figure 2.1 below shows an example of a generic determinant. Essentially, using this method, the wavefunction is made up of every possible orbital of each electron. Each row in the matrix corresponds to different electronic co-ordinates and each column to a particular single-electron orbital, and the result is that each electron is 'assigned' to a particular orbital. Swapping any two

electrons results in a change of sign for the overall wavefunction. In HF theory, it is postulated that a wavefunction can be described by a single Slater determinant. The theory is limited in that it does not incorporate any of the effects of electron correlation. In order to consider electron correlation, you would need to use several determinants, but these computational methods are much more time-consuming. This will be discussed further in Section 2.1.4.

$$\phi_{SD} = \frac{1}{\sqrt{N!}} \begin{bmatrix} \phi_1(1) & \phi_2(1) & \dots & \phi_N(1) \\ \phi_1(2) & \phi_2(2) & \dots & \phi_N(2) \\ \vdots & \vdots & \ddots & \vdots \\ \phi_1(N) & \phi_2(N) & \dots & \phi_N(N) \end{bmatrix}$$

Figure 2.1: A Slater determinant

The molecular orbitals described by a Slater determinant are incorporated into electronic structure calculations using a pre-defined combination of single electron functions, which is known as a basis set. The term basis set refers to the specific type of atomic orbitals which are used to form molecular orbitals. In the case of HF, this is usually a collection of Gaussian-type functions. Slater type orbitals are also sometimes used, but will not feature in this work. Gaussian orbitals are formulated in terms of Cartesian co-ordinates. They are generally considered to be easier to use than Slater type orbitals, despite known inaccuracies in their ability to calculate electron behaviour either very close to or very far from the nucleus. On average, three Gaussian orbitals are required to give the same accuracy as one Slater orbital.

The simplest basis sets are known as minimal basis sets, and are denoted with the STO-xG nomenclature where x is the number of Gaussian functions used to make up each atomic orbital. Split valence basis sets involve using more than one basis function (comprised of a linear combination of basic Gaussian functions) to represent each valence orbital. They are named double zeta, triple zeta etc depending on the number of basis functions used. A particularly well-used group of split valence basis sets are the Pople basis sets; an example of this is 3-21G, which will be used widely throughout this work. The 3 denotes three primitive Gaussian functions making up each *core* atomic

orbital. The 2 and 1 represent the valence orbitals, which are each composed of two basis functions, the first made up of two primitive Gaussian orbitals and the second made of one primitive Gaussian orbital.

It is also possible where necessary to add a polarization function to the basis set, indicated by a "*" after its name, or a diffuse function indicated by a "+", e.g. 3-21+G* has both polarisation and diffuse functions. A polarised basis set allows variation in the shape of an orbital by adding some p functions to s block atoms, d functions to p block atoms etc. A diffuse function allows orbitals to occupy a larger than normal region in space and is suitable for species with lone pairs, excited state systems etc.

In order to minimise the energy for a given structure, which is the ultimate aim of an electronic structure calculation, we need to be able to determine which combination of a Slater determinant and orbitals reaches an energetic minimum and thus gives us our optimized structure. In order to calculate this, we begin with an approximate structure, and undertake a step-wise, iterative process of solving the Schrödinger equation that is known broadly as the self-consistent field method. The variational principle tells us that calculated HF energy for a trial wavefunction will always be slightly higher than the true energy for the exact wavefunction for that particular structure, so each step of a HF calculation seeks to find a set of parameters which gradually lower the energy. In this manner, a calculation proceeds until an optimised structure is found when an iterative step in a calculation no longer finds a successively lower energy value. Convergence is reached when the first derivative of the energy with respect to the molecular orbital coefficient is zero i.e. zero rate of change.

It is important to note that there are several variations of HF theory that can be used depending on the electronic configuration of the species in question. The least exhaustive form of HF theory is called restricted HF (RHF) where all orbitals are treated as doubly occupied. However, in many situations, as is the case with the work presented here due to it largely being concerned with radical species, this is insufficient. In restricted, open-shell HF (ROHF) theory, all but the valence orbitals are considered to be doubly occupied. In unrestricted HF (UHF), every electron is treated as being in an individual orbital. The UHF energy for a wave function is invariably lower than the corresponding ROHF energy, as the UHF wavefunction allows different spatial orbitals

for α and β spin electrons and does not constrain them in the same way as a restricted method. For systems with an unpaired electron, a closed-shell treatment means the unpaired electron would interact in the same way with both α and β spin electrons, whereas in reality this interaction would vary depending on its own spin. Thus in these cases an unrestricted treatment would be more suitable. However, an unrestricted treatment can lead to spin contamination, an artefact of using a linear combination of Slater determinants with overlapping terms between singlet and triplet or doublet and quartet states etc. The result is that a UHF calculation rarely produces a ‘pure’ spin state: it often retains some character from a higher spin state.

There are a number of other limitations of HF theory that are now widely accepted and have led to the rise of several post-HF methods which attempt to rectify them.

2.3.2 Post Hartree-Fock Methods

As previously discussed, HF theory deals with the interaction of electrons with the same spin by using a Slater determinant to ensure the wavefunction is antisymmetric in nature. This type of interaction is known as *exchange correlation*. However, HF theory does not include any treatment of the interaction between electrons of opposite spin – *electron correlation*. It is estimated that the HF methodology is able to account for about 99% of the energy of a system, but that the remaining one percent is due to electron correlation. In restricted HF theory, electrons are paired in orbitals. Considering both *intra* orbital electron pairs, which are all spin-paired, and *inter* orbital electron pairs, which are both opposite and same spin pairs, in a given system there are more pairs of electrons with opposite spins than pairs of electrons with the same spin. This means that electron correlation should have a larger effect on a molecule’s energy than exchange correlation and explains why it is a major consideration when deciding if HF is a suitable method for a particular calculation.

There are two forms of electron correlation, *static* and *dynamic*. Static electron correlation relates to electrons that are permanently separated spatially, for example those in different molecular orbitals. It is sometimes also called a near-degeneracy effect because it prevails in systems where there are several orbital configurations with almost identical energies, and make it difficult to determine which configuration is a true representation of the lowest energy structure. Dynamic electron correlation is concerned with the interaction between rapidly moving electrons occupying the same

orbital space. Using simple diatomics for illustrative purposes, it is mainly dynamic correlation for a short bond distance such as the H-H distance in H₂, but as bond dissociation occurs and the distance between the orbitals increases, the main component of the correlation energy is static.

2.3.3 Multi-Determinant Methods

Dynamic electron correlation can be dealt with by using *multi-determinant methods* such as Configuration Interaction (CI). These stem from the understanding that a single Slater determinant is not adequate to accurately describe a wavefunction and work by substituting one or more of the HF orbitals with virtual orbitals as summarised in Equation 2.6. While HF theory centres on finding the best Slater determinant for minimising energy, the accuracy of the method can be substantially improved by using a combination of determinants that give a more detailed representation of a molecular orbital.

$$\Psi = a_0 \Phi_{\text{HF}} + \sum_{i=1} a_i \phi_i$$

Equation 2.6

In this equation, the $a_0 \Phi_{\text{HF}}$ term relates to the HF determinant, and the second term is a summation of all the substituted determinants, overall giving a linear combination of both HF and substituted elements to form the wavefunction.

There are various levels of substitution. A single substitution (S-type) involves replacing a single orbital within the determinant with a virtual orbital. These virtual orbitals are generated from excited Slater determinants, so called because a HF occupied molecular orbital is replaced with an unoccupied orbital of higher energy. A double substitution (D-type) is doubly excited relative to the HF determinant, and so on. Figure 2.2 shows how these excited determinants are formed.

CI calculations work by optimizing the value of co-efficients a (see Equation 2.6) to find the optimum level of substitution to minimize energy and again work iteratively.

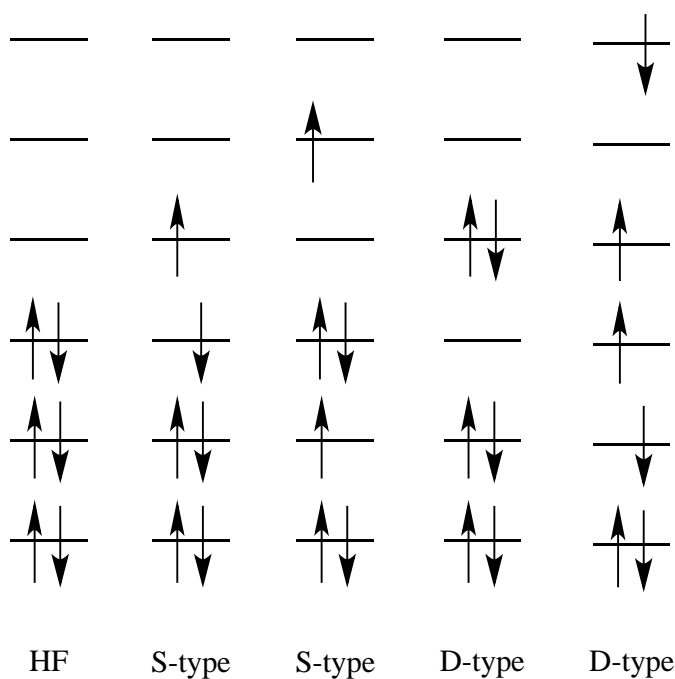


Figure 2.2: Illustration of Excited Slater Determinants

The Multi-Configurational Self-Consistent Field (MCSCF) method is another multi-determinant method, but an expansion on CI methods because it optimises not only the coefficients for each determinant but also optimises the molecular orbitals that construct each determinant. MCSCF methods are much more exhaustive, and harder to converge. Whereas with HF methods convergence is reached when the first derivatives of energy are zero, this is not always sufficient for this type of calculation and second order derivatives are required to ensure a true minimum.

2.3.4 Perturbation Methods

An alternative approach to dealing with dynamic electron correlation is through the use of many-body perturbation methods such as Møller-Plesset (MP) theory. This involves the ‘splitting’ of the Hamiltonian into two constituent parts – one that is the reference (or unperturbed) Hamiltonian, \hat{H}_0 , and the perturbed Hamiltonian, \hat{H}' (Equation 2.7).

$$H=H_0+\lambda H'$$

Equation 2.7

Here, λ is a variable co-efficient which determines the strength of the perturbation. The theory is based on the idea that the solution to a problem (in this case minimising energy) is most likely close to a solution already found. With this in mind, minor adjustments are made to the Hamiltonian via perturbation of \hat{H}_0 which are very small in comparison to the magnitude of \hat{H}_0 . Unlike multi-determinant methods which involve a linear expansion of wavefunctions, perturbation methods use an exponential expansion. The wavefunction and resulting energies can be expressed as a series of powers with relation to λ (Equations 2.8 and 2.9).

$$\psi = \psi^0 + \lambda \psi^{(1)} + \lambda^2 \psi^{(2)} + \lambda^3 \psi^{(3)} + \dots$$

Equation 2.8

$$E = E^0 + \lambda E^{(1)} + \lambda^2 E^{(2)} + \lambda^3 E^{(3)} + \dots$$

Equation 2.9

The first order substitution will result in no change to the energy of the system. However second order perturbations and above are frequently used and named accordingly e.g. MP2, MP3 etc. The higher order perturbations are analogous to the various level of substitution in the CI method. However, the MP method has a limit to the number of excited determinants that can be formed from a specified basis set, so it can function up to a pre-determined order only.

An alternative form of perturbation is the Coupled Cluster (CC) method, where all perturbations of a particular nature should be possible to an infinite order. Here, a solution for the wavefunction may be formed by the action of a single exponential operator on a single Slater determinant, usually that found by HF theory (Equation 2.10) and the exponential operator is made up of a linear expansion of excitations of increasing order (Equation 2.11) up to T_N where N is the number of electrons in the system.

$$\psi = e^{\hat{T}} \phi_0$$

Equation 2.10

$$\hat{T} = \hat{T}_1 + \hat{T}_2 + \hat{T}_3 + \dots + \hat{T}_N$$

Equation 2.11

One of the most popular CC models, Coupled Cluster Singles and Doubles (CCSD) stops the expansion in equation 2.11 at T_2 . For higher order terms, it uses exponential values of these terms, for example quadruple order would include the factor T_2^2 . By doing this, it makes CC calculations available for calculations involving larger systems.

2.3.5 Multi-Reference Methods

Static electronic correlation can be dealt with using multi-reference methods. As described in section 2.2.2, static correlation deals with pairs of electrons with opposite spin which are separated spatially. This is especially important for molecules such as singlet diradicals, which are the main focus of this work and will be discussed further in the following chapter.

The basic CI methods discussed previously used a HF wavefunction as a reference, with a single determinant as a starting point. However, it is possible to use a MCSCF function as a starting point, as described in 2.2.3, where the molecular orbitals as well as multiple determinants are optimised. By beginning in this manner, excitations can stem from all determinants – this is known as a *Multi Reference Configuration Interaction* method. The ‘size’ of the self-consistent field is dependent on the number of reference points from the original MCSCF calculation, but can essentially include all possible configurations of the electrons in a given system including excited states, radicals etc. It also means they can be used to examine situations of bond formation/breaking and so can be used with accuracy to optimise species such as transition states.

These methods can be very accurate, but also very time consuming. They are frequently truncated to single and double excitations as with CC methods. They can be further limited by using perturbation methods to determine which configurations have a notable interaction with the reference configuration and considering only these. However, this can mean that a particular configuration has a ‘drop-off’ point, where it falls suddenly below the stipulated threshold and no longer factors into a calculation, leading to unusual results.

2.4 Density Functional Methods

2.4.1 Traditional Density Functional Methods

Relatively recently, a third type of electronic structure method has become the most commonly used in the study of organic chemistry – *density functional* methods. Although calculations based on density functional theory (DFT) are not strictly considered to be *ab initio*, there are many similarities between the two classes.

Density functional methods are based on the Hohenberg-Kohn theorem developed in the 1960s which postulated that ground state electronic energy is determined completely by electron density.¹⁸ In other words, the electron density determines the Hamiltonian and the energy of a molecule becomes a functional of its electron density. Hohenberg and Kohn believed there was a specific functional which could exactly determine ground state energy and electron density. However, they did not state the form of this functional.

Current DFT methods separate electronic energy into a number of terms:

$$E = E_T + E_V + E_{ee} + E_{XC}$$

Equation 2.12

In this equation, the energy is split into:

- i) kinetic energy (T);
- ii) potential energy (V) including nucleus-electron attraction and nucleus-nucleus repulsion;
- iii) electron-electron repulsion (ee);
- iv) and exchange correlation (XC) which incorporates the remaining electron-electron interactions.

All of the above terms are functions of the electron density, ρ , with the obvious exclusion of the nucleus-nucleus component of the potential energy. The first three terms equate to the standard energy associated with charge distribution. The *correlation* energy, E_c is made up of dynamic electron correlation, which has already been defined in section 2.2.2 as the energy associated with the interaction between moving opposite spin electrons in a limited orbital space. It also includes *exchange* energy, E_x , associated with the antisymmetric nature of the electronic wavefunction. The exchange

correlation energy is a functional of the electron density (Equation 2.13). The correlation energy can be thought of as the mixed-spin interactions, and the exchange energy as the same spin interactions.

$$E_{XC}(\rho) = E_X(\rho) + E_C(\rho)$$

Equation 2.13

E_{XC} can be represented as an integral incorporating the electronic spin densities and their gradients, Δ .

$$E_{XC}(\rho) = \int f[\rho_\alpha(\vec{r}), \rho_\beta(\vec{r}), \nabla\rho_\alpha(\vec{r}), \nabla\rho_\beta(\vec{r})] d^3\vec{r}$$

Equation 2.14

If the exchange and correlation functionals are considered in terms of just electron density they are said to be local functionals. If they are considered also in terms of their gradients, they are called gradient-corrected functionals. The local functionals give rise to the Local Density Approximation (LDA) where electron density is a function of spatial configuration alone and so the electron density calculated by these methods is technically valid only for a particular point in space. It was developed to reproduce accurately the exchange energy for a uniform electron gas, but breaks down in more complex situations as it relies on a number of limited approximations to make it applicable to wider systems. Gradient approaches give rise to the General Gradient Approximation (GGA) and allow for the effects of electron density changing with position in space. This makes GGA methods inherently more applicable to real molecules.

Under the umbrella constructs of LDA/GGA methods there are a variety of different functionals available which include various corrections to make them more widely useful. For example, gradient corrections can be added to LDA methods to increase their accuracy. With a number of modified functionals for both exchange and correlation available, a DFT method is chosen by one of each type of functional. A commonly used DFT method is BLYP, which pairs together a gradient-corrected exchange functional by Becke with a gradient-corrected correlation functional designed by Lee, Yang and Parr.

A primary advantage of density functional methods is that they tend to be significantly cheaper than ab initio methods and can deal well with electron correlation without the exhaustive processes required by the methods in section 2.2.

2.4.2 Hybrid Density Functional Methods

The final class of methodology to be described here is the Hybrid DFT method, which combines elements of both HF and DFT calculations. The first hybrid methods were designed by Becke, who based the method on the fact that DFT calculations are carried out in an iterative manner similar to the ab initio calculations described above. Because HF theory and DFT both contain an element of exchange energy, it seemed logical to attempt to put the two methods together. He combined a mixture of Hartree-Fock and DFT exchange with DFT correlation.

$$E_{XC(\text{hybrid})} = c_{\text{HF}}E_{X(\text{HF})} + c_{\text{DFT}}E_{X(\text{DFT})}$$

Equation 2.15

Using the example of the DFT functional BLYP from the previous section, it is possible to illustrate the formation of such a hybrid functional as below (Equation 2.16). In this example, the DFT exchange functional chosen is Becke's 1988 functional, and the correlation functional VWN3 is used in conjunction with the correlation gradient correction LYP. The overall DFT hybrid functional is called B3LYP.

$$E_{XC(\text{B3LYP})} = E_{X(\text{LDA})} + c_0(E_{X(\text{HF})} - E_{X(\text{LDA})}) + c_X \Delta E_{X(\text{B88})} + E_{C(\text{VWN3})} + c_C(E_{C(\text{LYP})} - E_{C(\text{VWN3})})$$

Equation 2.16

Here the coefficients, c , allow any composition of the various exchange and correlation components to be factored in. The B3LYP method specified by Becke, has fixed quantities for each of these coefficients. By varying these coefficients, numerous different hybrid functionals can be constructed. When undertaking a computational study using previously published hybrid DFT methods, an important first step is benchmarking and evaluation of the various methods to see which is likely to give the

best results for the system in question. This is explored further in Chapter 3.

2.5 Simulation Techniques

The various methods of electronic structure calculation examined help us to describe and locate stationary points on a potential energy surface, such as products, reactants, transition states and intermediates. Knowing the electronic structure and vibrational energy levels of these species, we can quickly familiarise ourselves with their microscopic properties. In the introduction to this work, though, it was stated that these microscopic properties could be used to predict the macroscopic properties of a reactive system. We have some elements of this through the location markers we are able to develop over the surface of our PES. However, the study of dynamics simulation helps bring together the discussions of potential energy surfaces and phase space from Chapter 1 with the computational methods described in Chapter 2.

So far the discussion has centred on time-independent calculations. However, to thoroughly explore the reactions of a given molecule, and to be able to detect nonstatistical effects, it is vital to elucidate the aspects of mechanism which cannot be seen simply from consideration of stationary points. Simulation allows a reactive species, given a well-defined set of initial parameters, to evolve over time and to follow a particular trajectory over the PES. We now understand that although the results of two trajectories may look the same, the routes they take over the PES may have a large impact on their intermediate states and their product distribution.

There are a number of different simulation methods that can be employed. The main differentiator between them is the method in which initial sampling is conducted, and thus the way the starting point is defined. The term ensemble is used to describe an initial set of conditions such as atomic co-ordinates and momenta. The two most commonly used methods for constructing an ensemble are Monte Carlo (MC) methods and Molecular Dynamics (MD) methods.

2.5.1 Monte Carlo Methods

MC methods, which will not be used in this work, begin with a specified geometry of a given molecule and then the coordinates of a particular particle are altered by a small-magnitude distortion. At each step, to ensure that the new structure is not too dissimilar

from the input geometry, thresholds are set where the new geometries must either lead to a lowering of energy or have only an infinitesimally small increase in energy. The step size in MC methods must therefore be very small; the distortion is essentially at random and so needs to be ‘checked’ regularly to ensure it adheres to the energy requirements described. As such, MC methods often require thousands of steps and within this are only able to explore a reasonably limited volume of the available phase space for a reaction. However, at each step, only the energy need be recalculated, as all other changes are input parameters. In theory, is also only necessary to recalculate the energy in the region of the distortion, because the rest of the molecule should be unchanged. However this approach can be inaccurate, especially in the case of smaller molecules. MC methods are almost entirely non-deterministic, that is, because each step relies on random changes, there is essentially no chance of two trajectories giving the same result. One of the main disadvantages to MC methods is that they factor in no treatment of atomic velocities and so they cannot be used in the detection of time-dependent phenomena.

2.5.2 Molecular Dynamics Methods

In contrast, MD methods (to be used in this study) generate a time-dependent arrangement of particles by starting with a set of co-ordinates with specific velocities, and solving with respect to Newton’s second law at each step (Equation 2.17), where the force, F , on each atom is equal to the product of its mass, m , and acceleration, a .

$$F=ma$$

Equation 2.17

The time between each step and the number of steps can be set to show the evolution of the system over any user-specified time limit, but it is considered unwise to use this method to study a period of time much longer than 50 picoseconds(ps) due to the vast number of steps that would be required and the fact that any numerical errors at a particular step will be propagated and amplified throughout the trajectory. While this is a reasonably short timescale for many reactions, in the case of the reactions to be studied here and the timescale of IVR it is considered sufficient. The trajectories run in this study will be given around 1 ps.

MD methods are intrinsically deterministic. A set of co-ordinates given the same initial velocities should give the same result each time a simulation is run. At each step, not only the energy but the forces on each atom need to be calculated. Unlike MC calculations, the energy for the entire molecule also needs to be re-evaluated at each step because all particles move at each step. To mitigate the effects of marginal computational error and rounding, the total energy of the system is monitored as the trajectory progresses to ensure there is no notable fluctuation.

Classical MD methods would traditionally involve a number of single-point electronic structure calculations where potential energies would be calculated for each internal coordinate of the system at a number of different atomic positions.¹⁹ These energies would subsequently be fitted to a mathematical function that could be used to propagate the trajectory and determine potential energy and its derivatives for further steps. The obvious limitation of this methodology lies in the vast number of potential energies that need to be calculated at the outset, rendering it ineffectual for large systems. In practice, the initial conditions for these methods would be created using a combination of ab initio potential energies for the most ‘critical’ internal coordinates and an empirical potential energy term derived from experimental force constants, bond energies etc. to describe the other coordinates. However, determining the significance of particular internal co-ordinates from the outset would invariably be impractical, and a lack of availability of experimental data compounded the difficulties. This gave rise to the development of alternative dynamics methods, which could be used more reliably for larger systems.

At present, it is commonplace to use a ‘direct dynamics’ method, meaning that dynamics trajectories are calculated ‘on the fly’ using electronic structure theory methods.²⁰ In one specific type of MD which will be used in this work, Born-Oppenheimer molecular dynamics (BOMD), an initial potential energy is calculated using ab initio methods i.e. from the laws of quantum mechanics by solving the time-independent Schrödinger equation. At each step, Newton’s second law is solved to give the acceleration on each atom. There is also an explicit electronic wavefunction describing the system that is optimized to calculate potential energy. This combination of quantum mechanical and classical approaches is the foundation of BOMD. A primary advantage of direct dynamics methods is that they allow the evolution of a molecule’s electronic structure to be charted over time, so systems with more complex

electronic properties such as the biradicals presented here can be studied with enhanced accuracy.

2.6 Summary and Aims

It has been found in a number of cases that for thermally generated species, nonstatistical behaviour is exhibited. Two separate reactions will be studied in depth as the basis of the present work in Chapters 3 and 5. The first of these is the thermal rearrangement of spiropentane which will be studied computationally, by molecular dynamics simulation. Also, a synthetic investigation into finding a route to a benzoyl peroxide containing a Dewar benzene functionality will be carried out, and the thermal decomposition of the resulting molecule considered.

3 NONSTATISTICAL DYNAMICS IN THE THERMAL REARRANGEMENT OF SPIROPENTANE

3.1 Introduction

Biradicals are compounds which possess two unpaired electrons. One of the most prolific names in the field of biradical research is Salem,^{21,22} who has been involved in trying to determine exactly what is meant by the term diradical - a name used synonymously with biradical but which may turn out to have a subtly different meaning. The widely accepted view now is that a diradical is a species in which there is sufficient distance between the two unpaired electrons for them to not 'see' one another, for example in an electronic paramagnetic resonance (EPR) spectrum. On the other hand, a biradical can be thought of as a species where the two unpaired electrons are spatially oriented in such a way that they may interact with one another. Another view is that a diradical can be defined by the speed of bond closure relative to internal rotations.²³ Any species where loss of stereochemical configuration can occur much more quickly than a reclosure is considered to be more diradical in character than biradical. However, for the purposes of this work the two terms will be considered together under the name biradical.

The traditional view of a biradical is one in which two near degenerate, singly occupied orbitals (SOMOs) each contain an unpaired electron. In the case of a singlet, these two electrons will have antiparallel spins, whereas the triplet state will have two electrons of the same spin. In accordance with Hund's rule, in cases where the two unpaired electrons are in molecular orbitals with little spatial separation, the singlet state tends to be higher in energy than the triplet state for a given molecule. Conversely, where there is a large separation the triplet state will tend to have higher energy.

In order to fully understand the reactivity of biradicals, it is important to consider their orbital structure. They can be thought of as having two atomic orbitals, delocalised in space, which interact either by a small element of orbital overlap or exchange energy. Where the two electrons occupy individual orbitals, they can be described by one of two wavefunctions appertaining to either the singlet or the triplet state. These wavefunctions are thought of as covalent in nature and the singlet and triplet states are similar in energy. There are two further possible configurations that are considered ionic or

zwitterionic in nature, whereby the two electrons both occupy one orbital. Both zwitterionic configurations correspond to the singlet state.

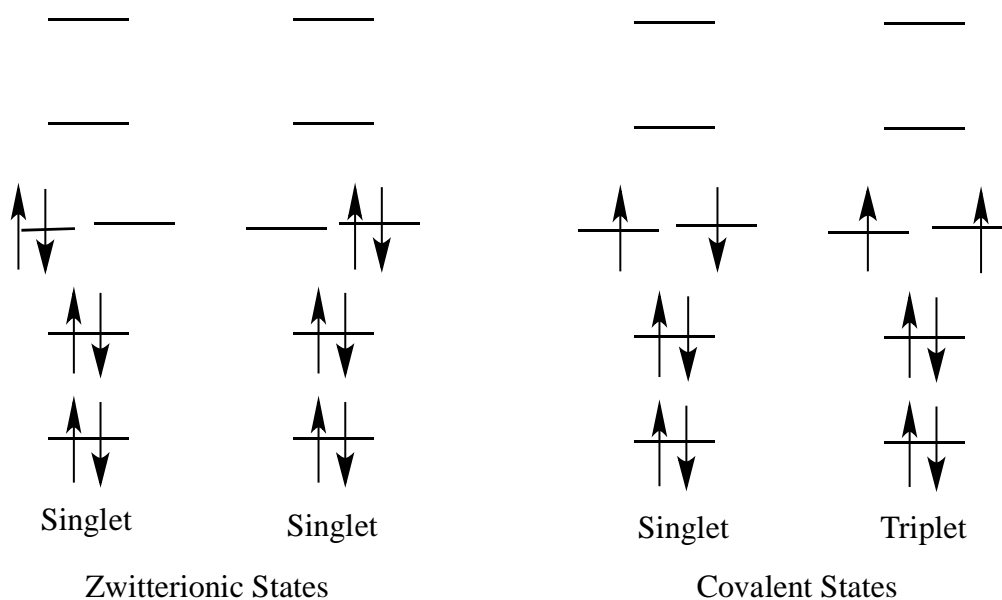


Figure 3.1: Biradical Electronic Configurations

The amount of zwitterionic or covalent character that a biradical has depends largely on the symmetry of the molecule. In systems with low symmetry, all the possible states described above can contribute to the overall configuration. This combination of states can make biradicals difficult to describe using more basic computational methods such as Hartree Fock or perturbation methods, and gives rise to the necessity for multi-reference methods as described in Chapter 2. For the purposes of this study, multi-reference calculations already carried out will be used as a starting point for some calculations.

The work in this chapter focuses on the thermal rearrangements of spiropentane, the simplest, saturated, spirocyclic hydrocarbon featuring two fused cyclopropane rings. In a study that involved the pyrolysis of small hydrocarbon rings including cyclopropane derivatives to form biradicals, it was found that calculated values for heats of formation of the biradicals were consistently smaller than experimental activation energies.²⁴ This

suggests that the biradicals would form shallow minima on the surface and appear as 'true' intermediates on a PES. The biradical species were found to have only short lifetimes of around 10^{-10} s.

However, later findings by Hoffmann were at odds with this view.²⁵ He studied the decomposition of cyclobutane to two ethylene fragments, and identified a tetramethylene diradical as the likely intermediate (Figure 3.2).

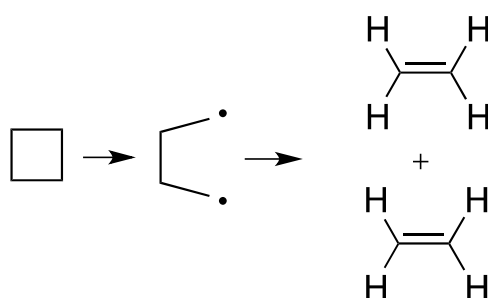


Figure 3.2: The Fragmentation of Cyclobutane

Similarly to the vinylcyclopropane example in Section 1.5.3, the stepwise vs. concerted mechanism question was important. By conducting labelling studies, it was found that the fragmentation occurred with loss of stereospecificity and this was considered evidence in favour of a stepwise mechanism with a biradical intermediate. Hoffmann's computational study was carried out using the extended Hückel method developed within the group. Initial calculation of the PES for the fragmentation appeared to show two minima in addition to the minima for cyclobutane and ethylene, which appeared to be structurally identifiable as *trans* and *gauche* conformers of the biradical. However, secondary calculations which varied the C2-C3 bond length in these structures found that it was possible to move on a directly downwards pathway from either conformation towards ethylene fragmentation, suggesting that the minima were not true minima. Instead, the findings supported the idea of a 'minimum' with a barrierless exit, similar in principle to a biradical plateau, where the biradical species could spend some time in a particular energetic state before moving on to complete the reaction. The consequences of this on calculated rate constants could be vast, as it was found that the biradicals could be spending as long as a few picoseconds on such a plateau. It could also possibly

give rise to other nonstatistical effects described in the opening chapters, such as large changes in conformation or loss of stereospecificity.

As such, singlet biradicals are found to lend themselves well to the study of nonstatistical dynamics. Short lifetimes give rise to the potential for further reaction occurring more rapidly than IVR. The potential for a unique plateau region to exist on a PES is also of interest.

3.2 The Thermal Rearrangements of Spiropentane

The first major element of this work focuses on a computational study of the dynamics of a small singlet biradical. The primary aim will be to elucidate mechanistic details of a thermal rearrangement in a multistep reaction, and to look for evidence of nonstatistical effects such as unusual product distributions due to incomplete IVR and TS barrier recrossings.

Spiropentane **10** (SP) is the simplest spirocyclic, unsaturated hydrocarbon and can be formed from the addition of singlet methylene **8** to methylenecyclopropane **9** in a highly exothermic reaction (Figure 3.3). The vast excess energy released by its formation means that it exists, at least initially, in a vibrationally excited state that makes it ideal for the study of nonstatistical dynamics. At moderate pressures this 'hot' spiropentane can undergo a unimolecular rearrangement to form methylenecyclobutane **11** (MCB), with an activation energy that is roughly 42 kJmol^{-1} higher than the energy needed for initial bond dissociation.²⁶ This indicates a multistep reaction and points towards a mechanism involving a biradical intermediate. At lower pressures, ethylene and allene **12a** and **12b** can be formed and at higher pressures spiropentane is found to be the primary product (see below).^{27,28}

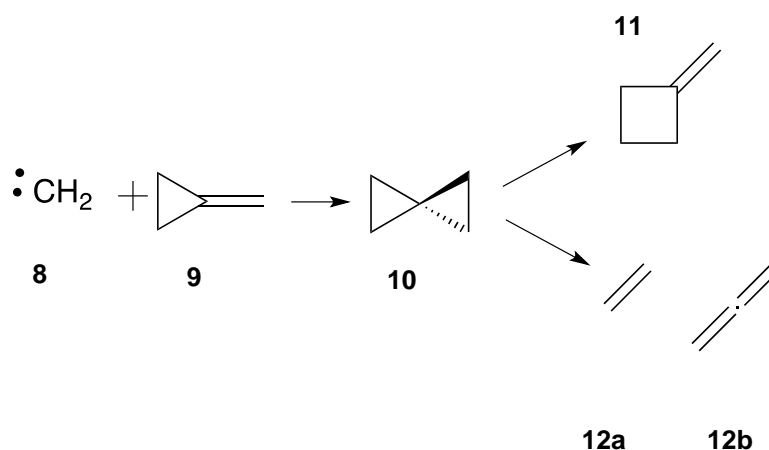


Figure 3.3: Thermal Rearrangements of Spiropentane

It is possible that the rearrangement from SP to MCB can progress in two ways as shown in Figure 3.4. In the top pathway, the first bond cleavage is a peripheral bond (not bonded to the central carbon), for example between C1-C2 as shown to give biradical

12a, followed by a radial bond fission C3-C5 to biradical **12c** and a bond formation between either C4 or C5 and C2 or C1. The alternative pathway involves a radial C1-C3 homolysis first to form **12b**, followed by peripheral bond fission to form biradical **12d**. Either pathway is identical in terms of possible atom distributions in the methylenecyclobutane product – the only difference is the order in which the bonds are cleaved. Each pathway should give rise to eight potential label distributions that should be formed with equal probability.

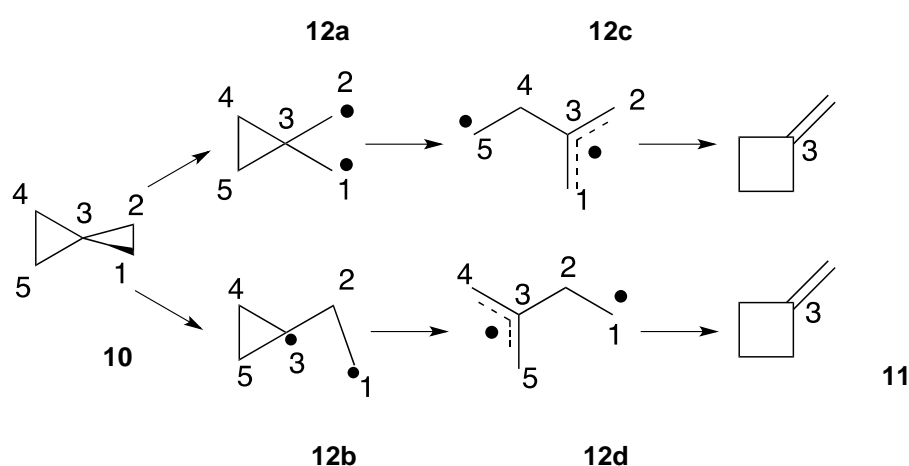


Figure 3.4: Mechanistic Pathways for the Rearrangement of SP to MCB

3.2.1 Labelling Studies

In 1968 Doering et al. added singlet CD_2 **13** to methylenecyclopropane to form SP, and then recorded the deuterium label distribution in the MCB rearrangement products **15a** - **15c**.²⁹ Their findings are summarised in Figure 3.5 below.³⁰ They determined that the label distribution was roughly as expected for a statistical model, and that in this system IVR in the excited spirocyclic molecule was deemed to be complete before any rearrangement occurred. They also noticed significant other products including 1-methyl-2-methylene cyclopropane **20** (MMCP, 41%) and ethylidene cyclopropane **21** (ECP, 17%). **10** and **11** accounted for 24% and 18% of the final products respectively, and these product ratios were found to be pressure independent.

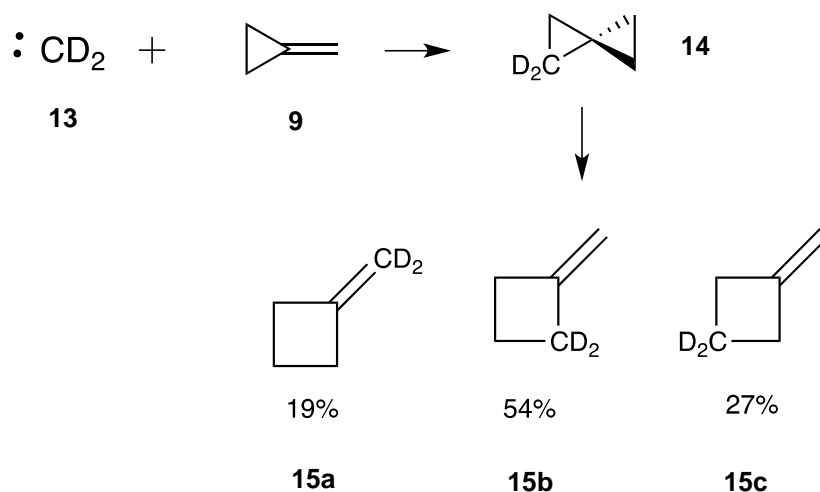


Figure 3.5: Labelling Study of SP to MCB Rearrangement

However, in 1971 Rynbrandt and Rabinovitch³¹ studied the addition of deuterated methylene to hexafluorovinylcyclopropane **16** (HVC) to form vibrationally excited hexafluorobicyclic propyl **17** (HBC) (Figure 3.6). This excited form of **17** can react further by extrusion of CF_2 from the original or nascent cyclopropane ring to give tetrafluorovinylcyclopropane **18a** or **18b** (TVC). The position of the deuterium label was varied to exist either in the original methylene or in the cyclopropane ring of **16** to investigate the magnitude of any potential isotope effects. They found the secondary isotope effects to be negligible.

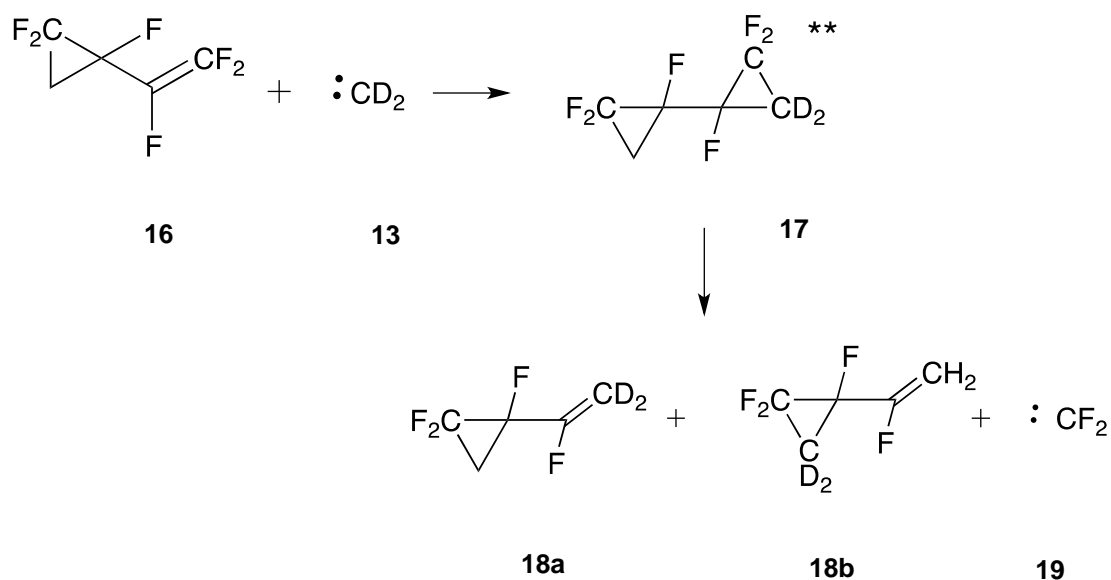


Figure 3.6: Formation and Fragmentation of HBC

They found that some HBC did decompose before IVR, with a preference for CF₂ extrusion from the newly formed ring. This varied from a ratio of between 1.2 and 1.9 depending on pressure, with the greatest nonstatistical effects evident at higher pressure (256 kPa). While it was possible that secondary isotope effects affected the results, this should also affect the rate of IVR by roughly the same order of magnitude.

3.2.2 Pressure Dependence and Product Ratios

A later study investigated the product ratios for the reaction of singlet methylene with methylenecyclopropane (Figure 3.7). They found that at low pressures (in this case 30 kPa) the major products were formed by dissociation to ethylene and allene. By raising the pressure to 40 kPa, formation of **11** was maximised. At pressures much above this, **10** became the primary product. Isoprene was also found, but in very low yields and only at pressures below 25 kPa. A summary of the findings from the Frey and Doering experiments can be found in Table 3.1.

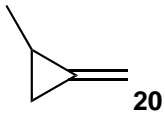
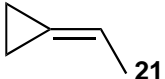
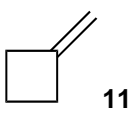
Product	Doering (30 kPa)	Frey (30 kPa)	Frey (40 kPa)	Frey (130 kPa)
 10	24	22	32	45
 12a, 12b	0	33	20	10
 20	41	20	21	21
 21	17	15	14	15
 11	18	10	12	9

Table 3.1: Product Distributions from Doering and Frey Experiments (by Percentage)

Frey detailed two distinct reaction pathways to the formation of the five products in the table. Allene, SP and MCB were hypothesised to be the result of an addition pathway, where SP would be a common intermediate to form either of the other two or where SP itself could be formed as the final product following a collisional deactivation step. In the absence of quenching, it could form either allene or MCB (in its excited state). This excited MCB could also be a route to allene (Figure 3.7). The results predict that the only route to MCB is through SP. While it was found that there were likely to be two routes to the formation of allene, the authors were unable to elucidate any details about the mechanism of that step, including whether there is a common intermediate.

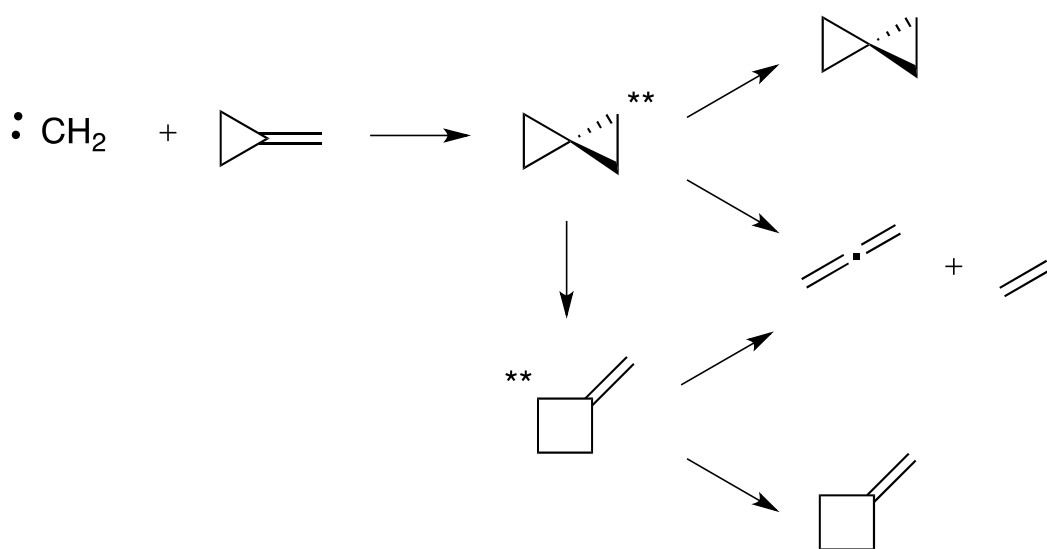


Figure 3.7: Proposed Addition Pathways

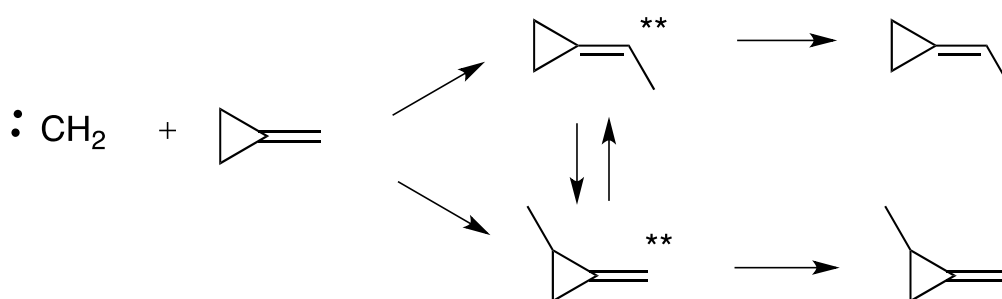


Figure 3.8: Proposed Insertion Pathways

The alternative pathway was named the insertion pathway, and gives rise to MMCP **20** and ECP **21** (Figure 3.8). Similarly, either can be formed in a vibrationally excited state and then undergo a quenching event. However, there is the potential for rapid interconversion between the two.

3.2.3 Stereomutation Pathways

Both experimental and theoretical studies have identified a number of potential stereomutations that can occur in SP.^{32,33} It can be envisaged that these stereomutations would result in different stereoisomers of SP in accordance with conrotatory, disrotatory or monorotatory pathways and it has been found experimentally that the stereomutation of Spiropentane-*cis*-1,2-d₂ occurs more quickly than isomerisation to MCB. This is summarised in Figure 3.9. Given the rearrangement mechanisms for SP to MCB outlined in Section 3.2 which involve a biradical intermediate, these stereomutations should have no effect on the product distribution of the four possible MCB isomers that can arise from SP.

A study by Johnson in 1999 used ab initio MCSCF methods (CASPT2) to explore how these stereomutations occur. Pathways **a** and **b** occur via either con- or disrotation exclusively and give rise to *cis* isomers. The *trans* isomer in route **c** can only be achieved through two monorotation steps or by a single conrotatory and single disrotatory step. The authors discovered a slight preference for the monorotation pathway.

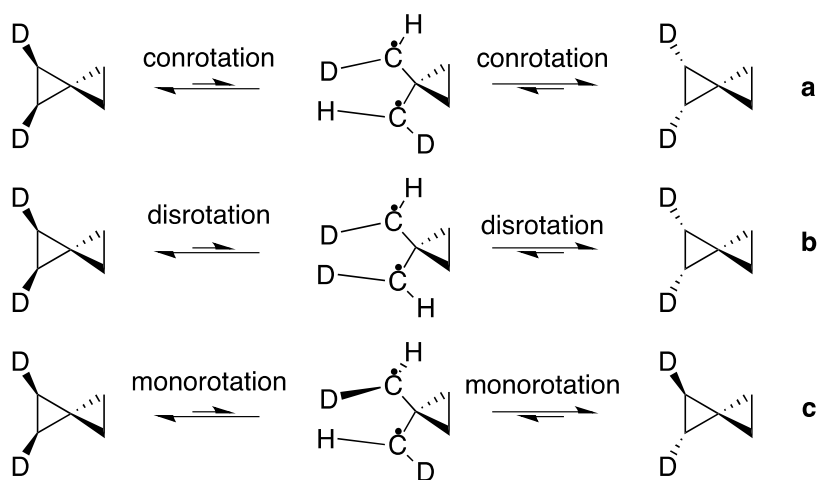


Figure 3.9: Possible Stereomutation Pathways of Spiropentane

They also noted that there was a significant difference in the energy required to break either a radial or peripheral bond in spiropentane (see Figure 3.4). They found that the

breaking of a peripheral bond required less energy than breaking a radial bond, which was attributed to the increased 2s bonding character in the radial bonds.

3.2.4 Previous Computational Studies

Most recently in 2009, Carpenter et al. compiled a PES for the rearrangement of SP to methylenecyclobutane (MCB) using a combination of high-level ab initio computational techniques (MkCCSD(T)/cc-pVTZ//CASSCF(12,12)/cc-pVDZ) and experimental data.³⁴ A summary of the connections between structures of interest can be seen at Figure 3.10. A route from SP to MCB featuring two biradical intermediates and three transition states was delineated, where the relative enthalpy values for the biradicals came from computational work and other stationary points were literature values from experiment. The enthalpies shown for the primary structures have been used as a starting point for the dynamics calculations carried out in this work.

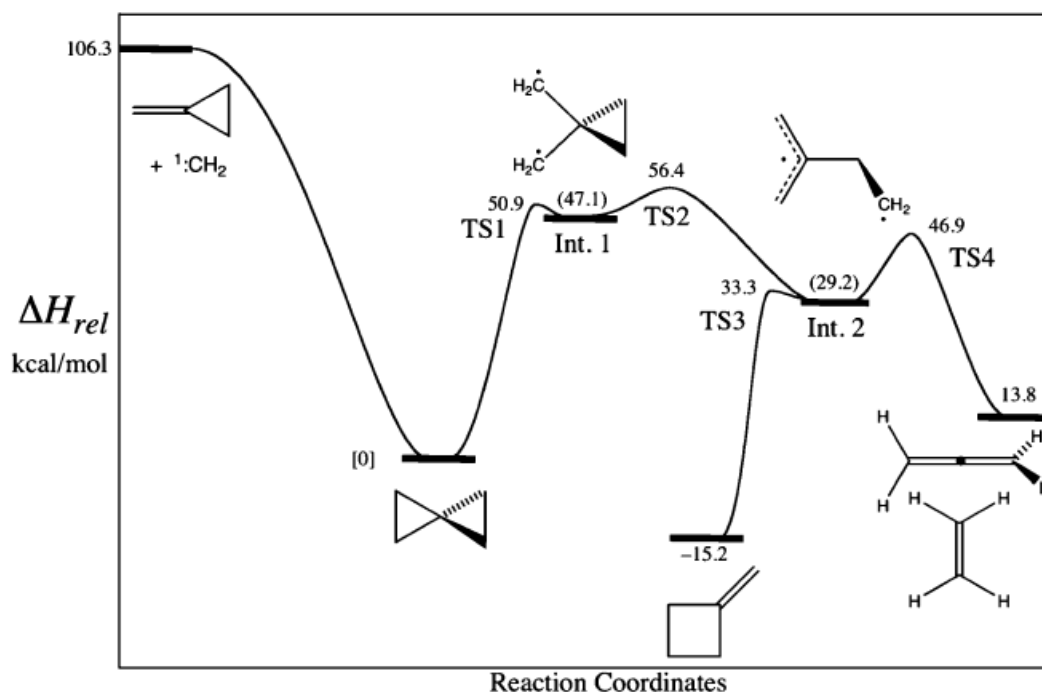


Figure 3.10: Summary of Enthalpies combined by Carpenter

3.3 DFT Benchmarking

The first step in the present study was to choose a suitable computational methodology for carrying out dynamics simulations. The use of hybrid DFT functionals was selected, as they appear to offer a reasonable pay off between accuracy and complexity. While the geometry optimisations carried out in Carpenter's study were very high-level ab initio calculations, these are not viable for a dynamics trajectory with hundreds of steps.

DFT benchmarking was carried out using the data summarised in Figure 3.10. A variety of well known and commonly used DFT hybrid functionals were selected and electronic structure calculations were carried out using each functional in an attempt to optimise the key structures in the SP to MCB rearrangement, using input geometries taken from Carpenter's paper. Exact details of the methodology can be found in Chapter 4, where sample input and output files are also present. The results of the benchmarking can be found in Table 3.2, and are summarised in Graph 3.1. The literature values are shown at the top of the table, relative to SP which was assigned an enthalpy of 0 kJmol⁻¹. A root mean square analysis was carried out to identify which functionals gave the best overall 'fit' to the experimental data.

The RMS analysis alone identified the functional B1B95 as giving the best agreement with the reference values. However, as can be seen in the graph and data table, the results for this functional were unpredictable as it resulted in a very close match with the enthalpy value for TS3, but was very different in the case of the other two transition states. While all functionals appeared to give much lower enthalpy values for all stationary points than the literature values, PBE1PBE was ultimately chosen. The results were all consistently lower than the literature values, without too much variation in the ΔE between points, giving an potential energy diagram very similar in shape to the reference. Although this was the case for a number of functionals, PBE1PBE also gave the closest match to the energy of TS2, which would be the starting point for the dynamics simulations.

Theory Level	Structure	Enthalpy	E (kJ/mol)	E Rel	Deviation	Dev. Sq.	Dev.	RMS
Lit. Values	Spiropentane		0.0	0.0				
	TS1		50.9	212.8				
	Birad1		47.1	196.9				
	TS2		56.4	235.8				
	Birad2		29.2	122.1				
	TS3		33.3	139.2				
	MCB		-15.2	-63.5				
B3LYP	Spiropentane	-194.1	-509524.1	0.0	0.0	0.0		
	TS1	-194.0	-509350.5	173.6	-39.2	1537.1		
	Birad 1							
	TS2	-194.0	-509337.7	186.4	-49.4	2439.5		
	Birad2							
	TS3	-194.0	-509424.7	99.3	-39.9	1588.7		
	MCB	-194.1	-509634.6	-110.5	-47.0	2208.8	1943.5	44.1
O3LYP	Spiropentane	-194.0	-509342.8	0.0	0.0	0.0		
	TS1	-193.9	-509154.2	188.6	-24.2	583.5		
	Birad1							
	TS2	-193.9	-509138.6	204.1	-31.6	1000.1		
	Birad2							
	TS3	-194.0	-509217.7	125.0	-14.2	200.4		
	MCB	-194.0	-509440.5	-97.8	-34.2	1172.2	739.1	27.2
PBE1PBE	Spiropentane	-193.8	-508901.6	0.0	0.0	0.0		
	TS1	-193.8	-508720.1	181.5	-31.2	976.3		
	Birad1							
	TS2	-193.8	-508694.7	206.9	-28.8	832.1		
	Birad2							
	TS3	-193.8	-508777.3	124.4	-14.8	220.1		
	MCB	-193.9	-508997.7	-96.0	-32.5	1056.2	771.2	27.8
B1B95	Spiropentane	-194.0	-509239.2	0.0	0.0	0.0		
	TS1	-193.9	-509039.7	199.5	-13.3	176.1		

	Birad1					0.0		
	TS2	-193.9	-509020.5	218.7	-17.1	290.7		
	Birad2					0.0		
	TS3	-193.9	-509102.1	137.0	-2.2	4.7		
	MCB	-194.0	-509331.6	-92.5	-29.0	838.4	327.5	18.1
mPW1PW91	Spiropentane	-194.0	-509412.6	0.0	0.0	0.0		
	TS1	-194.0	-509234.7	177.9	-34.8	1212.2		
	Birad1							
	TS2	-193.9	-509209.9	202.7	-33.0	1091.3		
	Birad2							
	TS3	-194.0	-509293.5	119.2	-20.0	400.9		
	MCB	-194.1	-509510.6	-97.9	-34.4	1183.2	971.9	31.2
B3PW91	Spiropentane	-194.0	-509353.3	0.0	0.0	0.0		
	TS1	-193.9	-509172.7	180.6	-32.1	1033.0		
	Birad1							
	TS2	-193.9	-509152.7	200.6	-35.1	1232.2		
	Birad2							
	TS3	-194.0	-509235.4	117.9	-21.3	452.2		
	MCB	-194.0	-509452.8	-99.5	-36.0	1292.9	1002.6	31.7
mPW1LYP	Spiropentane	-193.9	-509166.5	0.0	0.0	0.0		
	TS1	-193.9	-508998.3	168.3	-44.5	1977.6		
	Birad1							
	TS2	-193.9	-508982.4	184.2	-51.6	2662.0		
	Birad2							
	TS3	-193.9	-509071.3	95.3	-43.9	1929.6		
	MCB	-194.0	-509278.4	-111.8	-48.3	2333.9	2225.8	47.2
mPW1PBE	Spiropentane	-193.9	-509207.0	0.0	0.0	0.0		
	TS1	-193.9	-509028.2	178.8	-34.0	1156.5		
	Birad1							
	TS2	-193.9	-509003.0	203.9	-31.8	1012.1		
	Birad2							

	TS3	-193.9	-509086.1	120.8	-18.3	336.5		
	MCB	-194.0	-509304.3	-97.3	-33.8	1141.5	911.7	30.2
mPW3PBE	Spiropentane	-193.9	-509173.3	0.0	0.0	0.0		
	TS1	-193.9	-508991.4	181.9	-30.8	950.0		
	Birad1					0.0		
	TS2	-193.9	-508971.2	202.1	-33.6	1130.5		
	Birad2					0.0		
	TS3	-193.9	-509053.4	119.9	-19.3	372.6		
	MCB	-194.0	-509272.2	-98.9	-35.4	1252.7	926.4	30.4
BHandH	Spiropentane	-192.5	-505411.2	0.0	0.0	0.0		
	TS1	-192.4	-505219.9	191.3	-21.4	459.8		
	Birad1							
	TS2	-192.4	-505183.7	227.5	-8.2	67.7		
	Birad2							
	TS3	-192.4	-505273.3	137.9	-1.3	1.6		
	MCB	-192.5	-505504.6	-93.4	-29.8	889.2	354.6	18.8
BHandHLYP	Spiropentane	-193.9	-509158.4	0.0	0.0	0.0		
	TS1	-193.9	-508999.6	158.7	-54.0	2920.0		
	Birad1							
	TS2	-193.9	-508967.4	190.9	-44.8	2011.0		
	Birad2							
	TS3	-193.9	-509061.9	96.5	-42.7	1826.6		
	MCB	-194.0	-509266.6	-108.2	-44.7	1999.3	2189.2	46.8
B98	Spiropentane	-194.0	-509307.1	0.0	0.0	0.0		
	TS1	-193.9	-509131.1	176.0	-36.8	1352.2		
	Birad1							
	TS2	-193.9	-509119.6	187.4	-48.3	2334.3		
	Birad2							
	TS3	-193.9	-509203.7	103.4	-35.8	1280.3		
	MCB	-194.0	-509421.3	-114.2	-50.7	2571.5	1884.6	43.4
B3P86	Spiropentane	-194.8	-511350.6	0.0	0.0	0.0		

	TS1	-194.7	-511167.7	182.9	-29.9	891.6		
	Birad1							
	TS2	-194.7	-511148.9	201.6	-34.1	1163.9		
	Birad2							
	TS3	-194.7	-511232.1	118.5	-20.7	427.8		
	MCB	-194.8	-511451.5	-100.9	-37.4	1396.1	969.9	31.1
B971	Spiropentane	-194.0	-509354.9	0.0	0.0	0.0		
	TS1	-193.9	-509173.3	181.6	-31.2	972.8		
	Birad1							
	TS2	-193.9	-509161.7	193.2	-42.5	1806.6		
	Birad2							
	TS3	-194.0	-509244.2	110.7	-28.5	810.6		
	MCB	-194.0	-509466.0	-111.1	-47.6	2265.6	1463.9	38.3
B972	Spiropentane	-194.0	-509351.4	0.0	0.0	0.0		
	TS1	-193.9	-509160.2	191.2	-21.6	464.9		
	Birad1		0.0					
	TS2	-193.9	-509141.9	209.5	-26.2	687.8		
	Birad2		0.0					
	TS3	-194.0	-509225.4	126.0	-13.2	175.3		
	MCB	-194.0	-509449.2	-97.8	-34.3	1175.6	625.9	25.0

Table 3.2: DFT Benchmarking Results by RMS Analysis



Graph 3.1: Results of DFT Benchmarking

No DFT functionals used were able to optimize the geometries of the two biradical intermediates, despite a number of different methods employed to find them. In Graph 3.1, these have been set at the calculated values from Carpenter's paper for illustrative purposes. Methods to find the biradicals included fixing the distance between the two carbon atoms believed to be the radical centres, and running IRC calculations from the central transition state in each direction to try and converge at the closest minima. Almost certainly, the DFT methods chosen were unable to accurately find the biradicals due to the effects described in the introduction to Chapter 3, namely their multireference character. (see Section 2.3.5). However, carrying out molecular dynamics at a multireference level would be unrealistically time consuming and so the priority was to find a DFT functional that could best describe the starting point for the trajectories. Given that there was a wealth of experimental data that could be used to support the choice of the given functional, it was considered sufficient to use a simple DFT method in this case.

3.4 Molecular Dynamics Results

Two distinct sets of molecular dynamics simulations were carried out as part of this investigation. The first set, starting at the structure for the unimolecular transition state **TS2**, were carried out to attempt to map the SP to MCB rearrangement over a PES, and to try to link the stereochemistry in SP to the corresponding MCB products. A comparison of three DFT functionals was also carried out to see if there was a notable difference in the product ratios predicted by each.

During the course of this set of dynamics, it became apparent that a number of interesting rearrangements were occurring in SP itself, so a second set of trajectories were calculated to look at the formation of SP in its vibrationally excited state and its subsequent reactions.

3.4.1 Unimolecular Dynamics

Initially trajectories were run using Gaussian 03, beginning with the geometry of the second transition state **TS2** (the global maximum on the calculated PES) that was optimised using the PBE1PBE functional. A summary of the structures optimised using PBE1PBE is at Figure 3.11. Using random seed numbers to randomly populate vibrational energy levels based on the normal distribution, the trajectory was first run in an arbitrary direction, assigned "forward." The initial velocities assigned by Gaussian were then extracted from the dynamics output, reversed, and used to start a trajectory running in the "backward" direction. By linking the two trajectories together and labelling the composite atoms, it is possible to produce a full trajectory that passes through all the stationary points of interest.

Initial results for PBE1PBE after running approximately 200 trajectories showed that a reasonable proportion did not end with either SP or MCB. Many formed a single cyclopropane ring (CP) via radial C1-C2 bond formation (see Figure 3.12 for starting structure) and then remained at this "biradical-like" geometry with only minor fluctuations in bond length. For the remainder, no bond formation was seen. In all the cases where the MCB product was formed, it was as different structural and stereoisomers with little apparent selectivity.

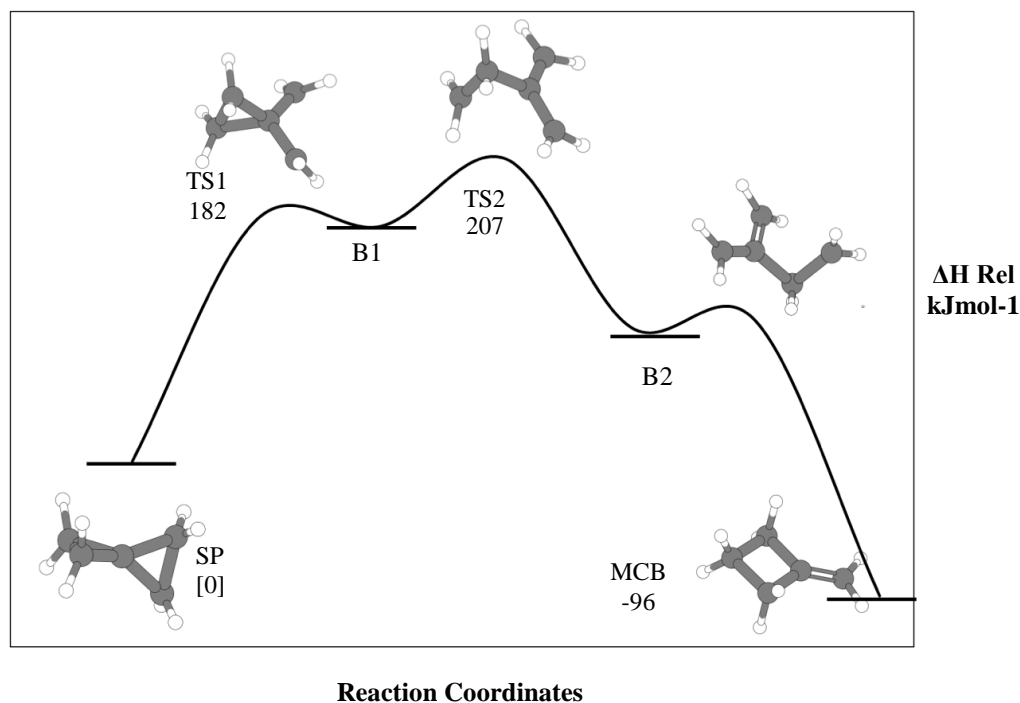


Figure 3.11: Summary of structures optimised using PBE1PBE/3-21G, with locations of B1 and B2 taken from Carpenter's paper

To test both the success rate and the stereochemical dependence of the DFT method, two more DFT hybrid functionals (B1B95 and O3LYP) were chosen to run 200 trajectories and to draw comparisons. B1B95 had the lowest RMS score in the benchmarking tests, and appeared to calculate the energy difference between SP and TS1 the most accurately. O3LYP gave the closest result to the experimental value for the relative energy of MCB. The computed structures for **TS2** by each of the three functionals can be seen in Figure 3.12 and a summary of the MD results can be seen in Table 3.3.

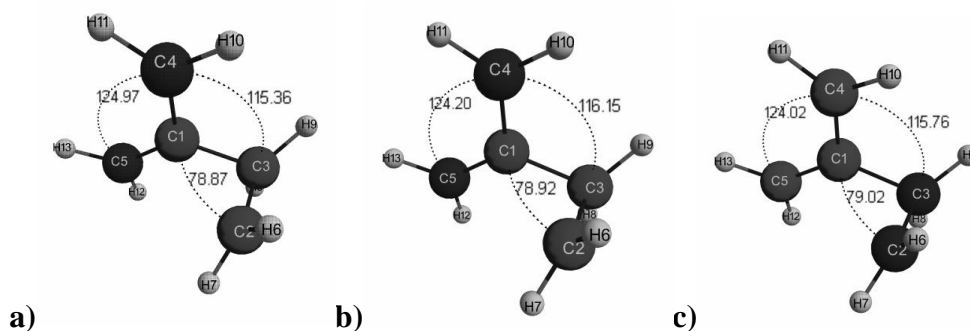


Figure 3.12:TS2 Geometries from a) B1B95 b) O3LYP and c) PBE1PBE Using the 3-21G Basis Set

The results, while potentially lacking a degree of statistical significance due to the small number of trajectories run, indicated that the preference for which species is formed could be highly functional dependent.

<u>Trajectory Outcome</u>	<u>% Occurrence</u>		
	PBE1PBE	O3LYP	B1B95
SP	29	19	15
MCB	14	21	8
Single CP Ring	11	9	25
CP ring reopens to form MCB	5	7	8
CP forms, then reopens	3	5	2
SP stereomutation	0	0	3

Table 3.3: Results of Comparative MD tests after 200 trajectories

Interestingly, the optimisations carried out using B1B95 found the smallest barrier to **B1**, with the relative enthalpy of **TS1** to SP being 38% closer to the literature value than its nearest competitor. It was also this functional that found the only occurrences of SP stereomutation within this limited data set. In all occurrences, SP was formed by initial C1-C2 radial bond formation, followed by C4-C5 peripheral bond formation. For all instances of a stereomutation, the newly formed C4-C5 peripheral bond was broken. O3LYP had mixed results, with seemingly little preference for forming either SP or MCB initially.

However, using both O3LYP and B1B95, trajectories were calculated where initial closure to CP occurred, followed by subsequent rearrangement to MCB. Where this occurred, there appeared to be a bimodal distribution of lifetimes for the biradical, with some formation of MCB occurring at 150-350fs, and some at 800-1000fs. This gave rise to stereoisomers of MCB that were not produced if MCB were the initial and only product.

Unfortunately, after closer inspection of the calculations run in Gaussian, it became apparent that there were problems relating to the conservation of energy throughout the trajectories, which renders modelling of a closed system inaccurate. While the initial conditions for the trajectories were selected from a canonical (NVT) ensemble given a specific rotational temperature (see Chapter 4 for details), MD simulations for an isolated system are microcanonical (NVE) in nature and attempt to preserve a fixed total energy at each step. Despite making various changes to how the trajectories were calculated, for example using an alternative Velocity Verlet integrator,³⁵ it was ultimately necessary to begin them again, this time using GAMESS-US.

In total, using GAMESS-US, 1500 usable trajectories were run in each direction with good conservation of energy. When the two halves of the trajectories were combined, only 200 were found to be "complete" in the sense that SP was the product in one direction and MCB in the other using reversed initial velocities. For the purposes of this discussion, the data will be grouped into three subsets: complete trajectories, "forward" trajectories which form MCB, and "reverse" trajectories that form SP. While the forward and backward data sets cannot be used to map overall stereochemistry, they can be used to look for product distributions in the two respective products.

The SP products were labelled **10a-d**. As closure of the first CP ring occurred each time with the same stereochemistry, the four isomers of SP were assigned by the relative positions of the four hydrogen atoms on the latter formed CP ring to the carbon atoms in the first ring. The MCB products were labelled **11a-d**. Their configurations were devised using the methylene carbon and the carbon opposite the methylene group as anchors.

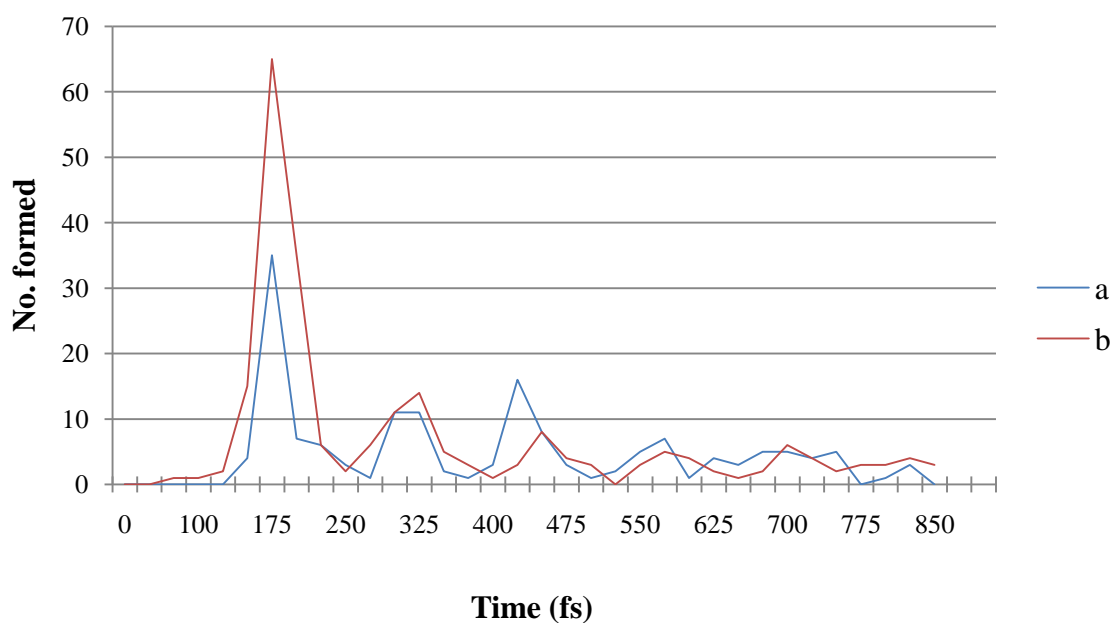
Figure 3.13 shows a summary of the MD results for complete trajectories along with the results of a parametric statistical test designed to find the uncertainties (shown in red) in the branching ratios 1-4 (shown in blue) at a 95% confidence level. The numbers shown in black are the counts for each outcome. The data shows that for each branching ratio there is a notable degree of uncertainty, but the proportion of full trajectories run to complete trajectories was low enough to make it impractical to attempt to run further simulations. Table 3.4 summarises the correlation between SP and MCB product distributions.

<u>SP Configuration</u>	<u>MCB Configuration</u>	<u>% of Trajectories</u>	<u>Ratio 11b : 11a</u>
10a	11a	18	1.8
	11b	32	
10b	11a	33	1.2
	11b	39	
10c	11a	18	1.2
	11b	22	
10d	11a	14	1.7
	11b	24	

Table 3.4: Summary of correlated product distributions

The table above indicates that from SP configurations **10a** and **10d** there is a notable degree of selectivity for the MCB product **11b**. This preference is much less pronounced in **10b** and **10c**. As we would predict, **11c** and **11d** were not formed at all from **TS2** in the complete trajectories. However, this is merely an artefact of the chosen structure for **TS2** and the C1-C3 bond, and should not be considered significant. Experimentally, **TS2** could have been formed with a C1-C2 bond instead depending on the pathway from SP to MCB (see Figure 3.4), and these results would be reversed. The formation of **11c** and **11d** would require the starting C1-C3 bond to break, which cannot happen without rearrangement via **B1**. However, they did occur in the larger data set for forward direction only and will be discussed shortly.

Overall, there is a preference for formation of **11b** over **11a**, which is perhaps predictable within an initial period of time bearing in mind the conformation of **TS2**: the C2-C4 dihedral angle of 87.4° is smaller compared with the C2-C5 dihedral of 98° in **TS2**. Using the results from the entire forward data set, Graph 3.2 shows the formation of the two isomers of MCB as a function of time. Those which form MCB most rapidly (within 175 fs) appear to do so with preference for **11b**. We then see a multimodal pattern for the formation of **11a** and **11b** as the lifetime of **B2** increases and internal rotations around C1-C3 give rise to both products in a more even distribution. The time interval between peaks in formation was found to be roughly equal to that taken for an internal bond rotation.



Graph 3.2: Formation of MCB isomers as function of time

The total number of forward trajectories in which **11a-d** were formed is 489, 14% of which were formed after initial C1-C2 radial bond closure to form a CP ring as in **B1** (see Figure 3.14 for a summary of products). The CP ring then has to reopen by breaking radial bond C1-C2 or C1-C3 and subsequent formation of MCB occurs by closure of C2 or C3 with either C4 or C5. Not only does this imply barrier recrossing over **TS2**, but it gives rise to interesting stereochemical outcomes. In the case of initial CP ring formation, isomers **11c** and **11d** are formed (see Figure 3.15). In other words, the only route to these isomers is by re-traversing the transition state. In every case, the bond that reopens is the C1-C3 bond, suggesting that the **B1** intermediate state reopens with selective excitation. It is not, however, the newly formed bond which is breaking.

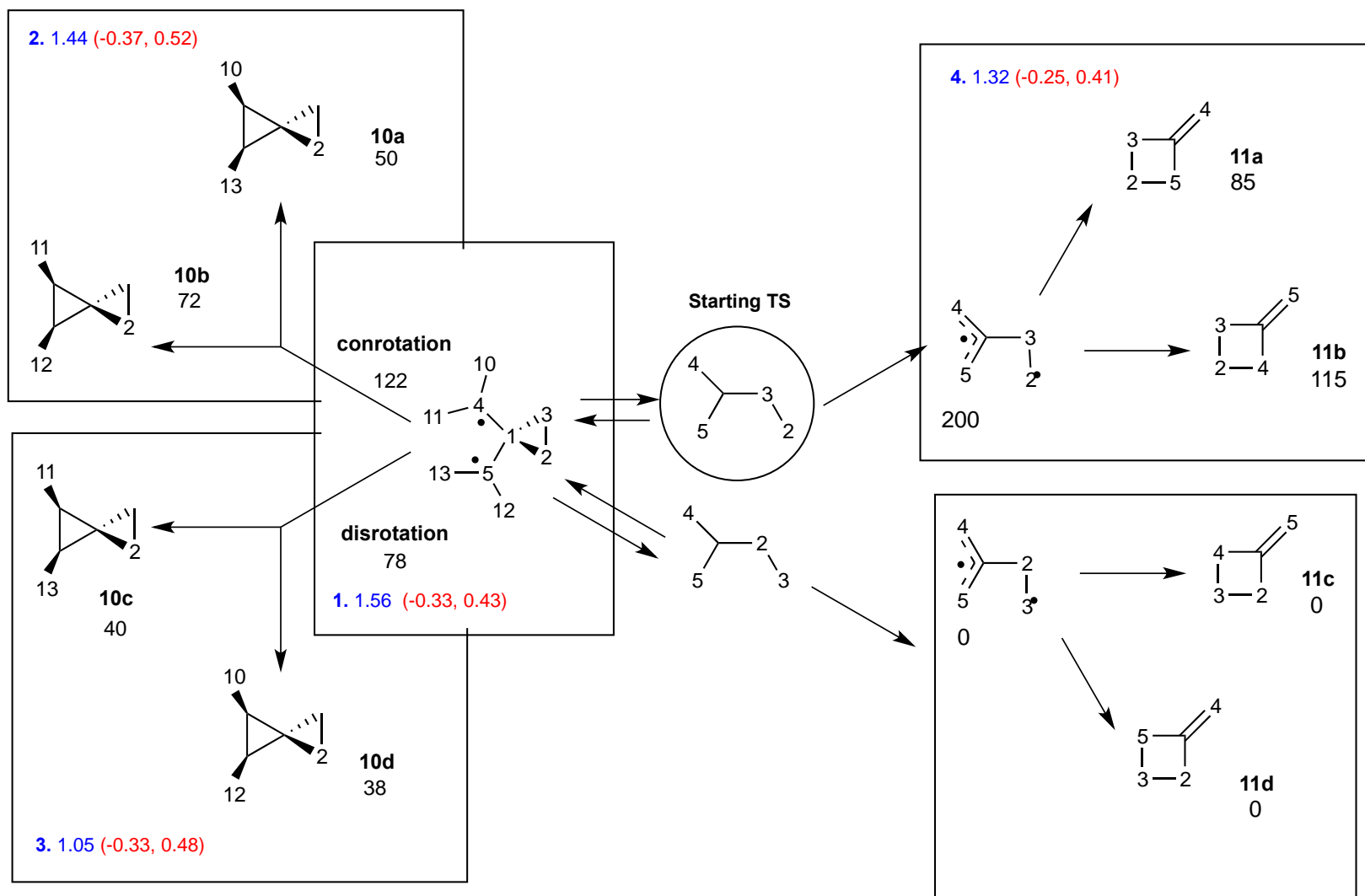


Figure 3.13: Summary of stereochemical outcomes for complete trajectories, showing branching ratios in red and the statistical uncertainties in the branching ratios in blue

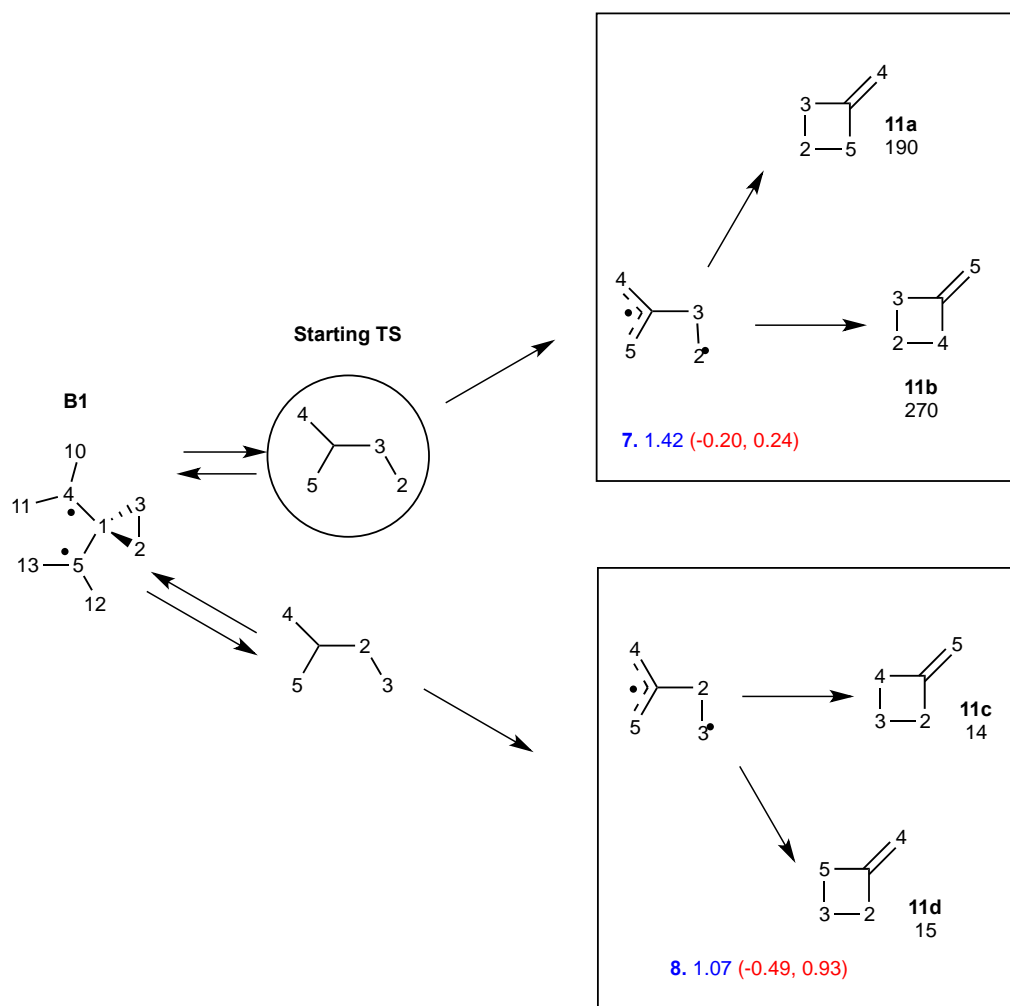


Figure 3.14: Summary of results from forward trajectories, showing branching ratios in red and the statistical uncertainties in the branching ratios in blue

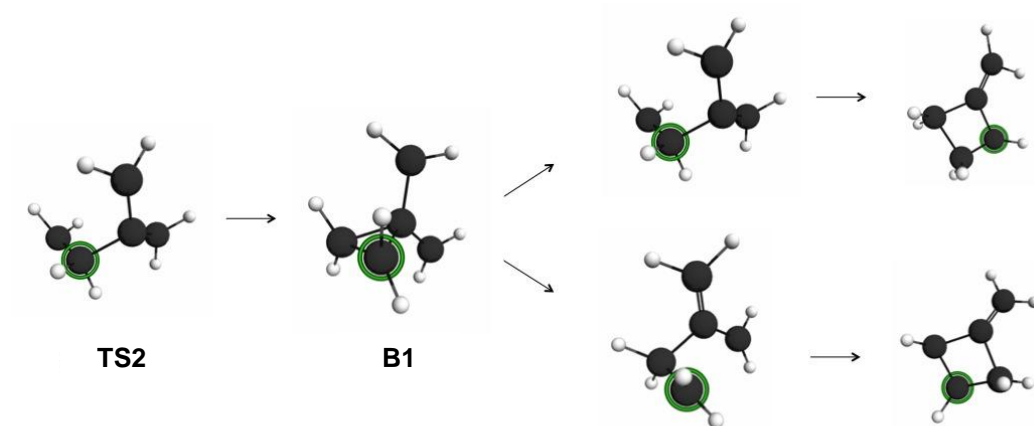
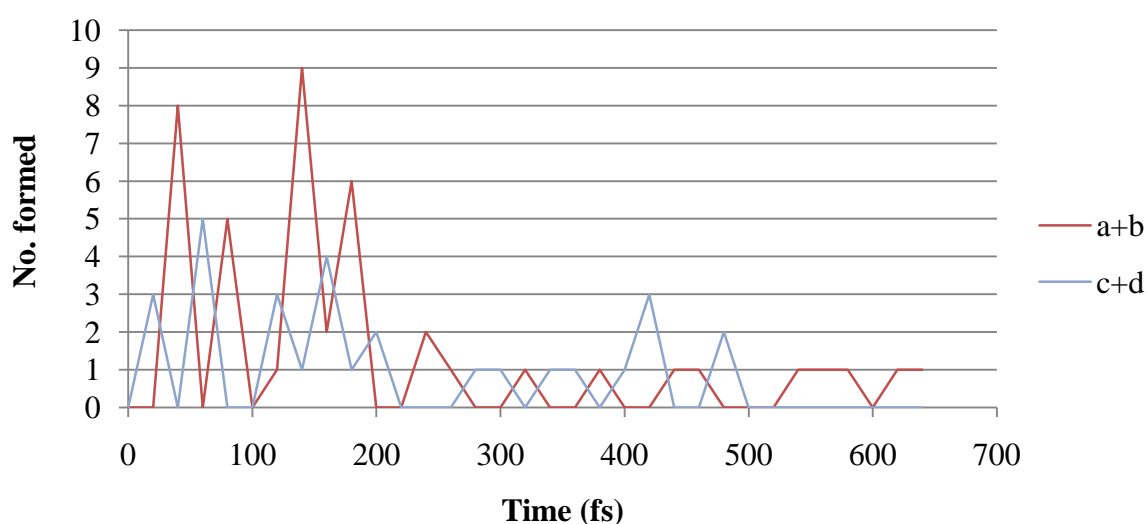


Figure 3.15: Possible rearrangement pathways via B1

A clue to the origin of this effect may lie in the previous study into the acetone radical cation, discussed in Section 1.5.2. There we saw a preference for the newly formed bond breaking within an initial time period, but that this preference shifted as the time progressed, and rapidly oscillating excitation shifted from one symmetrical bond to the other. Upon closure of **TS2** to form the biradical **B1**, the two radial bonds outside the CP ring become equivalent by virtue of symmetry. Graph 3.3 combines the incidences of **11a** with **11b** and the incidences of **11c** with **11d** as a function of the lifetime of **B1**. In other words, the graph shows incidences of C1-C2 or C1-C3 cleavage as a function of biradical lifetime.



Graph 3.3: Comparison of MCB isomers **11a/11b** and **11c/11d** as function of time

The graph indicates the possibility of an oscillation between which bond is preferentially broken, with a levelling out as time increases and IVR gives rise to a more statistical product distribution. The fact that no initial period is seen where the newly formed bond is broken is interesting, but given that the time interval between oscillations appears to be in region of only around 20 fs, this result may be an artefact of the relative rates of bond cleavage and energy transfer. However, as evidenced by roofing on the peaks this oscillation cannot be confirmed without a larger data set. What we can clearly deduce is that for a given period of time before IVR is complete in **B1** we do witness a degree of selective excitation. In this case, a levelling off appears to occur around 300 fs.

While it is noted that **TS2** is chiral, and so has an enantiomer from which we could potentially start trajectories, the effect of including this other enantiomer is believed to be trivial in this case and would most likely result in no change to the product ratios.

The reverse trajectories gave rise to all four stereoisomers of spirocyclopentane with no evidence of subsequent stereomutation. Their mechanism of formation from **B1**, i.e. disrotatory or conrotatory, is also noted. These results are summarised in Figure 3.16.

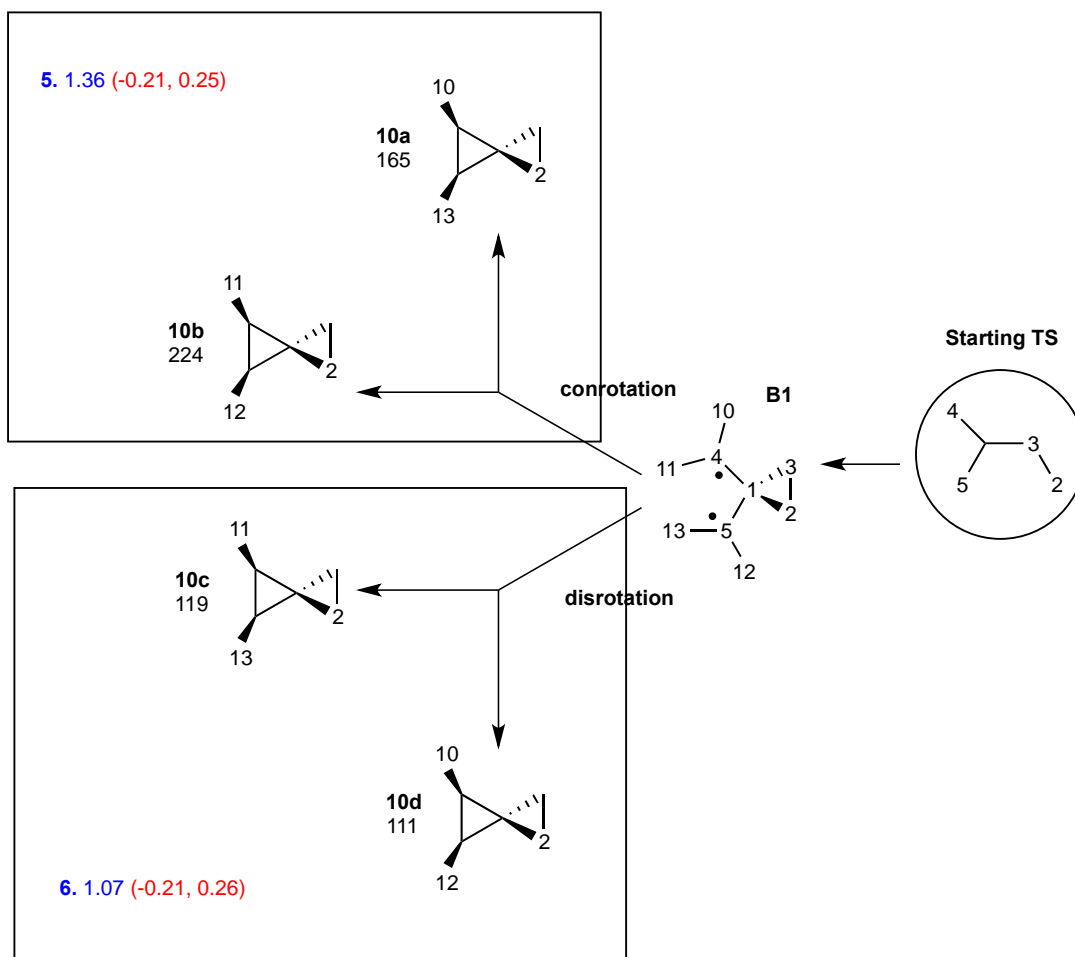


Figure 3.16 Summary of results from forward trajectories

The data suggest a clear preference for **B1** closing in a conrotatory manner to form **10a** and **10b**. However, after watching the progress of the trajectories more closely it became apparent that the conrotatory/disrotatory description is insufficient to describe the way in which SP is formed. A structure of **B1** can be envisaged where a CP ring has formed between C1-C2-C3 and the two methylenes *exo* to the ring are almost coplanar with C1 (Figure 3.17).

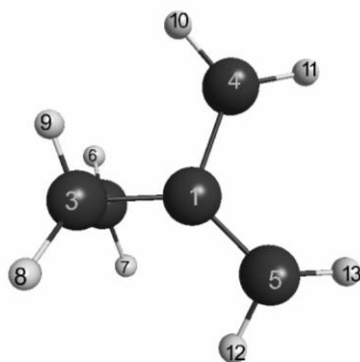


Figure 3.17: Initial structure of **B1**

This structure does appear to exist transiently immediately after ring closure (for around 10 fs) and in this state the two radial bonds to C4 and C5 should be roughly equivalent by symmetry. What is actually seen is that both of bonds rotate, but with differing frequency. In roughly 60% of the trajectories viewed, it is the C1-C5 bond that rotates more quickly, with up to six rotations before ring closure to form SP. In contrast, the C1-C4 bond rotates only once or twice in this time. In the other 40%, the C1-C4 bond rotates more rapidly and the opposite is seen. The final SP product distribution appears to be primarily a complex result of selective excitation in one of the radial bonds coupled with the lifetime of **B1** and the frequency of the two bond rotations.

However, no clear hypothesis could be formed to explain the nature of this selective excitation in a particular bond. The formation of **B1** from **TS2** occurred within a wide range of times and via numerous bond stretches and rotations, but no clear link could be made between the method of biradical formation and the resultant bond rotations, nor between the frequency and selectivity bond rotations and the final SP product distribution. What is clear, however, is that **B1** is not truly symmetrical and that a non-statistical product ratio arises as a result.

3.4.2 Bimolecular Dynamics

A second experiment was designed in which MD simulations would be used to watch the reaction progress following the reaction of singlet methylene with MCP. These dynamics started from a bimolecular transition state **TS4** as shown in Figure 3.15.

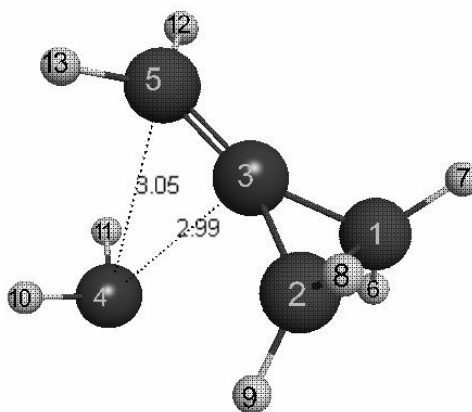


Figure 3.18: TS4, starting point for dynamics

It was envisaged that this set of dynamics might give more information about the possible stereomutations of SP. In total, 756 trajectories were run in which methylene and MCP underwent successful collision. The results of these trajectories are summarised in Table 3.5 using the same product naming convention for SP as in the previous section. (The carbon atoms are labelled differently but configuration of Hs can be treated in the same manner).

<u>Trajectory Outcome</u>	<u>% Occurrence</u>
10b	66
10b reopens via C3-C4	6
10b reopens via C3-C5	9
10b reopens via C4-C5	1
10d	1
MCB	3
cis/transstereomutation	6
cis/cis' stereomutation	5
peripheral stereomutation	3

Table 3.5: Summary of trajectory results following collision

In this case, the number of incidences of MCB formation was considered too low to draw any meaningful conclusions. However, within the limited data available the product distribution appeared to be roughly statistical. Where SP was formed, the vast majority closed with retention of the configuration from **TS4** and in 78% of cases, C4 formed a bond with C3 before C5.

There were some unexpected results from the stereomutations. Of the 14% of trajectories where a stereomutation occurred, four fifths occurred in the manner described in the Johnson study, whereby a peripheral bond breaks to form **B1** and then recloses with a different stereochemistry. The results of this show roughly equal proportions of *cis-trans* isomerisation to *cis-cis'* isomerisation. Where the *cis-trans* isomerisations occurred within around 300 fs (around 30%), there was 70 : 30 preference for monorotation : disrotation and conrotation. However, in the majority of cases the second CP ring took much longer to reclose. Upon the peripheral bond breaking, one of the *exo* bonds would undergo only one or two rotations while the other rotated several times. In almost all instances, the bond undergoing more rotations was the C3-C4 bond which the results have already showed to be the more recently formed bond in most cases. The data was examined to see if there was a link between the lifetime of the re-opened biradical and the eventual SP configuration but no correlation was found, possibly due to an insufficient number of data points.

In the other fifth of the trajectories where a stereomutation occurs, after initial formation of SP a radial bond breaks to form a structure that looks something like **12b** (Figure 3.4). While this structure is predicted en route from SP to MCB, it was not noted as one of the SP to SP mutation pathways. In the case of initial radial bond fission, then the positions of the two carbons outside of the CP can exchange relative to it, which in the dynamics gave rise to two new SP configurations. While this only occurred in 3% of cases overall, it is likely a significant enough number of the total stereomutations to result in an unexpected product distribution.

Finally, it is worth noting that a large (total 16%) number of the trajectories which initially formed **10b** then reopened by either peripheral or radial bond fission, but did not reclose to form either SP or MCB. In contrast to the results of the stereomutations, where a newly formed bond between C3 and C4 appeared to behave more 'energetically', in cases where trajectories appear to remain 'stuck' at a biradical structure

it is not either of the newly formed bonds to C4 which breaks more quickly. This is what we would expect for species which spend a long time at an intermediate structure, as we would expect IVR to complete and any preference for bond breaking to diminish.

3.5 Summary and Conclusions

Although there were energy conservation problems with a handful of the original Gaussian trajectories beginning with **TS2**, the results do imply a product dependence on the DFT functional used. While time did not permit any further investigation as part of this study, potential future work may benefit from the use of newly designed DFT hybrids such as complete-active-space DFT (CAS-DFT)³⁶ which have been designed specifically for systems with multireference character.

The unimolecular dynamics appear to go some way towards uncovering evidence of non-statistical effects. The distribution of MCB products appears to be dependent on the time of their formation, and we see this dependence tailing off as more time is spent at the biradical structure. While the structure of the transition state lends itself to a particular product, a route through **B2** should, in a traditional view, compensate for this effect as the biradical is able to undergo large conformational changes. It appears that trajectories making a rapid exit from the biradical region do so with little conformational change, supporting the presence of a plateau in this region. There is also evidence of barrier recrossing where a cyclopropane ring closes and subsequently reopens, and where we see this effect, it gives rise to configurations of MCB which would otherwise be unachievable by our chosen route into the PES. There is also evidence of selective excitation in the seemingly symmetrical bonds of **B1**, which appears to oscillate between the bonds and again give rise to a nonstatistical product distribution.

The results from the bimolecular dynamics, while limited in number, point towards a more complex pathway for the SP stereomutation than a simple mono-, dis- or conrotatory mechanism. However, where these pathways have been found, a preference for monorotation prevails which is in keeping with the literature. There is evidence that a second route to the stereomutation is also available by an alternative, non-symmetrical intermediate, and the results indicate that the product distribution here can be, in part,

determined by the fact that a more recently formed bond appears to break more frequently – perhaps evidence of selective excitation.

An important caveat regarding the MD simulations is that the statistical significance of the results is limited by their time consuming nature. In order to minimise uncertainties in the data, it would be necessary to run several times more trajectories in both cases. This is particularly true in the case of the collision dynamics, where there were insufficient data points to begin looking for time and product correlations. In part, this was due to a large amount of data loss as a result of technical issues with the cluster used to perform the calculations. However, the majority of the results are pronounced enough to go some way towards finding nonstatistical effects and would provide a solid basis for further study.

4 EXPERIMENTAL SECTION FOR CHAPTER 3

4.1 Geometry Optimisation Details

Geometry optimisations were carried out using the Gaussian03 Revision E.01.³⁷ Below are optimisation results for five stationary points on the PES relating to **10**, **11**, **TS1**, **TS2** and **TS3** which were selected from benchmarking to be the basis for MD simulation in section 3.4.1. They were calculated using the 3-21G basis set³⁸ and the unrestricted PBE1PBE DFT hybrid functional comprised of Perdew, Burke and Ernzerhof's exchange functional and a gradient-corrected correlation functional from the same group.^{39,40} For comparative MD purposes, **TS2** was also optimised using the DFT hybrids O3LYP^{41,42} and B1B95.^{43,44} Calculations for all other functionals have been omitted from this section. A sample input file and a selection of output files for optimisation can be found in Sections 4.1.1 and 4.1.2 respectively.

TS4, the starting point for the second set of dynamics results, was optimised at the PBE1PBE/6-31G* level by a QST2 calculation.⁴⁵ This type of calculation requires reactant and product geometries rather than a guess for the TS. The sample input and output files can be found at Sections 4.1.3 and 4.1.4.

4.1.1 Sample Gaussian Input - Geometry Optimization

```
%mem=1800MB
%Chk=ts2pbe1pbe.chk
%mem=1800MB
%NProcS=4
# UPBE1PBE/3-21G opt=(ts, call, noeigentest) guess=(mix,always)
```

TS between biradicals

```
0 1
C 0.361569 -0.019149 0.082799
C -1.417268 0.003699 -0.666016
C -1.021721 -0.135831 0.768971
C 0.972392 1.351150 0.010129
C 1.124234 -1.181468 -0.188230
H -1.648452 0.974484 -1.079722
H -1.613533 -0.874347 -1.261483
H -1.200786 -1.108569 1.214491
H -1.278748 0.683113 1.429464
H 0.638546 2.098452 -0.695847
H 1.881316 1.537722 0.565367
H 0.798408 -2.155122 0.153757
H 2.038170 -1.120292 -0.761429
```

4.1.2 Optimised Geometries and Energies - Section 3.3

Geometries are in the form: Atom No | Atomic No | Atom Type | X | Y | Z. Cartesian coordinates are in Ångströms and energies are in Hartrees. Corrections are in Hartrees/Particle. Frequencies are in cm^{-1} .

Spiropentane

UPBE1PBE/3-21G

1	6	0	-1.271661	-0.455366	-0.621172
2	6	0	-1.271612	0.455380	0.621187
3	6	0	0.000000	-0.000007	-0.000040
4	6	0	1.271649	0.621179	-0.455365
5	6	0	1.271625	-0.621188	0.455372
6	1	0	-1.566212	-0.007006	-1.563893
7	1	0	-1.566749	-1.489214	-0.477195
8	1	0	-1.566093	0.007023	1.563931
9	1	0	-1.566712	1.489227	0.477232
10	1	0	1.566131	1.563914	-0.006991
11	1	0	1.566787	0.477227	-1.489202
12	1	0	1.566179	-1.563894	0.006979
13	1	0	1.566663	-0.477269	1.489241

Imaginary Frequency: N/A

Sum of electronic and thermal Enthalpies: -193.830365

Zero-point correction 0.116647

Thermal correction to Enthalpy 0.122542

$\langle S^2 \rangle$ 0.0000

Transition State 1

UPBE1PBE/3-21G

1	6	0	0.000000	0.000000	0.218801
2	6	0	0.753586	0.007691	-1.123984
3	6	0	-0.753586	-0.007691	-1.123984
4	6	0	0.000000	1.232007	1.019694
5	6	0	0.000000	-1.232007	1.019694
6	1	0	1.246062	0.940434	-1.381234
7	1	0	1.276316	-0.901730	-1.393902
8	1	0	-1.246062	-0.940434	-1.381234
9	1	0	-1.276316	0.901730	-1.393902
10	1	0	0.788173	1.972997	0.923254
11	1	0	-0.723436	1.339891	1.821221
12	1	0	-0.788173	-1.972997	0.923254
13	1	0	0.723436	-1.339891	1.821221

Imaginary Frequency: 232.0555i

Sum of electronic and thermal Enthalpies: -193.761229

Zero-point correction 0.109091

Thermal correction to Enthalpy 0.115766

$\langle S^2 \rangle$ 0.8855

Transition State 2

UPBE1PBE/3-21G

1	6	0	0.386766	-0.017260	0.150105
2	6	0	-1.321058	-0.028594	-0.716146
3	6	0	-1.023042	-0.178995	0.724213
4	6	0	0.860455	1.353046	0.011613
5	6	0	1.168707	-1.138273	-0.096363
6	1	0	-1.559086	0.938143	-1.139440
7	1	0	-1.368163	-0.905416	-1.347195
8	1	0	-1.201099	-1.165854	1.148801
9	1	0	-1.338922	0.630890	1.378508
10	1	0	0.170976	2.186149	0.081996
11	1	0	1.913739	1.555058	-0.141571
12	1	0	0.812859	-2.132667	0.150138
13	1	0	2.138720	-1.045850	-0.571766

Imaginary Frequency: 933.9312i

Sum of electronic and thermal Enthalpies: -193.758487

Zero-point correction 0.108140

Thermal correction to Enthalpy 0.115067

$\langle S^2 \rangle$ 0.9225

Transition State 2

UO3LYP/3-21G

1	6	0	0.388035	-0.010539	0.148767
2	6	0	-1.324458	-0.027677	-0.720295
3	6	0	-1.032315	-0.161084	0.725116
4	6	0	0.880431	1.347700	0.006998
5	6	0	1.158663	-1.156156	-0.087345
6	1	0	-1.557176	0.934778	-1.155790
7	1	0	-1.369388	-0.909826	-1.344151
8	1	0	-1.214528	-1.140798	1.163505
9	1	0	-1.345257	0.659650	1.366923
10	1	0	0.214455	2.195283	0.115382
11	1	0	1.928924	1.531967	-0.194809
12	1	0	0.782882	-2.143571	0.155977
13	1	0	2.137955	-1.080939	-0.546485

Imaginary Frequency: 810.3412i

Sum of electronic and thermal Enthalpies: -193.920637

Zero-point correction 0.107237

Thermal correction to Enthalpy 0.114204

$\langle S^2 \rangle$ 0.8974

Transition State 2

UB1B95/3-21G

1	6	0	0.386766	-0.017260	0.150105
2	6	0	-1.321058	-0.028594	-0.716146
3	6	0	-1.023042	-0.178995	0.724213
4	6	0	0.860455	1.353046	0.011613
5	6	0	1.168707	-1.138273	-0.096363
6	1	0	-1.559086	0.938143	-1.139440
7	1	0	-1.368163	-0.905416	-1.347195
8	1	0	-1.201099	-1.165854	1.148801
9	1	0	-1.338922	0.630890	1.378508
10	1	0	0.170976	2.186149	0.081996
11	1	0	1.913739	1.555058	-0.141571
12	1	0	0.812859	-2.132667	0.150138
13	1	0	2.138720	-1.045850	-0.571766

Imaginary Frequency:	872.7795i
Sum of electronic and thermal Enthalpies:	-193.875626
Zero-point correction	0.108338
Thermal correction to Enthalpy	0.115239
$\langle S^2 \rangle$	0.8828

Transition State 3

UPBE1PBE/3-21G

1	6	0	-0.559374	0.009259	-0.180899
2	6	0	1.655698	-0.087694	0.509719
3	6	0	0.721201	-0.760930	-0.465785
4	6	0	-0.252646	1.399868	-0.144353
5	6	0	-1.721267	-0.555397	0.228581
6	1	0	2.635739	0.271259	0.211610
7	1	0	1.440545	-0.192499	1.567870
8	1	0	0.605533	-1.840040	-0.300353
9	1	0	1.051571	-0.599961	-1.499642
10	1	0	0.557935	1.789134	-0.750523
11	1	0	-0.943665	2.119666	0.287450
12	1	0	-1.855385	-1.632069	0.232359
13	1	0	-2.553934	0.053873	0.567647

Imaginary Frequency: 428.0769i

Sum of electronic and thermal Enthalpies: -193.782999

Zero-point correction 0.108140

Thermal correction to Enthalpy 0.110144

$\langle S^2 \rangle$ 0.7371

Methylenecyclobutane

UPBE1PBE/3-21G

1	6	0	-1.547930	0.000001	-0.000155
2	6	0	-0.432714	1.110217	0.000095
3	6	0	0.627587	-0.000002	0.000042
4	6	0	-0.432717	-1.110217	0.000092
5	6	0	1.951254	0.000000	-0.000070
6	1	0	-2.172881	0.000009	-0.895446
7	1	0	-2.173393	-0.000004	0.894779
8	1	0	-0.421260	1.739201	0.895987
9	1	0	-0.421099	1.739536	-0.895560
10	1	0	-0.421107	-1.739561	-0.895542
11	1	0	-0.421262	-1.739175	0.896005
12	1	0	2.519061	-0.926668	-0.000131
13	1	0	2.519060	0.926668	-0.000118

Imaginary Frequency: None

Sum of electronic and thermal Enthalpies: -193.866943

Zero-point correction 0.116300

Thermal correction to Enthalpy 0.121586

$\langle S^2 \rangle$ 0.0000

4.1.3 Sample Gaussian Input - TS4

Collision Transition State

%mem=1GB

%chk=collisionQST2.chk

%NProcS=4

UPBE1PBE/6-31G* opt=(QST2, calcall, noeigentest) guess=(mix,always)

TS for collision

0 1

C	-0.01986563	0.29828051	-0.62117201
C	-0.01981664	1.20902646	0.62118697
C	1.25179541	0.75363952	-0.00004
C	3.29667783	1.92160594	-1.45359671
C	2.52342033	0.13245851	0.45537201
H	-0.31441665	0.7466405	-1.56389296
H	-0.31495357	-0.73556745	-0.47719499
H	-0.31429756	0.76066947	1.56393099
H	-0.31491661	2.24287367	0.47723201
H	3.14814425	2.46320701	-0.26102829
H	3.98227572	1.75822449	-2.41206098
H	2.81797457	-0.81024754	0.006979
H	2.81845856	0.2763775	1.489241

0 1

C	-1.271661	-0.455366	-0.621172
C	-1.271612	0.455380	0.621187
C	0.000000	-0.000007	-0.000040
C	1.271649	0.621179	-0.455365
C	1.271625	-0.621188	0.455372
H	-1.566212	-0.007006	-1.563893
H	-1.566749	-1.489214	-0.477195
H	-1.566093	0.007023	1.563931
H	-1.566712	1.489227	0.477232
H	1.566131	1.563914	-0.006991
H	1.566787	0.477227	-1.489202
H	1.566179	-1.563894	0.006979
H	1.566663	-0.477269	1.489241

4.1.4 Optimised Geometry and Energy for TS4

UPBE1PBE/6-31G*

1	6	0	1.186634	-0.534411	-0.768762
2	6	0	1.269630	-0.452184	0.755845
3	6	0	0.396746	0.437470	-0.011194
4	6	0	-2.257058	-0.948037	0.025398
5	6	0	-0.414602	1.484785	-0.027437
6	1	0	0.673316	-1.400691	-1.180346
7	1	0	2.025837	-0.176731	-1.362712
8	1	0	2.166641	-0.035904	1.211012
9	1	0	0.816146	-1.267917	1.315504
10	1	0	-2.407124	-0.469980	1.004312
11	1	0	-2.848276	-0.447163	-0.756785
12	1	0	-0.801449	1.883211	-0.962615
13	1	0	-0.713192	1.989432	0.888528

Imaginary Frequency: 121.8518i

Sum of electronic and thermal Enthalpies: -194.742663

Zero-point correction 0.105380

Thermal correction to Enthalpy 0.113589

$\langle S^2 \rangle$ 0.6429

4.2 Molecular Dynamics Details for Section 3.4.1

Initially, Born-Oppenheimer molecular dynamics were run at the UPBE1PBE/3-21G theory level using Gaussian 03 Revision E.01. Trajectories were started from **TS2**. Initial conditions were selected using quasiclassical normal mode sampling based on a canonical ensemble, using the same method as employed in the classical trajectory program VENUS.⁴⁶ The input (rotational) temperature was 298 K. A random seed number was used to slightly perturb the initial conditions in each case and give rise to variation in trajectories - this was calculated using an internal random number generator. Due to the highly symmetrical nature of the various products, no termination criteria were used, as this would dampen the effects of stereomutation. Instead, trajectories were run for 1000 fs, considered a suitable limit for accurate results. Reverse trajectories were also begun using **TS2**, but with an additional input parameter of reversed initial velocities extracted from the forward trajectory. These were reversed by multiplying all values in the velocity matrix by -1.

DRC trajectories⁴⁷ were calculated using GAMESS-US Version 1 Oct 2010 R1.⁴⁸ Dynamics were again run for 1000 fs. Initial conditions were selected by Gaussian in the same manner as above. A collection of single step BOMD calculations with random seed numbers were calculated in Gaussian, and the initial velocities used in the GAMESS-US input files. Trajectories were also reversed in the same way as above.

Sample inputs are at Sections 4.2.1-4.2.3. Sample BOMD and DRC dynamics outputs are at Appendices A and B respectively, truncated at the end of the first step in each case.

4.2.1 Sample Gaussian Input - BOMD

Forward Trajectory

```
%NProcL=1
%NProcS=4
%Mem=1800MB
# UPBE1PBE/3-21G IOP(1/44= 7027874)
guess=(mix,always) scf=(xqc, MaxCycle=128) NoSymm
# BOMD(ReadStop ,ntraj=1, update=7, MaxPoints=1800, RTemp=298)
Spiropentane random seed 7027874

0 1
6 0 0.386766 -0.017260 0.150105
6 0 -1.321058 -0.028594 -0.716146
6 0 -1.023042 -0.178995 0.724213
6 0 0.860455 1.353046 0.011613
6 0 1.168707 -1.138273 -0.096363
1 0 -1.559086 0.938143 -1.139440
1 0 -1.368163 -0.905416 -1.347195
1 0 -1.201099 -1.165854 1.148801
1 0 -1.338922 0.630890 1.378508
1 0 0.170976 2.186149 0.081996
1 0 1.913739 1.555058 -0.141571
1 0 0.812859 -2.132667 0.150138
1 0 2.138720 -1.045850 -0.571766
0
```

Reverse Trajectory

%NProcS=4

UPBE1PBE/3-21G guess=(mix,always)

BOMD(ntraj=1, update=7, MaxPoints=1800, readMWvelocity) NoSymm

Seeds based on corrected vels

0 1

6 0 0.344969 -0.057854 0.064561

6 0 -1.367615 0.071335 -0.760209

6 0 -0.984084 -0.188354 0.758199

6 0 0.829253 1.306739 -0.039945

6 0 1.227547 -1.131032 -0.007971

1 0 -1.628497 0.889215 -1.114582

1 0 -1.596054 -0.846234 -1.350828

1 0 -1.318998 -1.205141 0.895092

1 0 -1.362345 0.613026 1.462632

1 0 0.158303 2.240053 0.439707

1 0 1.843959 1.560619 -0.180075

1 0 1.084252 -2.292105 0.248756

1 0 2.223199 -0.969371 -0.574966

0

7460043842132.00 -18645659390590.00 -10431331678830.00

-9720667203631.00 -64828590725570.00 1154163844192.00

16240246525510.00 10697454196450.00 -44869750820050.00

-33713079164240.00 -1378960674516.00 3826069631580.00

-31476330127500.00 46554052284370.00 -4682935466913.00

73993013948300.00 51308667676390.00 92036065123900.00
-3927487030861.00 -3581987940327.00 -2964633499041.00
89137830581370.00 139896274813700.00 -35565121645350.00
-8901925926018.00 -56194508201780.00 30283800790550.00
136235062155300.00 -25708621567130.00 14516479933890.00
-14664535081150.00 50631332895760.00 18204670458560.00
7572084607513.00 -57344361912370.00 20108028008680.00
-102738158239400.00 -3763601898319.00 53178270093100.00

4.2.2 Sample Gaussian Input - Initial Condition Sampling for GAMESS

%mem=1GB

%nprocs=8

%nprocl=1

#n UPBE1PBE/3-21G IOP(1/44= 6421946) guess=(mix,always) NoSymm
BOMD(ntraj=100, MaxPoints=1, RTemp=298) test

Biradical between spiropentane and methylenecyclobutane

0 1

C 0.38677 -0.01726 0.15011

C -1.32106 -0.02859 -0.71615

C -1.02304 -0.179 0.72421

C 0.86046 1.35305 0.01161

C 1.16871 -1.13827 -0.09636

H -1.55909 0.93814 -1.13944

H -1.36816 -0.90542 -1.3472

H -1.2011 -1.16585 1.1488

H -1.33892 0.63089 1.37851

H 0.17098 2.18615 0.082

H 1.91374 1.55506 -0.14157

H 0.81286 -2.13267 0.15014

H 2.13872 -1.04585 -0.57177

4.2.3 Sample GAMESS US Input - DRC

Forward Trajectory

\$CONTRL SCFTYP=UHF RUNTYP=DRC DFTTYP=PBE0 MAXIT=100 \$END

\$SYSTEM TIMLIM=9000 MWORDS=64 MEMDDI=64 \$END

\$BASIS GBASIS=N21 NGAUSS=3 \$END

\$GUESS MIX=.TRUE. \$END

\$DRC NSTEP=10000 DELTAT=0.1000 TOTIME= 0.0000

NPRTSM=10 NMANAL=.F. NVEL=.TRUE.

VEL(1)= -0.002488387 -0.002445898 -0.002241154

0.018151810 0.007781557 -0.001711298

-0.007557845 -0.005073861 -0.000235612

-0.010915384 0.011407942 0.001763922

0.008678341 0.005138657 0.010901739

-0.036180495 -0.043312993 -0.036907979

-0.061709168 -0.042818869 -0.044677763

0.151097064 0.059010316 -0.003991509

-0.069120637 -0.003908345 -0.000947233

0.078123611 -0.128847859 -0.024997013

0.022008054 -0.010756880 -0.045920856

-0.103209943 -0.070600272 0.052068945

-0.050884123 0.041100200 0.004432115

\$END

\$DATA

Spiropentane

C1

C 6.0 0.4526347 -0.0285118 0.1108249

C 6.0 -1.2943614 0.0526918 -0.7002992

C 6.0 -1.0257676 -0.1938047 0.7362450

C 6.0 0.7917109 1.3987261 0.0073953

C	6.0	1.1321697	-1.2341860	-0.0826813
H	1.0	-1.7292838	1.0270942	-1.0442086
H	1.0	-1.2377274	-0.9792471	-1.3461346
H	1.0	-1.3044675	-1.2624314	0.9035486
H	1.0	-1.1873970	0.5545061	1.3153673
H	1.0	0.0107006	2.1301465	-0.1724958
H	1.0	1.7485830	1.8047201	-0.3289327
H	1.0	0.8337904	-2.1654422	0.0965990
H	1.0	2.1944203	-1.0488051	-0.2748994

\$END

Reverse Trajectory

\$CONTRL SCFTYP=UHF RUNTYP=DRC DFTTYP=PBE0 MAXIT=100 \$END

\$SYSTEM TIMLIM=9000 MWORDS=64 MEMDDI=64 \$END

\$BASIS GBASIS=N21 NGAUSS=3 \$END

\$GUESS MIX=.TRUE. \$END

\$DRC NSTEP=10000 DELTAT=0.1000 TOTIME= 0.0000

NPRTSM=10 NMANAL=.F. NVEL=.TRUE.

VEL(1)= 0.002488387 0.002445898 0.002241154

-0.018151810 -0.007781557 0.001711298

0.007557845 0.005073861 0.000235612

0.010915384 -0.011407942 -0.001763922

-0.008678341 -0.005138657 -0.010901739

0.036180495 0.043312993 0.036907979

0.061709168 0.042818869 0.044677763

-0.151097064 -0.059010316 0.003991509

0.069120637 0.003908345 0.000947233

-0.078123611 0.128847859 0.024997013

-0.022008054 0.010756880 0.045920856

0.103209943 0.070600272 -0.052068945

0.050884123 -0.041100200 -0.004432115

\$END

\$DATA

Spiropentane

C1

C 6.0 0.4526347 -0.0285118 0.1108249

C 6.0 -1.2943614 0.0526918 -0.7002992

C 6.0 -1.0257676 -0.1938047 0.7362450

C 6.0 0.7917109 1.3987261 0.0073953

C 6.0 1.1321697 -1.2341860 -0.0826813

H	1.0	-1.7292838	1.0270942	-1.0442086
H	1.0	-1.2377274	-0.9792471	-1.3461346
H	1.0	-1.3044675	-1.2624314	0.9035486
H	1.0	-1.1873970	0.5545061	1.3153673
H	1.0	0.0107006	2.1301465	-0.1724958
H	1.0	1.7485830	1.8047201	-0.3289327
H	1.0	0.8337904	-2.1654422	0.0965990
H	1.0	2.1944203	-1.0488051	-0.2748994

\$END

4.3 Molecular Dynamics Details for Section 3.4.2

Born-Oppenheimer molecular dynamics were run at the UPBE1PBE/3-21G theory level using Gaussian 03 Revision E.01. Trajectories were started from bimolecular **TS4**. Initial conditions were selected using quasiclassical normal mode sampling based on a canonical ensemble, using the same method as employed in the classical trajectory program VENUS.⁴⁶ The input (rotational) temperature was 298 K. A random seed number was used to slightly perturb the initial conditions in each case and give rise to variation in trajectories - this was calculated using an internal random number generator. Trajectories were run for 1000 fs. A "Phase" parameter was used to specify a decreasing bond distance between two atoms, to ensure collision of the two molecules. Please see Appendix A for sample Gaussian BOMD output.

5 NONSTATISTICAL DYNAMICS IN THE THERMAL DISSOCIATION OF A DEWAR BENZENE FUNCTIONALISED PEROXIDE

5.1 Introduction to Chapter Five

The second major element of this work focuses on the attempted synthesis of a novel compound featuring a peroxide bond and a Dewar benzene moiety, which should react to generate a radical pair. The molecule has been designed with the aim of using it to compare the rate of IVR with the rate of homolytic bond fission across the O-O bond, and to look for evidence of incomplete IVR leading to an energetically non-symmetrical dissociation of the molecule.

5.1.1 Thermal Decomposition of Benzoyl Peroxide

It is known that standard benzoyl peroxide can undergo thermal decomposition via the cleavage of an O-O bond to give two benzoic radicals (Figure 5.1).⁴⁹ The activation energy for this reaction in the solid state has been determined to be $\approx 125 \text{ kJmol}^{-1}$.⁵⁰

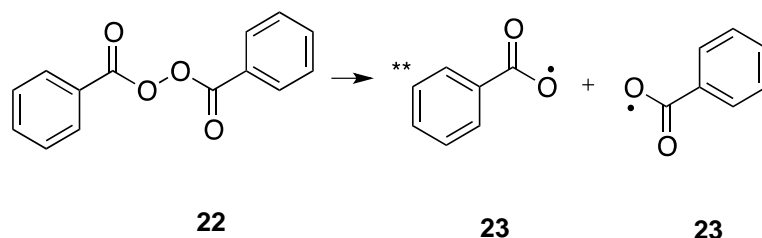
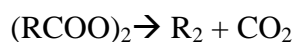


Figure 5.1: Thermal Decomposition of Benzoyl Peroxide

In 1937, Walker and Wild proposed the following general mechanisms for the decomposition of acyl peroxides:⁵¹



Equation 5.1



Equation 5.2



Equation 5.3

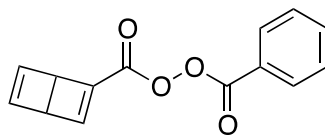
Equation 5.1 refers to the isolated molecule, whereas Equations 5.2 and 5.3 are for the reaction in solution, where R'H may be solvent, a second peroxide molecule or a minor decomposition product. By pyrolysis of acetyl peroxide in toluene at temperatures between 70 and 90 °C, they determined experimentally that a reaction of the type shown in Equation 5.2 occurred much more frequently than the type in Equation 5.3. While they noted that the solution contained a complex mixture of products which would be difficult to resolve spectroscopically, they were able to reach this conclusion by measuring the evolution of gaseous by-products and a much larger proportion of methane (RH) was found than ethane (R'R).

In 1940, Brown conducted a study into the decomposition of benzoyl peroxide in benzene which was heated thermostatically to 80 °C. Periodically, samples of the reaction mixture were extracted, rapidly cooled to room temperature, and titrated against iodine solution to test for peroxide content. He found that the primary products of the reaction were carbon dioxide, biphenyl and benzoic acid. Brown noted that the rate of pyrolysis changed over time, such that the initial rate remained reasonably low for around 15 minutes, then rose to a maximum after around 2 hours. Following this, there was a steady decrease in rate to a constant. He attributed these effects to two reaction 'phases.' The initial phase and steady rate increase could be explained by a unimolecular decomposition of the benzoyl peroxide to two benzoic radicals. The second phase would involve parallel first and second order reactions: a rate peak relating to the first order decomposition of the benzoic radical to carbon dioxide and phenyl radicals, and then a second order reaction of the benzoic radical as an oxidant to form benzoate ions. The levelling off of reaction rate would occur when both the first and second order reactions were occurring simultaneously.

5.1.2 The Reactivity of Dewar Benzene

The modified benzoyl peroxide **24** seen in Figure 5.2 was designed specifically for this work. It contains a highly strained, antiaromatic Dewar benzene ring, which is known to rearrange as an isolated species to the standard isomer of benzene in a highly exothermic reaction ($\Delta H \approx -250 \text{ kJ mol}^{-1}$)⁵²⁵³. An isolated molecule of Dewar benzene is

known to have a half-life of around 2 days at room temperature, and the activation enthalpy for its rearrangement has been determined to be around 96 kJmol^{-1} .^{54,55}



24

Figure 5.2: A Functional Group Isomer of Benzoyl Peroxide

A 2008 study by Robello and co-workers⁵² looked into the thermal isomerisation of Dewar benzene derivatives, at various temperatures and in non-polar solvents (toluene and *o*-xylene). Previous work had already determined the half-life of hexamethyldewarbenzene to be over 1000 years at room temperature, indicating that Dewar benzene is stabilised by the addition of electron donating groups (EDGs).⁵⁶ They compared lifetimes and activation energies for a number of Dewar benzene derivatives; selected results are summarised in Table 5.1.

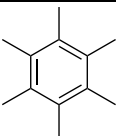
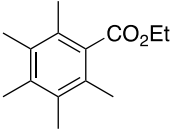
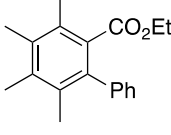
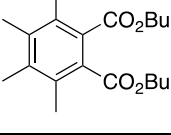
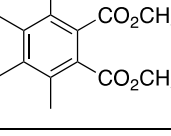
Product	E_a (kJ mol ⁻¹)	Temp range (°C)	Half life in years (at 20 °C)
 a	37.2	21	>1000
 b	25.6	90-110	70
 c	23.0	100-130	47
 d	25.1	90-110	2.9
 e	24.0	50-110	1.4

Table 5.1: Summary of Half-Lives for Dewar Benzene Derivatives

The results of Robello's study appear to support the hypothesis that the addition of electron withdrawing groups (EWGs) destabilises Dewar benzene derivatives, and that the addition of electron donating groups can counteract this effect.

The combination of the Dewar benzene and the peroxide bond in a single molecule should enable interesting conclusions to be drawn about the relative rates of IVR and pyrolysis. It is predicted that similarly to standard benzoyl peroxide, the modified benzoyl peroxide **24** will pyrolyse via homolytic bond fission at the peroxide bond, and that this will occur somewhat more slowly than the isomerisation of Dewar benzene to standard benzene. Depending on the relative rates of homolysis and IVR, it is possible that one of the benzoic radicals will be higher in energy than the other, in this case **23***, having formed from the 'end' of the molecule which was previously Dewar benzene. This can be seen in the reaction scheme below (Figure 5.3). Note that species predicted to be formed with selective vibrational excitation are denoted with a "*". Given the required activation energy for the decomposition of benzoyl peroxide, it is likely that the release of energy from the benzene isomerization will be enough to cause pyrolysis of the peroxide.

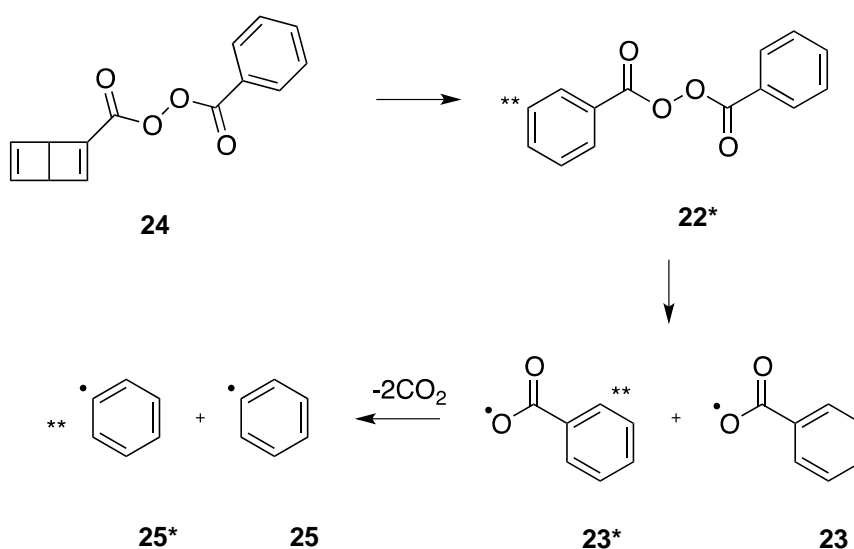


Figure 5.3: Proposed Thermal Decomposition of Dewar Benzene Functionalised Peroxide

If synthesis of **24** under mild conditions is possible, then controlled thermal decomposition should yield information about energy distribution between any resulting benzoic radicals. It is also possible that CO₂ cleavage from **23** and **23*** could occur, to form a phenyl radical. The rate of decarboxylation should be proportionately higher for higher energy radicals, and so in this case **23*** would be expected to undergo more rapid decarboxylation, leading to a greater concentration of **25*** being formed than **25**. By selectively labelling one of the benzene rings and detecting the proportion of labelled to unlabelled phenyl radicals, it should be possible to ascertain whether one benzoic radical is significantly higher in energy than the other. The product ratio can be followed by ¹³C labelling of one end of the molecule and using NMR to investigate the mixture of products when the reaction is carried out in an aromatic solvent (Figure 5.4).

No literature data has been found to support any change in the rate of Dewar benzene isomerisation when labelled with ¹³C. The only step in the reaction in Figure 5.4 that could potentially be affected by isotope effects to any notable degree is the decomposition of **28** to **29**, but with a nominal mass change from ¹²C to ¹³C these would be minimal. Furthermore, we would expect that the labelling would dampen rather than falsely exaggerate any results.

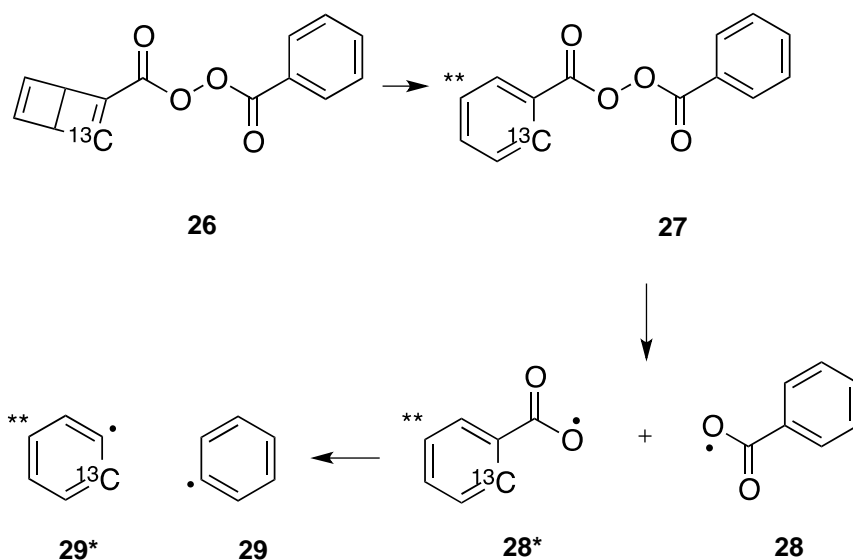


Figure 5.4: Proposed Labelling Study to Determine Rate of Decarboxylation

5.2 Synthetic Work

The synthesis of **24** was attempted in two main stages. As the peroxide coupling would be the final stage in the process, it was necessary first to attempt to make the Dewar benzene, and separately to investigate ways in which to form the peroxide bond under suitably mild conditions that would not cause isomerisation of the Dewar benzene.

5.2.1 Dewar Benzene Synthesis

The most widely published means of preparing a Dewar benzene appears to be via the [4 + 2] cycloaddition of cyclobutadiene to an alkyne.⁵⁷ The initial proposed synthetic route to **24** is shown in Figure 5.5.

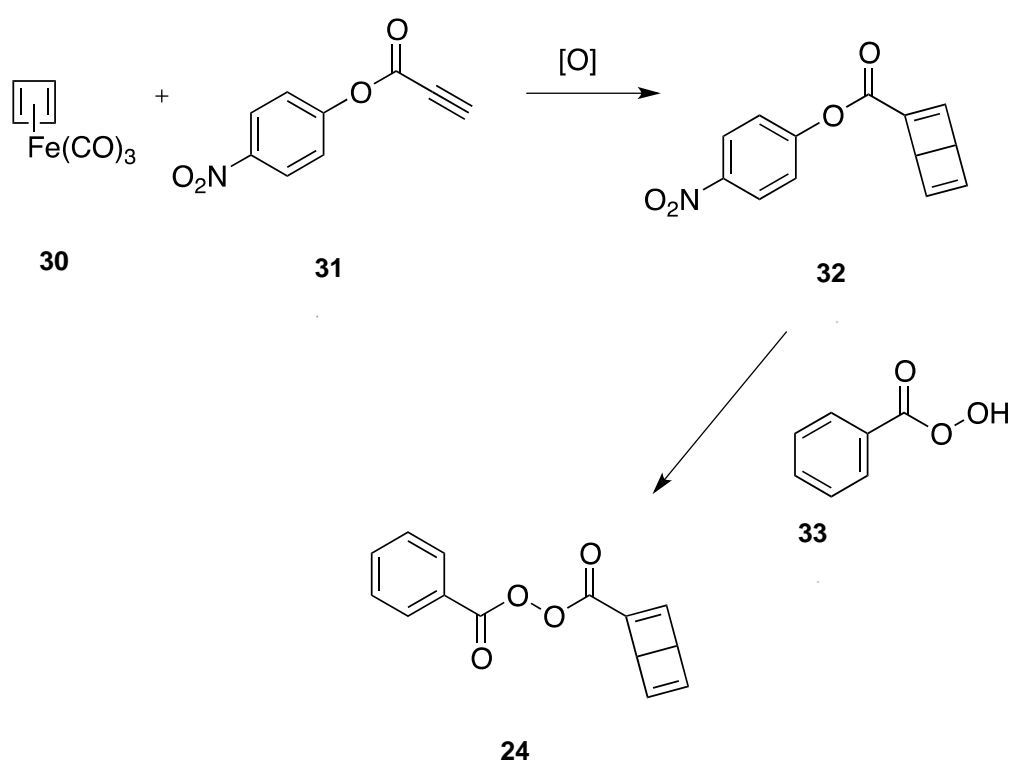


Figure 5.5: Proposed Synthesis of **24**

The first step in the synthesis was the formation of a cyclobutadieneiron tricarbonyl complex **30** from cis-1,2-dichlorocyclobutene **31** and diiron nonacarbonyl (Figure 5.6). Cyclobutadiene is known to undergo rapid dimerization to form a mixture of bi- and tricyclic products so requires careful procedures with controlled liberation rates.⁵⁸ This was prepared successfully using a literature procedure.⁵⁹

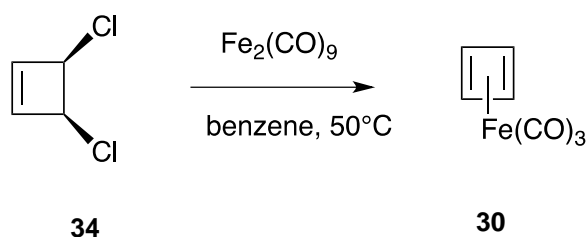


Figure 5.6: Synthesis of cyclobutadieneiron tricarbonyl **30**

Oxidation of **30** liberates cyclobutadiene, which can be trapped by a suitably activated alkyne to form a Dewar benzene.⁶⁰ As described above, the lifetime of Dewar benzenes is greatly shortened by the addition of EWGs. However, for the cycloaddition of cyclobutadiene to an alkyne to be achieved, an EW substituent on the alkyne would be highly favourable. It was also necessary to functionalise the Dewar benzene with a labile leaving group, in order for the eventual coupling of the Dewar benzene with perbenzoic acid **33**. For the purposes of functionalising the Dewar benzene for further synthesis, a *p*-nitrophenol group (PNP) was first added to propiolic acid to give alkyne ester **31** (Figure 5.7).

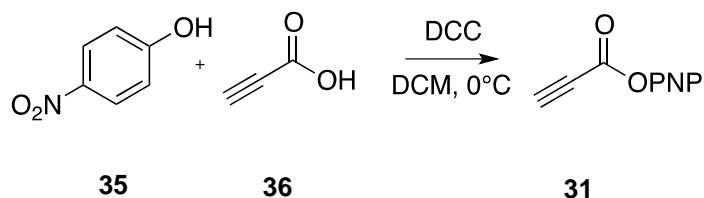


Figure 5.7: First Preparation of Alkyne Trapping Agent

Attempts to liberate cyclobutadiene using ceric ammonium nitrate (CAN) at -78°C and trap with alkyne **31** as per the literature procedure were unsuccessful, despite exhaustive testing of a number of altered conditions. It was initially predicted that the most likely cause of reaction failure was the dimerization of cyclobutadiene. To test whether liberation of this was possible at the given temperature and under a nitrogen atmosphere, a test reaction was conducted using diethylazodicarboxylate **37** as a trapping agent and freshly recrystallized lead tetraacetate as the oxidant (Figure 5.8).

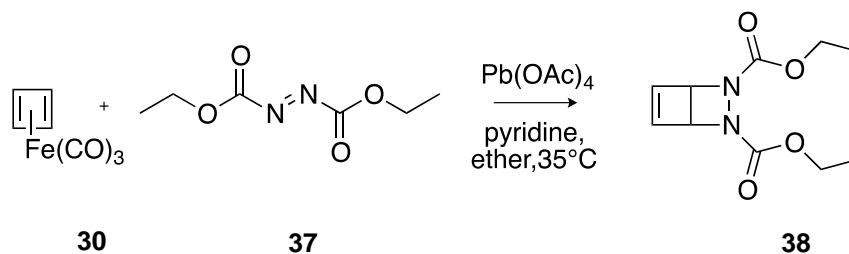


Figure 5.8: Successful Trapping of Cyclobutadiene using **37**

This reaction was conducted successfully, with **38** being formed in a moderate yield. Based on this, it appeared that the most likely cause for the failure of trapping with **31** was either unsuitability of CAN as an oxidant or the substituents on the trapping agent.

A number of different oxidising agents were trialled alongside trapping agent **31** including lead tetraacetate and trimethylamine N-oxide (TMAO), both of which did not yield the desired Dewar benzene. A range of solvents and temperatures were also used. To ensure there was no oxidation of the trapping agent occurring before the liberation of cyclobutadiene, **31** was stirred with each oxidising agent for around an hour, and the resulting mixture analysed by NMR. In all cases, the alkyne was unaffected by the oxidant.

The next step involved the testing of alternative alkynes with different substituents. Given the importance of symmetry in the final peroxide molecule to the results of the study, it was noted that it would be necessary to make an equivalent substitution within the Dewar benzene molecule. A literature procedure was found which used CAN as an oxidant at -78°C to liberate cyclobutadiene from **30**, followed by warming to 0°C to facilitate cycloaddition to dimethyl butynedioate **39** (Figure 5.9).⁶¹

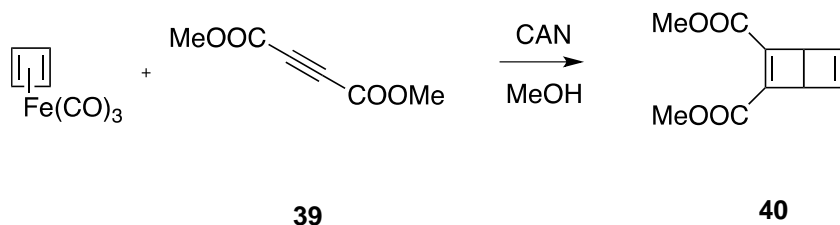


Figure 5.9: Successful Trapping of Cyclobutadiene using **39**

Given that **40** was prepared with two EWGs on the alkyne, an NMR study was conducted to test the rate of decomposition of the Dewar benzene over time. Any Dewar benzene synthesised would need to be reasonably stable for a period of time to allow subsequent reaction steps. The samples were stored at 0 °C and a series of ^1H NMR spectra taken over the course of 84 hours (Figure 5.10)

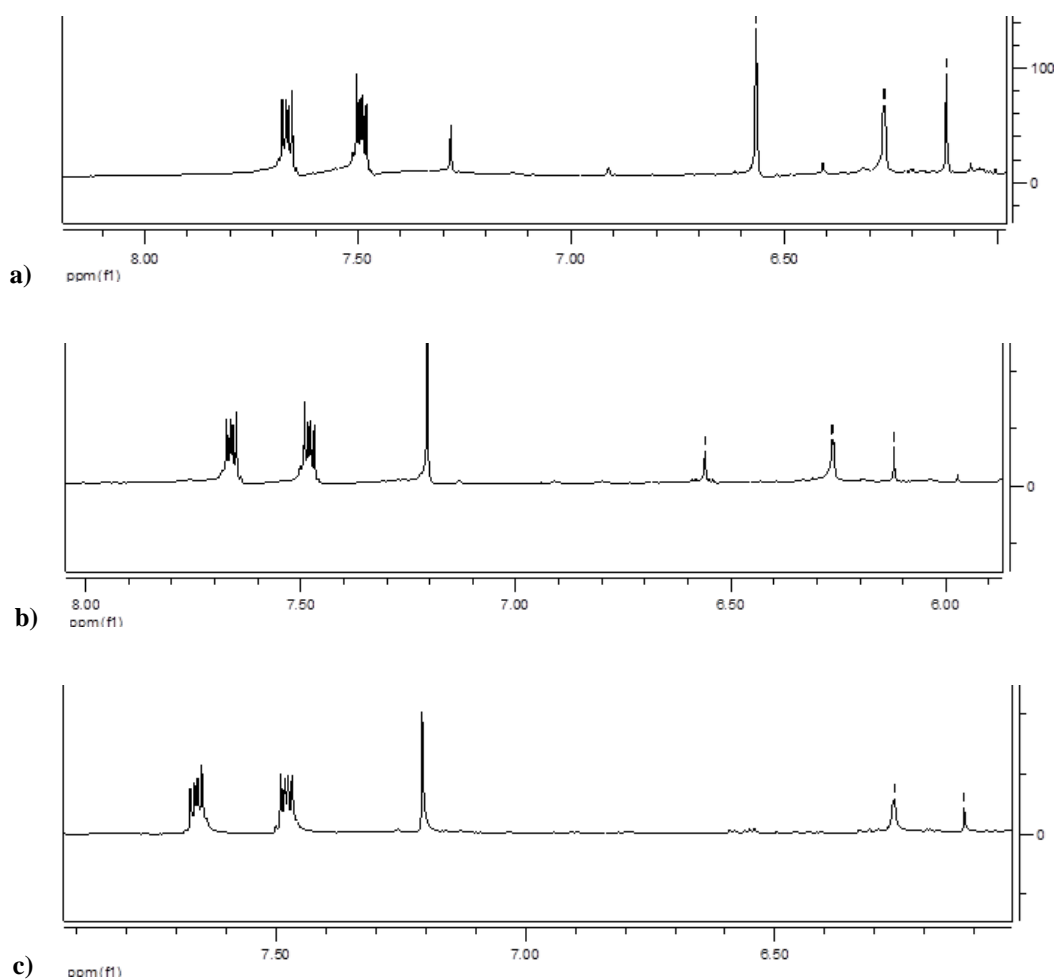


Figure 5.10: NMR spectra of **40** taken at a) 12hrs, b) 36hrs and c)84hrs

The NMRs show a gradual attenuation in the signal at 6.6 ppm, which is the signal relating to the bridging hydrogens of **40**. The signal appears to disappear completely after a period of around 84 hours. The reaction procedure for the synthesis of **40** was modified so that the entire process including work up and concentration occurred at around at 0 °C and the initial yield of product appeared to be greatly improved, with

little isomerisation occurring before characterisation. However, attempts to purify **40** via column chromatograph as per the literature procedure were entirely unsuccessful.

Unfortunately, because of the symmetrical nature of alkyne **39**, the cycloaddition product would have little use moving forwards through the synthesis. The final stage involving formation of the peroxide bond would require the Dewar benzene to be unsymmetrically substituted. However, with optimised reaction conditions, the next stage of the synthesis was to synthesise a suitably activated, unsymmetrical alkyne that would be a useful precursor for the formation of the peroxide but that would also have the right electronic properties to undergo a cycloaddition with cyclobutadiene.

As an ideal candidate for the cycloaddition, some effort was focused on the mono-esterification of acetylenedicarboxylic acid (Figure 5.11) to form **42**, which is both unsymmetrical and should readily undergo cycloaddition. There is literature precedent for conducting this reaction using a phase transfer catalyst (PTC), tetra-*n*-butylammonium bromide (TBAB) under basic conditions.⁵⁵ The selectivity of this reaction is thought to stem from the complexation of the PTC in solution with a singly deprotonated species, thus sterically hindering the removal of the second proton. The PTC serves to enable the deprotonated, ionic species to pass into the organic phase of the reaction where methylation (by addition of methyl iodide) occurs. However, in this instance the method was unsuccessful. This may be due to the length of the carbon chain, which the authors of the literature procedure cited as a one of the main factors affecting yield. Longer carbon chains were able to form ‘cyclic’ structures which were more efficiently complexed with the PTC.

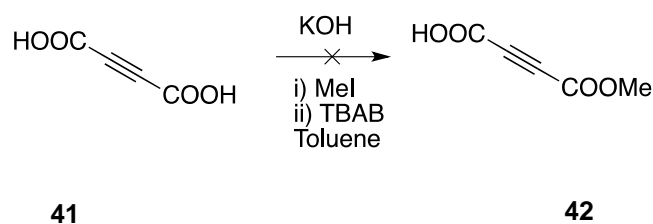


Figure 5.11: Attempted monoesterification of acetylenedicarboxylic acid using a PTC

Monoesterification was also attempted using mild coupling agents such as *N,N'*-dicyclohexylcarbodiimide (DCC) in single equivalents via dropwise addition, but this was also unsuccessful.

An alternative route to **42** was identified (Figure 5.12) involving lithiation to remove the alkynic proton and subsequent addition of CO₂. A literature procedure exists for the analogous reaction, using ethyl propiolate as a reactant rather than methyl propiolate, **43**.⁶² The procedure involves deprotonation of ethyl propiolate followed by the addition of CO₂ gas, but the methyl equivalent was chosen here as it is slightly less electron donating and so should form an easier substrate for the cycloaddition. The original procedure used dry ice as a CO₂ source, which was kept in a separate reaction vessel and allowed to sublime, then introduced to the reaction vessel via syringe. This was unsuccessful, as was following the literature procedure using the ethyl ester. There was the possibility that moisture was being introduced into the reaction vessel using this method, so it was modified to use CO₂ gas directly from a cylinder using a pressure regulator and drying tube. This gas was bubbled directly into the solution using a long needle, but also proved unsuccessful. Finally, a third method of adding dry ice powder directly into the reaction vessel was tested, to see if the gradual temperature rise from -78 °C to 0 °C as it dissolved would aid reaction and reduce decarboxylation. Despite focused attempts, no methods to add CO₂ gave rise to the desired product.

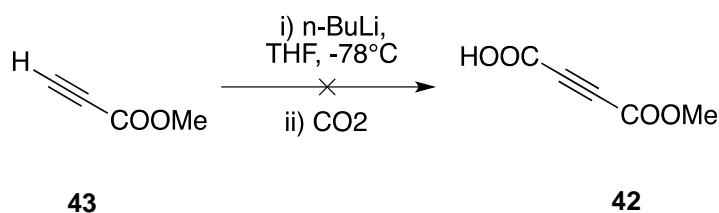


Figure 5.12: Alternative route to monomethyl ester from methyl propiolate

A tetrahydropyranprotected alkyne was also tested to see if the lithiation could be successful. While a D₂O shake and subsequent GC/MS analysis indicated that all the lithiations were a success, addition of CO₂ proved difficult once again. It is believed that this may be due to a relatively high rate of the competing decarboxylation reaction, particularly during the work-up phase of the reaction. However, no insight has been gained into why the literature procedure was irreproducible in this case.

5.2.2 Formation of the Peroxide Bond

Work has also been done on forming the peroxide bond between any Dewar benzene formed and a peroxybenzoic acid derivative. In the absence of any suitable Dewar benzene, a successful coupling was attempted between mCPBA and benzoyl chloride (Figure 5.13).

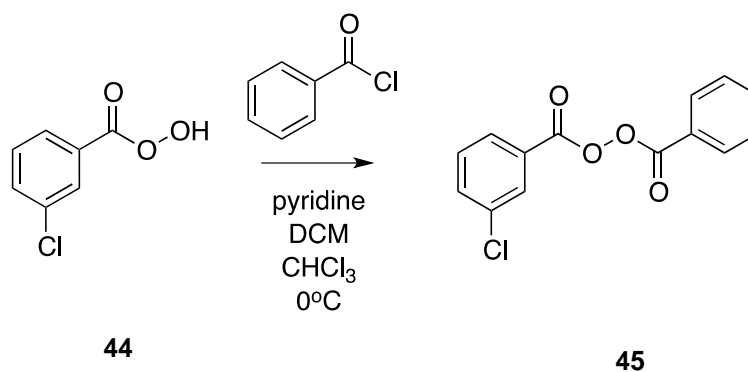


Figure 5.13: Coupling of mCPBA and benzoyl chloride

In order for the nonstatistical effects to be tested accurately, any substituents on the Dewar benzene would also have to be present and symmetrical on the benzene ring in the other half of the molecule. To this end, tests were carried out to ensure that symmetrically substituted peroxybenzoic acids could be made. An example synthesis is shown in Figure 5.14.

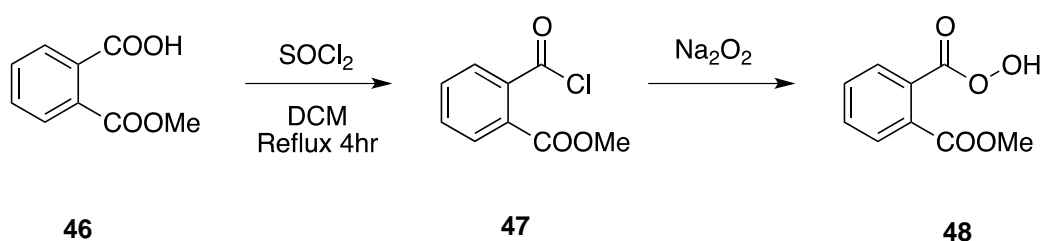


Figure 5.14: Peroxybenzoic acid synthesis

As it appears necessary to use EWGs to facilitate the trapping of cyclobutadiene, the reduced lifetime of the Dewar benzene means that it would be reasonable to attempt the trapping as the final step in the overall synthesis. Therefore, peroxide couplings with

alkynes were also attempted. Anhydride **50** was synthesised from 2-butynoic acid **49** and successfully coupled with mCPBA to give peroxide **51**.

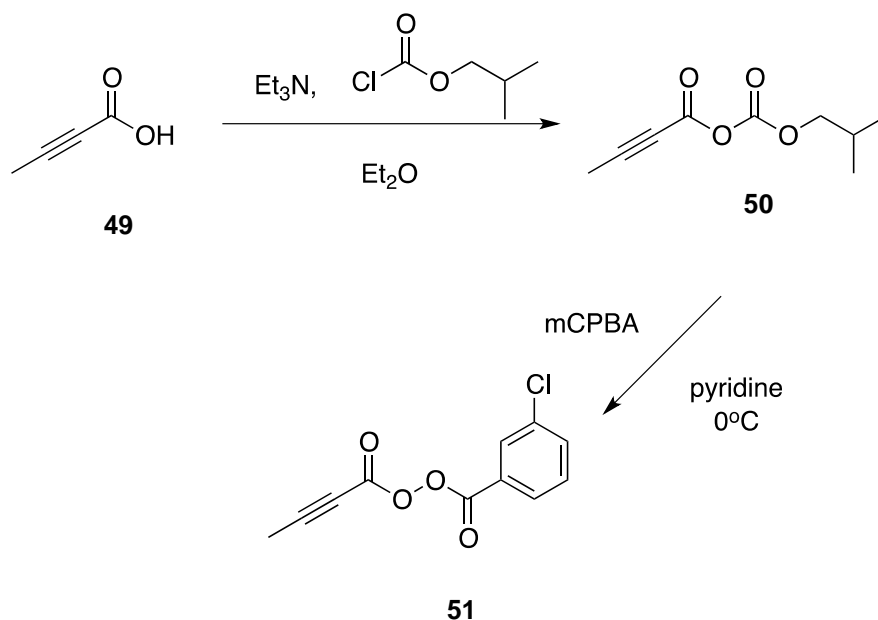


Figure 5.15. Anhydride synthesis

5.3 Summary and Conclusions

A new system was designed to investigate the relative rates of IVR and thermal bond dissociation in a peroxide containing Dewar benzene. Unfortunately the synthetic work was largely unsuccessful and so the work in this chapter did not give rise to any studies on nonstatistical dynamics.

If the synthesis of peroxide **24** were completed at a later date, the next step would be to incorporate a ^{13}C label as shown in Figure 5.4. A suitable solvent would need to be chosen for the pyrolysis that would act as a ‘trapping’ agent for any resulting benzoic or phenyl radicals. Standard techniques such as ^{13}C NMR spectroscopy and high-resolution mass spectrometry could reasonably be used to determine the ratio of labelled to non-labelled trapping products. For a reaction displaying incomplete IVR, the ratio of products containing a label within a certain timeframe would be predicted to be higher, given the residual excess energy in that ‘end’ of the molecule. Doubly labelled biphenyl is a potential major product.

6 EXPERIMENTAL SECTION FOR CHAPTER 5

6.1 General Experimental Procedures

Many of the compounds described in this work were air and/or moisture sensitive and all reaction vessels were carried out in oven dried glassware which was also dried under reduced pressure with a heat gun immediately prior to use and cooled under inert gas.

With the exception of the carboxylation reactions, which were partially carried out under an atmosphere of carbon dioxide gas, all reactions were performed under a nitrogen atmosphere, and air sensitive reactants were introduced through suba seals via a syringe and needle. Where required, solvents were degassed on a Schlenk line using the freeze-pump-thaw method. Dry solvents were purchased from Aldrich or Acros, with the exception of DCM which was drawn from an MBraun SPS-800 solvent purification system.

All reactions were performed using magnetic stirring apparatus and after reaction work-up were concentrated using a rotary evaporator at automatically selected pressure.

Compounds **33**, **45**, **48** and **51** or their by-products/reactants are potentially explosive or pyrophoric and were all prepared using a blast shield and concentrated in a rotary evaporator inside a fume hood. They were not left to become completely dry, and as such yields are crude only. As these were only test reactions with potentially dangerous by-products, attempts were not made to purify them beyond that needed for basic characterisation. All peroxides were assayed by iodometric titration for confirmation.

6.2 Instrumentation

^1H and ^{13}C NMR spectra were obtained from a Bruker DPX400 or DPX 500 spectrometer. All J values are in Hz and δ values are reported in ppm downfield from TMS.

Infrared spectra were obtained using a Perkin-Elmer 1600 series IR or Smiths Detection Identify IR. Samples were prepared as thin films on sodium chloride plates using either nujol or DCM, with the exception of compound **30** which was run as a solution in HPLC grade pentane.

Low-resolution GC/MS was obtained on a Perkin-Elmer Autosystem XL-GC / TurboMass GC/MS using a Supelco SLB fused silica capillary column (30 m x 0.32 mm x 0.3 μ m). High resolution MS was obtained on a Water LCT Premier XE MS.

Thin-layer chromatography was performed using Merck 60 F₂₅₄ aluminium-backed plates. Plates were analysed by visual inspection, UV lamp (245 nm), or using permanganate stain, anisaldehyde stain or ceric ammonium molybdate stain. Permanganate stain was prepared from potassium permanganate (1 g), sodium carbonate (2 g) and deionised water (100 ml). Anisaldehyde stain was prepared using anisaldehyde (15 ml), ethanol (250 ml) and sulphuric acid (2.5 ml). Cerium ammonium molybdate stain was prepared from ceric ammonium molybdate (4 g), ammonium molybdate (4 g) and water (360 ml).

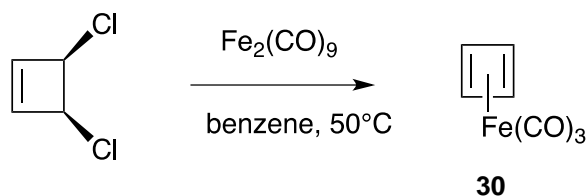
Column chromatography was done as flash chromatography using silica gel (60 \AA , 35-70 μ m). Columns were packed as slurries in eluent and run using bellows.

Melting points were determined using a Stuart Scientific SMP1 melting point apparatus.

Chemical names and structures were generated using ChemDraw.

6.3 Experimental Procedures

Cyclobutadiene Iron tricarbonyl (30)



In a two-necked, 100ml flask fitted with a condenser and stirrer bar and connected to a nitrogen supply, cis-3,4-dichlorocyclobutene (0.77ml, 8.2mmol) was added to anhydrous benzene (10ml). Diiron nonacarbonyl (2.9g, 8.0mmol) was added, the flow of N_{2(g)} was stopped but the tap left open, and the mixture was heated to 50-55 $^{\circ}$ C with

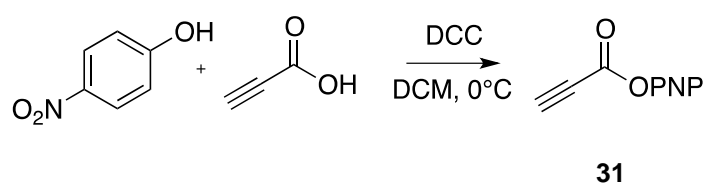
stirring. After around 15min, or when initial evolution of carbon monoxide had diminished, an additional 1g portion of diiron nonacarbonyl was added. Further 1g portions were then added periodically, governed by the rate of CO evolution. Additions continued until gas evolution appeared to stop, and the mixture was stirred at 50°C for a further hour. In total, roughly 8g of the nonacarbonyl complex are required. The flask contents were filtered through Celite and washed thoroughly with ice-cold pentane until the washings ran colourless, taking care not to allow the remaining brown residue to dry as it is frequently pyrophoric. Following the filtration, the remaining residue was immediately wetted with plenty of water. The washings were concentrated on a rotary evaporator to remove most of the benzene and pentane, yielding **30** as pale yellow-green crystals (0.74g, 47%);

$^1\text{H NMR}$ (400MHz, CDCl_3): δ 3.94 (4H,s);

IR (solution, pentane) 2053, 2000, 1982;

MS (GCMS) m/z (% relative intensity): 191.9 (M^+ , 22), 163.9 ($\text{M}^+ - \text{CO}$, 30), 136.0 ($\text{M}^+ - 2\text{CO}$, 10), 108.1 ($\text{M}^+ - 3\text{CO}$, 100), 82.1 (95), 56.1 (92).

4-Nitrophenyl Propiolate (**31**)



In a 100ml flask flushed with nitrogen and fitted with a Suba seal, propiolic acid (0.074ml, 1.2mmol) was added via syringe to dry DCM (10ml) with stirring. The reaction was cooled to 0°C and *N,N'*-dicyclohexylcarbodiimide (0.272g, 1.3mmol) was added. After around 10 minutes, *p*-nitrophenol (0.5g, 3.6mmol) was added to the mixture, which was maintained at 0°C and stirred for a further 5hrs. The resulting pale yellow solution was filtered to remove any residual solid, washed with 0.5M HCl and then with saturated NaHCO_3 , dried over MgSO_4 and concentrated on a rotary evaporator to give the crude product as a yellow oil. This was purified by gradient

silica gel flash column chromatography (10:1, 5:1, 1:1 petrol ether:EtOAc) to give **3** as a yellow oil, (0.17g, 73%);

^1H NMR (400MHz, CDCl_3): δ 3.1 (1H, s), 7.3 (2H, d, $J=9.2$), 8.25 (2H, d, $J=9.2$)

2,3-Dicarboethoxy-2,3-diazabicyclo[2.2.0]hex-5-ene (38)

30

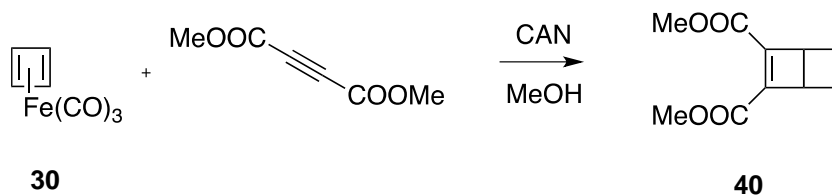
38

A solution of **30**(0.2g, 1mmol) and diethylazodicarboxylate (0.18g, 1mmol) in freshly distilled pyridine (1ml) was prepared in a 5ml flask. Roughly one fourth of this mixture was added dropwise via syringe to a 25ml flask under nitrogen at 35°C, already charged with a suspension of lead tetraacetate (freshly recrystallized from glacial acetic acid, 0.24g, 0.5mmol) in ether (1.5ml) and pyridine (2ml). The rate of addition was controlled so as to keep the reaction temperature at 35 – 40°C. Once evolution of CO had stopped, a second aliquot of the iron tricarbonyl complex solution was added dropwise to the flask, along with a second portion of lead tetraacetate (0.24g, 0.5mmol). This procedure was repeated until approximately 1g of lead tetraacetate had been consumed, and then the mixture was left to stir at 35°C for a further 3 hours. The viscous brown mixture formed was poured into ether (10ml) and the supernatant organic liquid was decanted and put aside. The inorganic solids remaining were dissolved in a small amount of water and washed with more ether, the washings were then combined with the first organic extract and concentrated on a rotary evaporator to give **38** as a brown oil (0.18g, 57%);

^1H NMR (400MHz, CDCl_3): δ 1.4 (6H, t, $J=7$), 4.2 (4H, q, $J=7$), 5.15 (2H, d, $J=2.9$), 6.65 (2H, d, $J=2.9$);

MS (GCMS) m/z (% relative intensity): 226.0 (M^+ , 13), 180.1 ($M^+ - OCH_2CH_3$, 5), 154 ($M^+ - OCOCH_2CH_3$), 81 (154 ($M^+ - 2OCOCH_2CH_3$, 100)

Dimethyl bicyclo[2.2.0]hexa-2,5-diene-2,3-dicarboxylate (40**)**⁵⁷

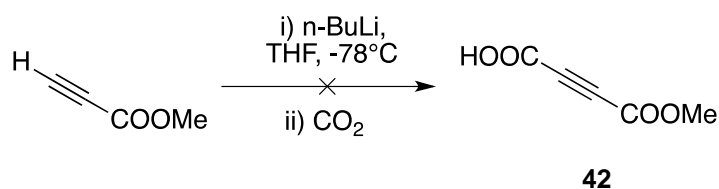


A 10ml flask was dried, flushed with nitrogen and charged with anhydrous methanol (5ml). To this, **30**(0.2g, 1mmol) was added with stirring. To a second 2-necked, 50ml flask, which was also dried and flushed with nitrogen, cerium ammonium nitrate (2.28g, 4.2mmol) was added and the flask sealed with a Suba seal. The flask was cooled to 0°C, at which point anhydrous methanol (10ml) was added with stirring, followed by dimethyl acetylenedicarboxylate (0.52ml, 4.2mmol). The mixture of **30** in methanol was slowly added to the second flask via syringe, and then the contents were stirred for a further two hours at 0°C. Saturated $NaHCO_3$ (10ml) solution was added to the reaction mixture, which was then filtered and washed twice with acetone (2x10ml) and DCM (2x10ml). The extracts were combined and concentrated on a rotary evaporator to leave behind an aqueous layer. This was extracted with diethyl ether (3x10ml), the washings were combined and dried over Na_2SO_4 and then concentrated to give **40** as a yellow oil (0.13g, 65%);

MS (GCMS) m/z (% relative intensity): 194.1 (M^+ , 8), 164.2 ($M^+ - 2Me$, 10), 163.1 ($M^+ - MeO$, 100), 76.1 ($M^+ - 2COOMe$, 25);

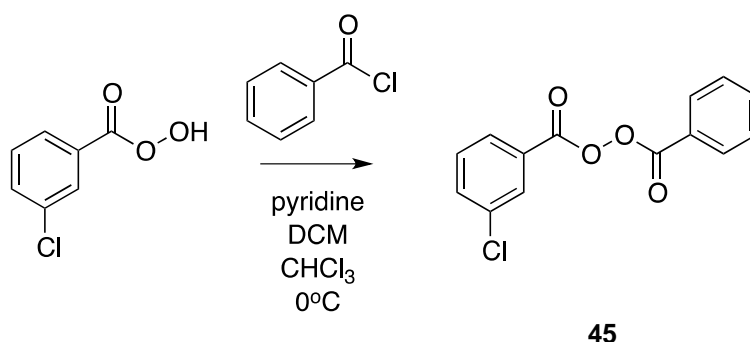
1H NMR (400MHz, $CDCl_3$): δ 3.41 (6H,s), 6.24 (2H,s), 6.61 (2H,s)

2-Butynedioic acid monomethyl ester (42)⁶³



Methyl propiolate (0.84ml, 10mmol) in anhydrous THF (60ml) was cooled to -78°C . 2.5M *n*-BuLi (4.75ml, 12mmol) was added dropwise to the solution with stirring over 30 minutes. CO_2 gas was then bubbled through the solution at -78°C for 15 minutes. The reaction mixture was hydrolysed with saturated NH_4Cl solution, then THF removed under reduced pressure. The remaining mixture was extracted with diethyl ether, and the organic layer set aside. The aqueous layer was acidified to pH 1 using dilute HCl and evaporated to dryness, leaving behind a white solid which was stirred vigorously three times in ether and filtered off. The ether extracts were combined, dried over Na_2SO_4 , and concentrated under reduced pressure.

Benzoic 3-chlorobenzoic peroxyanhydride (45)



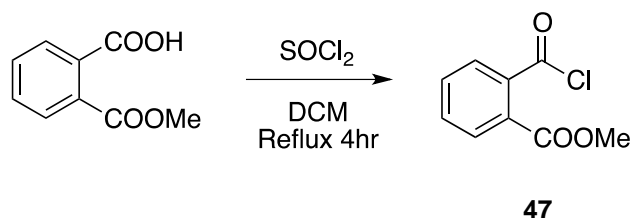
mCPBA (0.345 g, 2 mmol) was dissolved in chloroform (5 ml) in a round-bottomed flask, charged with a magnetic stirrer. Benzoyl chloride (0.23 ml, 2 mmol) was added and the flask was cooled to 0°C in an ice bath. In a separate flask, a solution of pyridine (0.22 ml, 2.8 mmol) in DCM (5 ml) was made up, and then added in a

dropwise manner to the first flask. This was stirred for around 30 minutes at 0 °C. The resulting organic solution was washed with 0.2M HCl_(aq), deionised water, saturated sodium carbonate solution and then deionised water for a second time. It was then dried over sodium sulphate and concentrated in vacuo with care to give **45** as white crystals (crude yield 82% by iodometric titration) NB For safety reasons this compound was not fully dried, as it was not required for further synthesis

¹H NMR (500MHz, CDCl₃): δ 8.16 (1H, m), 8.03 (2H, m), 7.94 (1H, m), 7.50-7.59 (2H, m), 7.46-7.60 (2H, m), 7.32-7.41 (1H, m);

¹³C NMR (125MHz, CDCl₃): δ 162.8, 161.8, 135.1, 134.9, 132.3, 129.9, 129.8, 128.9, 128.8, 128.6, 128.4, 128.0, 127.9, 127.3.

Methyl 2-(chlorocarbonyl)benzoate (**47**)⁶⁴

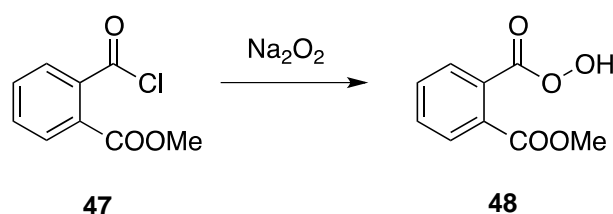


Mono-methyl phthalate (0.9 g, 5mmol) was dissolved in dry DCM (25 ml) and fitted with a condenser and guard tube. Thionyl chloride was added (0.51 ml, 7 mmol) and the mixture was heated to reflux with stirring for 5 hours, and then concentrated in vacuo to give **47** as cream-coloured crystals (0.82 g, 83%);

¹H NMR (400MHz, CDCl₃): δ 7.94 (2H, m), 7.64 (2H, m), 3.95, (3H, s);

IR (nujol): ν 2850, 1780, 1705, 1450, 1375, 1340;

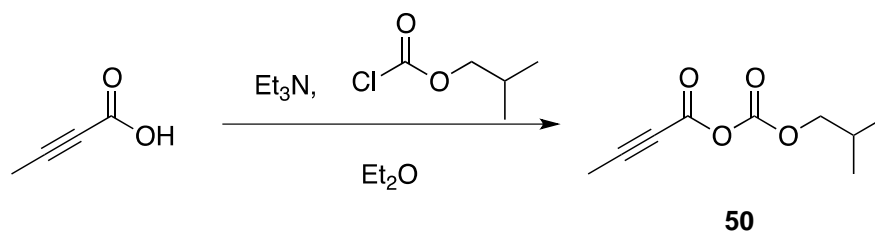
2-(methoxycarbonyl)benzoperoxoic acid (**48**)⁶⁵



Sodium peroxide (0.78 g, 10 mmol) was dissolved in a mixture of ice and water (100 ml) in a conical flask, which was charged with a magnetic stirrer and placed in an ice bath. Compound **47** (1.3 g, 7 mmol) was added slowly over the course of half an hour and the reaction mixture was stirred at 0°C until it was deemed to be complete by TLC (around 6 hours). It was then filtered on a chilled Buchner funnel, and the solid was transferred to a second flask and shaken with iced water (50ml), then filtered again on a chilled Buchner funnel. The aqueous filtrates were combined and added to 10% sulphuric acid solution (50 ml) chilled to 0 °C. The acidic product crystallised as a white solid, which was extracted into chloroform then concentrated in vacuo to give **48** as a colourless oil, which gave a positive starch/iodide result (0.34 g, 27%);

$^1\text{H NMR}$ (400MHz, CDCl_3): δ 7.83 (2H, m), 7.54 (2H, m), 3.84 (3H, m)

But-2-ynoic (isobutyl carbonic) anhydride (**50**)

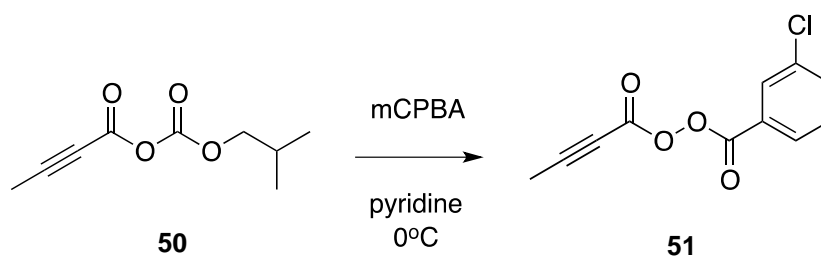


2-butyne-1-carboxylic acid (1.64 g, 20 mmol) was dissolved in dry ether (20 ml) in a 100 ml round-bottomed flask with stirrer bar that had been dried in the oven overnight, then sealed and flushed with nitrogen. The flask was immersed in an ice bath, and triethylamine

(2.92 ml, 21 mmol) was added in a dropwise manner. Isobutyl chloroformate (2.73 ml, 21 mmol) was also added dropwise, and the reaction was stirred at 0 °C for a further 1hr. An oven-dried sinter funnel was used to filter off any solid triethylamine hydrochloride, and the remaining solution was concentrated in vacuo to give **50** as a yellow oil (1.94 g, 54%);

¹H NMR (400MHz, CDCl₃): δ 3.99 (2H, d, *J* = 3.2), 2.52 (1H,m), 1.96 (3H, s), 0.93 (6H, d, *J* = 4)

But-2-ynoic 3-chlorobenzoic peroxyanhydride (**51**)



mCPBA (0.345 g, 2 mmol) was dissolved in dry DCM (5 ml) and pyridine (0.22 ml, 2.8 mmol) in a small round-bottomed flask, and cooled to 0 °C. **50** (0.57 g, 2.4 mmol) was added dropwise and the temperature maintained for a further hour whilst the reaction was stirred. The mixture was checked by TLC and found to be complete within this time. Chloroform (10 ml) was added, and the organics were washed with 0.2 M HCl (aq), saturated bicarbonate solution and brine, then dried over sodium sulphate and concentrated. The resulting brown oil was purified by column chromatography (7:1 hexane:EtOAc) to give **51** as a transparent oil (0.38 g, 67%);

¹H NMR (500MHz, CDCl₃): δ 8.04 (1H, m), 7.97 (1H, m), 7.93 (1H, m), 7.83 (1H, m), 1.91 (3H, s);

¹³C NMR (125MHz, CDCl₃): δ 160.8, 153.7, 131.1, 130.5, 130.2, 129.8, 128.6, 128.2, 85.1, 72.6, 3.2.

7 WORKS CITED

1. Eyring, H. *J. Chem. Phys.* **1935**, *3*, 107.
2. Rice, O. K.; Ramsperger, H. C. *J. Am. Chem. Soc.* **1927**, *49*, 1617.
3. Rice, O. K.; Ramsperger, H. C. *J. Am. Chem. Soc.* **1928**, *50*, 617.
4. Kassel, L. S. *Chem. Rev.* **1932**, *10*, 11.
5. Marcus, R. A.; Rice, O. K. *J. Phys. Colloid Chem.* **1951**, *55*, 894.
6. Baer, T.; Hase, W. L. *Unimolecular Reaction Dynamics: Theory and Experiments*; OUP: New York, 1996.
7. Carpenter, B. K. Potential Energy Surfaces and Reaction Dynamics. In *Reactive Intermediate Chemistry*; John Wiley & Sons, 2004; pp 925-957.
8. Uzer, T. Theories of Intramolecular Vibrational Energy Transfer. *Physics Reports* **1991**, *199* (2), 73.
9. Stannard, P. R.; Gelbart, W. M. *J. Phys. Chem.* **1981**, *85*, 3592.
10. McLafferty, F. W.; McAddo, D. J.; Smith, J. S.; Kornfield, R. *J. Am. Chem. Soc.* **1971**, *93*, 3720.
11. Depke, G.; Lifshitz, C.; Schwarz, H.; Tzidony, E. *Angew. Chem. Int. Ed. Eng* **1981**, *20*, 792.
12. Nummela, J.; Carpenter, B. K. *J. Am. Chem. Soc.* **2002**, *124*, 8512.
13. Frey, H. M.; Marshall, D. C. *J. Chem. Soc.* **1962**, 3981.
14. Baldwin, J. E.; Villarica, K. A.; Freedberg, D. I.; Anet, F. A. L. *J. Am. Chem. Soc.* **1994**, *116*, 10845.
15. Doubleday, C.; Li, G.; Hase, W. L. *Phys. Chem. Chem. Phys.* **2002**, *4*, 304.

16. Foresman, J. B.; Frisch, A. *Exploring Chemistry With Electronic Structure Methods, 2nd Ed.*; Gaussian Inc.: Pittsburgh, 1996.
17. Jensen, F. *Introduction to Computational Chemistry*, 2nd ed.; John Wiley & Sons Ltd: Chichester, 2007.
18. Hohenberg, P.; Kohn, W. *Phys. Rev.***1964**,*136*, 864.
19. Bunker, D. L. *Methods Comput. Phys.***1971**,*10*, 287.
20. Bolton, K.; Hase, W. L. Direct Dynamics Simulations of Reactive Systems. In *Modern Methods for Multidimensional Dynamics Computations in Chemistry*; World Scientific: Singapore, 1998; pp 143-179.
21. Salem, L.; Rowland, C. J. *Angew. Chem. Internat. Ed.***1972**,*11*, 92.
22. Maruani, J. *Molecules in Physics, Chemistry and Biology*; Kluwer Academic: Dordrecht; Vol. 3: Electronic Structure and Chemical Reactivity.
23. Bartlett, P. D. *Quart. Rev. Chem. Soc.***1970**,*24*, 473.
24. Benson, S. W.; O'Neal, H. E. *J. Phys. Chem.***1968**,*72*, 1866.
25. Hoffmann, R.; Swaminathan, S.; Odell, B.; Gleiter, R. *J. Am. Chem. Soc.***1970**,*92*, 7091.
26. Gajewski, J. J. *Hydrocarbon Thermal Isomerizations*; Academic Press: New York, 1981.
27. Frey, H. M.; Jackson, G. E.; Smith, R. A.; Walsh, R. *J. Chem. Soc., Faraday Trans.***1975**,*71* (1), 1991.
28. Flowers, M. C.; Frey, H. M. *J. Chem. Soc.***1961**, 5550.
29. Doering, W. V. E.; Gilbert, J. C.; Leermakers, P. A. *Tetrahedron***1968**,*24*, 6863.
30. DeTar, D. F. *J. Am. Chem. Soc.***1967**,*89*, 4058.

31. Rynbrandt, J. D.; Rabinovitch, B. S. *J. Phys. Chem.* **1971**, *75*, 2164.
32. Johnson, W. T. G.; Hrovat, D. A.; Borden, W. T. *J. Am. Chem. Soc.* **1999**, *121*, 7766.
33. Gilbert, J. C. *Tetrahedron* **1969**, *25*, 1459.
34. Carpenter, B. K.; Pittner, J.; Veis, L. *J. Phys. Chem. A* **2009**, *113*, 10557.
35. Hratchian, H. P.; Schlegel, H. B. *J. Phys. Chem. A* **2002**, *106*, 165.
36. Grafenstein, J.; Cremer, D. *Phys. Chem. Chem. Phys.* **2000**, *2*, 2091.
37. *Gaussian03 Revision E.01*; Frisch, M. J.; Trucks, G. W.; Schlegel, H. B.; Scuseria, G. E.; Robb, M. A.; Cheeseman, J. R.; Montgomery, Jr., J. A.; Vreven, T.; Kudin, K. N.; Burant, J. C.; Millam, J. M.; Iyengar, S. S.; Tomasi, J.; Barone, V.; Mennucci, B.; Cossi, M.; Scalmani, G.; Rega, N.; Petersson, G. A.; Nakatsuji, H.; Hada, M.; Ehara, M.; Toyota, K.; Fukuda, R.; Hasegawa, J.; Ishida, M.; Nakajima, T.; Honda, Y.; Kitao, O.; Nakai, H.; Klene, M.; Li, X.; Knox, J. E.; Hratchian, H. P.; Cross, J. B.; Bakken, V.; Adamo, C.; Jaramillo, J.; Gomperts, R.; Stratmann, R. E.; Yazyev, O.; Austin, A. J.; Cammi, R.; Pomelli, C.; Ochterski, J. W.; Ayala, P. Y.; Morokuma, K.; Voth, G. A.; Salvador, P.; Dannenberg, J. J.; Zakrzewski, V. G.; Dapprich, S.; Daniels, A. D.; Strain, M. C.; Farkas, O.; Malick, D. K.; Rabuck, A. D.; Raghavachari, K.; Foresman, J. B.; Ortiz, J. V.; Cui, Q.; Baboul, A. G.; Clifford, S.; Cioslowski, J.; Stefanov, B. B.; Liu, G.; Liashenko, A.; Piskorz, P.; Komaromi, I.; Martin, R. L.; Fox, D. J.; Keith, T.; Al-Laham, M. A.; Peng, C. Y.; Nanayakkara, A.; Challacombe, M.; Gill, P. M. W.; Johnson, B.; Chen, W.; Wong, M. W.; Gonzalez, C.; and Pople, J. A.; Gaussian, Inc., Wallingford CT, 2004.
38. Binkley, J. S.; Pople, J. A.; Hehre, W. J. *J. Am. Chem. Soc.* **1980**, *102*, 939.
39. Perdew, J. P.; Burke, K.; Ernzerhof, M. *Phys. Rev. Lett.* **1996**, *77*, 3865.
40. Perdew, J. P.; Burke, K.; Ernzerhof, M. *Phys. Rev. Lett.* **1997**, *78*, 1396.
41. Handy, N. C.; Cohen, A. J. *Mol. Phys.* **2001**, *99*, 403.
42. Lee, C.; Yang, W.; Parr, R. G. *Phys. Rev. B* **1988**, *37*, 785.

43. Becke, A. D. *Phys. Rev. A***1988**,*38*, 3098.
44. Becke, A. D. *J. Chem. Phys.***1996**,*104*, 1040.
45. Peng, C.; Ayala, P. Y.; Schlegel, H. B.; Frisch, M. J. *J. Comp. Chem.***1996**,*17*, 49.
46. Hase, W. L.; Duchovic, R. J.; Hu, X.; Komornicki, A.; Lim, K. F.; Lu, -H.; Peslherbe, G. H.; Swamy, K. N.; Linde, S. R. V.; Varandas, A.; Wang, H.; Wolfe, . *QCPE***1996**,*16*, 671.
47. Taketsgu, T.; Yanai, T.; Hirao, K.; Gordon, M. S. *Theochem.***1998**,*451*, 163.
48. Schmidt, M. W.; Baldridge, K. K.; Boatz, J. A.; Elbert, S. T.; Gordon, M. S.; Jensen, J. H.; Koseki, S.; Matsunaga, N.; Nguyen, K. A.; Su, S.; Windus, T. L.; Dupuis, M.; Montgomery, J. A. GAMESS US, Version 1 Oct 2010 (R1). *J. Comput. Chem.***1993**,*14*, 1347.
49. Brown, D. J. *J. Am. Chem. Soc.***1940**,*62* (10), 2657.
50. Zaman, F.; Beezer, A. E.; Mitchell, J. C.; Clarkson, Q.; Elliot, J.; Davies, A. F.; Wilson, R. J. *Int. J. Pharm.***2001**,*227*, 133.
51. Walker, O. J.; Wild, G. L. E. *J. Chem. Soc.***1937**, 1132.
52. Ferrar, L.; Mis, M.; Robello, D. R. *Tetrahedron Lett.***2008**,*49*, 4130.
53. Havenith, R. W. A.; Jenneskens, L.; Lenthe, J. H. v. *J. Mol. Struct. (Theochem)***1999**,*492*, 217-224.
54. Goldstein, M. J.; Leight, R. S. *J. Am. Chem. Soc.***1977**,*99*, 8112.
55. De La Zerda, J.; Barak, G.; Sasson, Y. *Tetrahedron***1989**,*45*, 1533.
56. Adam, W.; Chang, J. C. *Int. J. Chem. Kinetic.***196**,*1*, 487.
57. Watts, L.; Fitzpatrick, J. D.; Pettit, R. *J. Am. Chem. Soc.***1965**,*87*, 3253.
58. Li, Y.; Houk, K. N. *J. Am. Chem. Soc.***1996**,*118*, 880.

59. Pettit, R.; Henery, J. *Org. Syn. Coll.***1988**,*6*, 310.
60. Limanto, J.; Tallarico, J. A.; Porter, J. R.; Khuong, K. S.; Houk, K. N.; Snapper, M. L. *J. Am. Chem. Soc.***2002**,*124*, 14748.
61. Emerson, G. F.; Watts, L.; Pettit, R. *J. Am. Chem. Soc.***1965**,*87*, 3254.
62. Schmitt, M.; Bourguignon, J.-J.; Wermuth, C.-G.; Schott, D.; Rousseau, B.; Beaucourt, J.-P. *Journal of Labelled Compounds and Radiopharmaceuticals***1989**,*27*, 23.
63. Zheng, H.; McDonald, R.; Hall, D. *Chem. Eur. J.***2010**,*16*, 5454.
64. Raposo, M. M. M.; Sampaio, A. M. B. A.; Krisch, G. *J. Heterocyclic Chem.***2005**,*42*, 1245.
65. Brooks, B. T.; Brooks, W. *J. Am. Chem. Soc.***1933**,*55*, 4309.
66. Luo, T.; Dai, M.; Zheng, S.-L.; Schreiber, S. L. *Org. Lett.***2011**,*13*, 2834.

APPENDIX A

Sample Gaussian Output - BOMD

```
# UPBE1PBE/3-21G IOP(1/44= 7027874) guess=(mix,always) scf=(xqc, MaxCy  
cle=128) NoSymm # BOMD(ReadStop ,ntraj=1, update=7, MaxPoints=1800, RT  
emp=298)
```

```
-----  
Spiropentane random seed 7027874  
-----
```

Symbolic Z-matrix:

Charge = 0 Multiplicity = 1

6	0	0.38677	-0.01726	0.15011
6	0	-1.32106	-0.02859	-0.71615
6	0	-1.02304	-0.179	0.72421
6	0	0.86046	1.35305	0.01161
6	0	1.16871	-1.13827	-0.09636
1	0	-1.55909	0.93814	-1.13944
1	0	-1.36816	-0.90542	-1.3472
1	0	-1.2011	-1.16585	1.1488
1	0	-1.33892	0.63089	1.37851
1	0	0.17098	2.18615	0.082
1	0	1.91374	1.55506	-0.14157
1	0	0.81286	-2.13267	0.15014
1	0	2.13872	-1.04585	-0.57177

```
TRJ-TRJ-TRJ-TRJ-TRJ-TRJ-TRJ-TRJ-TRJ-TRJ-TRJ-TRJ-TRJ-TRJ-TRJ-TRJ-  
TRJ
```

```
-----  
INPUT DATA FOR L118
```

General parameters:

Max. points for each Traj. = 1800

Total Number of Trajectories = 1

Random Number Generator Seed = 7027874

Trajectory Step Size = 0.250 sqrt(amu)*bohr

Sampling parameters:

Vib Energy Sampling Option = Thermal sampling

TS Sampling direction = Forward

Vib Sampling Temperature = 298.0 K

Rot Energy Sampling Option = Thermal distribution (symmetric top)

Rot Sampling Temperature = 298.0 K

Start point scaling criteria = 1.000D-05 Hartree

Integration parameters:

Correction Scheme = Fifth order polynomial fit

Project trans/rot in grad. = True

Project in prediction step = True

Project in correction step = True

Integration Scheme = Bulirsch-Stoer method

Integration Step Size = 2.000D-01 femtosec

Truncation Error Criteria = 1.000D-08 bohr

Energy Error Criteria = 1.000D-04 Hartree

Hessian evaluation = Update for 7 steps.

Hessian update method = Bofill update

Back integrate previous updated step with new Hessian.

8 H	2.199540	2.187642	1.088977	3.447906	2.677158
9 H	2.215191	2.196091	1.088024	2.688340	3.404906
10 H	2.214998	2.787164	2.726175	1.083695	3.475494
11 H	2.211087	3.647191	3.518694	1.083366	2.794843
12 H	2.157893	3.119483	2.741702	3.488789	1.084532
13 H	2.156024	3.609116	3.525300	2.780107	1.084193

6	7	8	9	10
---	---	---	---	----

6 H	0.000000				
7 H	1.865026	0.000000			
8 H	3.129058	2.515101	0.000000		
9 H	2.546162	3.128985	1.816604	0.000000	
10 H	2.458158	3.737554	3.775790	2.525780	0.000000
11 H	3.665630	4.275318	4.332509	3.707362	1.866944
12 H	4.088888	2.916335	2.447056	3.711644	4.366787
13 H	4.234649	3.594334	3.758875	4.325392	3.839953

11	12	13
----	----	----

11 H	0.000000		
12 H	3.859579	0.000000	
13 H	2.645828	1.860168	0.000000

Symmetry turned off by external request.

Stoichiometry C5H8

Framework group C1[X(C5H8)]

Deg. of freedom 33

Full point group C1

Rotational constants (GHZ): 6.8377464 5.2231897 3.8426838

Standard basis: 3-21G (6D, 7F)

Integral buffers will be 131072 words long.

Raffenetti 2 integral format.

Two-electron integral symmetry is turned off.

61 basis functions, 99 primitive gaussians, 61 cartesian basis functions
 19 alpha electrons 19 beta electrons
 nuclear repulsion energy 164.4232010431 Hartrees.
 NAtoms= 13 NActive= 13 NUniq= 13 SFac= 7.50D-01 NAtFMM= 80
 NAOKFM=F Big=F
 One-electron integrals computed using PRISM.
 NBasis= 61 RedAO= T NBF= 61
 NBsUse= 61 1.00D-06 NBFU= 61
 SCF N**3 symmetry information disabled.
 Harris functional with IExCor= 1009 diagonalized for initial guess.
 ExpMin= 1.83D-01 ExpMax= 1.72D+02 ExpMxC= 1.72D+02 IAcc=1 IRadAn=
 1 AccDes= 1.00D-06
 HarFok: IExCor=1009 AccDes= 1.00D-06 IRadAn= 1 IDoV=1
 ScaDFX= 1.000000 1.000000 1.000000 1.000000
 <S**2> of initial guess= 1.0000
 Requested convergence on RMS density matrix=1.00D-08 within 128 cycles.
 Requested convergence on MAX density matrix=1.00D-06.
 Requested convergence on energy=1.00D-06.
 No special actions if energy rises.
 Keep R1 and R2 integrals in memory in canonical form, NReq= 5395914.
 Integral accuracy reduced to 1.0D-05 until final iterations.
 Initial convergence to 1.0D-05 achieved. Increase integral accuracy.
 SCF Done: E(UPBE+HF-PBE) = -193.866626340 A.U. after 23 cycles
 Conv = 0.6158D-08 -V/T = 2.0086
 S**2 = 0.9225
 Annihilation of the first spin contaminant:
 S**2 before annihilation 0.9225, after 0.0881
 QCSCF skips out because SCF is already converged.
 ExpMin= 1.83D-01 ExpMax= 1.72D+02 ExpMxC= 1.72D+02 IAcc=1 IRadAn=
 1 AccDes= 1.00D-06

HarFok: IExCor= 205 AccDes= 1.00D-06 IRadAn= 1 IDoV=1

ScaDFX= 1.000000 1.000000 1.000000 1.000000

Range of M.O.s used for correlation: 6 61

NBasis= 61 NAE= 19 NBE= 19 NFC= 5 NFV= 0

NROrb= 56 NOA= 14 NOB= 14 NVA= 42 NVB= 42

Symmetrizing basis deriv contribution to polar:

IMax=3 JMax=2 DiffMx= 0.00D+00

G2DrvN: will do 14 centers at a time, making 1 passes doing MaxLOS=1.

FoFDir/FoFCou used for L=0 through L=1.

DoAtom=TTTTTTTTTTTTTT

Differentiating once with respect to electric field.

with respect to dipole field.

Differentiating once with respect to nuclear coordinates.

Store integrals in memory, NReq= 4381253.

There are 42 degrees of freedom in the 1st order CPHF.

39 vectors were produced by pass 0.

AX will form 39 AO Fock derivatives at one time.

39 vectors were produced by pass 1.

39 vectors were produced by pass 2.

39 vectors were produced by pass 3.

39 vectors were produced by pass 4.

39 vectors were produced by pass 5.

14 vectors were produced by pass 6.

3 vectors were produced by pass 7.

Inv2: IOpt= 1 Iter= 1 AM= 3.24D-15 Conv= 1.00D-12.

Inverted reduced A of dimension 251 with in-core refinement.

Isotropic polarizability for W= 0.000000 55.01 Bohr**3.

End of Minotr Frequency-dependent properties file 721 does not exist.

Population analysis using the SCF density.

Alpha occ. eigenvalues -- -10.20499 -10.20111 -10.18951 -10.15979 -10.14667
Alpha occ. eigenvalues -- -0.87809 -0.74262 -0.67281 -0.63294 -0.54181
Alpha occ. eigenvalues -- -0.50145 -0.47456 -0.43618 -0.41911 -0.38869
Alpha occ. eigenvalues -- -0.37901 -0.34864 -0.31106 -0.16642
Alpha virt. eigenvalues -- -0.04379 0.10758 0.12641 0.14688 0.17100
Alpha virt. eigenvalues -- 0.18479 0.20232 0.20891 0.24455 0.24986
Alpha virt. eigenvalues -- 0.26747 0.28558 0.38342 0.42001 0.65862
Alpha virt. eigenvalues -- 0.67960 0.69822 0.73421 0.74647 0.75846
Alpha virt. eigenvalues -- 0.81064 0.83003 0.83458 0.88291 0.89408
Alpha virt. eigenvalues -- 0.96619 0.98443 1.01972 1.05138 1.08412
Alpha virt. eigenvalues -- 1.10103 1.10585 1.14771 1.15576 1.36651
Alpha virt. eigenvalues -- 1.38467 1.42401 1.60886 1.65324 1.74703
Alpha virt. eigenvalues -- 1.96327 2.10380
Beta occ. eigenvalues -- -10.20576 -10.19396 -10.18991 -10.17311 -10.13889
Beta occ. eigenvalues -- -0.87516 -0.74296 -0.68465 -0.62103 -0.54247
Beta occ. eigenvalues -- -0.50022 -0.47445 -0.43374 -0.42048 -0.39076
Beta occ. eigenvalues -- -0.37907 -0.34809 -0.31273 -0.17431
Beta virt. eigenvalues -- -0.04102 0.11089 0.12720 0.14711 0.17531
Beta virt. eigenvalues -- 0.18689 0.19215 0.21306 0.24264 0.24844
Beta virt. eigenvalues -- 0.26843 0.28722 0.37786 0.42387 0.66179
Beta virt. eigenvalues -- 0.68941 0.69564 0.72852 0.75079 0.75821
Beta virt. eigenvalues -- 0.80519 0.81277 0.84592 0.88813 0.89366
Beta virt. eigenvalues -- 0.96478 0.98582 1.02027 1.04886 1.08399

Beta virt. eigenvalues -- 1.10221 1.10706 1.14521 1.15677 1.36565

Beta virt. eigenvalues -- 1.38795 1.41834 1.59482 1.66212 1.75270

Beta virt. eigenvalues -- 1.96239 2.10513

Condensed to atoms (all electrons):

	1	2	3	4	5	6						
1 C	5.487451	-0.062696	0.215636	0.317531	0.465974	-0.002607						
2 C	-0.062696	5.622021	0.198203	-0.021887	-0.034658	0.371490						
3 C	0.215636	0.198203	5.513268	-0.076910	-0.064251	-0.038536						
4 C	0.317531	-0.021887	-0.076910	5.444760	-0.066419	-0.000317						
5 C	0.465974	-0.034658	-0.064251	-0.066419	5.339435	0.000980						
6 H	-0.002607	0.371490	-0.038536	-0.000317	0.000980	0.443817						
7 H	-0.004500	0.373774	-0.038354	0.001076	0.001681	-0.019324						
8 H	-0.035654	-0.031093	0.378654	0.002693	-0.001476	0.001682						
9 H	-0.033991	-0.031241	0.379720	-0.000435	0.001978	-0.002746						
10 H	-0.043873	0.000280	-0.000687	0.379656	0.002323	0.000903						
11 H	-0.043322	0.000827	0.002167	0.383615	-0.001287	0.000055						
12 H	-0.048642	0.001382	-0.004519	0.002632	0.388157	-0.000019						
13 H	-0.049970	-0.000259	0.003057	-0.002324	0.389155	0.000008						
	7	8	9	10	11	12						
1 C	-0.004500	-0.035654	-0.033991	-0.043873	-0.043322	-0.048642						
2 C	0.373774	-0.031093	-0.031241	0.000280	0.000827	0.001382						
3 C	-0.038354	0.378654	0.379720	-0.000687	0.002167	-0.004519						
4 C	0.001076	0.002693	-0.000435	0.379656	0.383615	0.002632						
5 C	0.001681	-0.001476	0.001978	0.002323	-0.001287	0.388157						
6 H	-0.019324	0.001682	-0.002746	0.000903	0.000055	-0.000019						
7 H	0.431911	-0.002845	0.001683	-0.000011	-0.000015	0.000333						
8 H	-0.002845	0.452938	-0.015518	-0.000014	-0.000037	0.002660						
9 H	0.001683	-0.015518	0.455540	0.000894	0.000077	0.000031						
10 H	-0.000011	-0.000014	0.000894	0.483012	-0.022634	-0.000060						

11 H -0.000015 -0.000037 0.000077 -0.022634 0.462559 0.000007
12 H 0.000333 0.002660 0.000031 -0.000060 0.000007 0.490380
13 H 0.000022 0.000020 -0.000051 0.000024 0.001634 -0.024298

13

1 C -0.049970
2 C -0.000259
3 C 0.003057
4 C -0.002324
5 C 0.389155
6 H 0.000008
7 H 0.000022
8 H 0.000020
9 H -0.000051
10 H 0.000024
11 H 0.001634
12 H -0.024298
13 H 0.482524

Mulliken atomic charges:

1

1 C -0.161334
2 C -0.386144
3 C -0.467447
4 C -0.363671
5 C -0.421592
6 H 0.244614
7 H 0.254569
8 H 0.247990
9 H 0.244059
10 H 0.200188

11 H 0.216356
12 H 0.191953
13 H 0.200459

Sum of Mulliken charges= 0.00000

Atomic charges with hydrogens summed into heavy atoms:

1
1 C -0.161334
2 C 0.113039
3 C 0.024602
4 C 0.052873
5 C -0.029180
6 H 0.000000
7 H 0.000000
8 H 0.000000
9 H 0.000000
10 H 0.000000
11 H 0.000000
12 H 0.000000
13 H 0.000000

Sum of Mulliken charges= 0.00000

Atomic-Atomic Spin Densities.

	1	2	3	4	5	6
1 C	-0.084619	-0.047161	0.035798	0.078377	-0.042242	0.002016
2 C	-0.047161	0.664906	-0.063640	0.017749	-0.051164	-0.014566
3 C	0.035798	-0.063640	-0.030709	0.013287	0.000373	0.002046
4 C	0.078377	0.017749	0.013287	-1.143622	0.011946	0.000207
5 C	-0.042242	-0.051164	0.000373	0.011946	0.687125	0.000590
6 H	0.002016	-0.014566	0.002046	0.000207	0.000590	-0.015005
7 H	0.001859	-0.010687	0.001176	-0.000520	0.003361	0.001328

8 H -0.003588 0.001895 0.003212 -0.000564 0.000334 -0.000210
 9 H -0.002742 0.001593 0.005619 -0.002760 0.000295 -0.000332
 10 H 0.000256 0.001490 -0.001164 0.008591 0.000195 -0.000190
 11 H 0.001269 0.000201 -0.000003 0.009815 -0.000693 -0.000013
 12 H -0.001525 0.000990 -0.000173 -0.000232 -0.004547 -0.000005
 13 H -0.000768 -0.000369 -0.000051 0.000348 -0.004380 0.000006

7 8 9 10 11 12

1 C 0.001859 -0.003588 -0.002742 0.000256 0.001269 -0.001525
 2 C -0.010687 0.001895 0.001593 0.001490 0.000201 0.000990
 3 C 0.001176 0.003212 0.005619 -0.001164 -0.000003 -0.000173
 4 C -0.000520 -0.000564 -0.002760 0.008591 0.009815 -0.000232
 5 C 0.003361 0.000334 0.000295 0.000195 -0.000693 -0.004547
 6 H 0.001328 -0.000210 -0.000332 -0.000190 -0.000013 -0.000005
 7 H -0.023708 0.000104 -0.000050 0.000000 -0.000002 -0.000077
 8 H 0.000104 0.000957 -0.000497 0.000026 -0.000001 0.000256
 9 H -0.000050 -0.000497 0.001454 0.000285 0.000006 0.000002
 10 H 0.000000 0.000026 0.000285 0.048275 -0.001126 0.000001
 11 H -0.000002 -0.000001 0.000006 -0.001126 0.046377 0.000007
 12 H -0.000077 0.000256 0.000002 0.000001 0.000007 -0.026489
 13 H 0.000004 0.000000 0.000002 -0.000010 -0.000029 0.000455

13

1 C -0.000768
 2 C -0.000369
 3 C -0.000051
 4 C 0.000348
 5 C -0.004380
 6 H 0.000006
 7 H 0.000004
 8 H 0.000000

9 H 0.000002
 10 H -0.000010
 11 H -0.000029
 12 H 0.000455
 13 H -0.027517

Electronic spatial extent (au): $\langle R^{*2} \rangle = 410.1823$

Charge= 0.0000 electrons

Center Number	Atomic Number	Forces (Hartrees/Bohr)		
		X	Y	Z
1	6	0.000000010	-0.000001639	0.000000165
2	6	0.000000594	0.000002231	-0.000000783
3	6	-0.000000522	-0.000000297	-0.000001279
4	6	0.000001230	-0.000000028	0.000002985
5	6	-0.000001996	-0.000000663	-0.000001288
6	1	0.000001603	0.000003731	0.000000622
7	1	-0.000000140	0.000004154	-0.000002910
8	1	-0.000002071	-0.000001155	-0.000003013
9	1	-0.000000319	-0.000001410	0.000000302
10	1	0.000002387	-0.000000947	0.000004689
11	1	0.000001672	-0.000001666	0.000004519
12	1	-0.000002290	-0.000001218	-0.000003437
13	1	-0.000000159	-0.000001092	-0.000000572

Cartesian Forces: Max 0.000004689 RMS 0.000002034

Internal Coordinate Forces (Hartree/Bohr or radian)

0.39133681D+00	0.39402653D+00	0.40734161D+00	0.41209904D+00
0.42107939D+00	0.00000000D+00	0.00000000D+00	0.00000000D+00
0.00000000D+00	0.00000000D+00	0.00000000D+00	

Get start point for trajectory 1

Thermal Sampling of Vibrational Modes

Mode	Wavenumber	Vib. quant.#	Energy (kcal/mol)
------	------------	--------------	-------------------

1	-933.933		-0.490169E-01
2	197.965	0	0.283005
3	246.258	0	0.352044
4	372.099	0	0.531943
5	384.781	1	1.65022
6	406.337	0	0.580888
7	485.833	0	0.694533
8	543.540	0	0.777030
9	624.982	0	0.893457
10	686.980	0	0.982088
11	774.134	0	1.10668
12	804.396	0	1.14994
13	835.490	0	1.19439
14	980.389	0	1.40154
15	988.326	0	1.41288
16	1047.336	0	1.49724
17	1109.132	0	1.58558
18	1194.688	0	1.70789

19	1235.967	0	1.76690
20	1275.912	0	1.82401
21	1363.774	0	1.94961
22	1489.280	0	2.12903
23	1498.157	0	2.14172
24	1510.594	0	2.15950
25	1532.674	0	2.19107
26	3147.476	0	4.49954
27	3182.078	0	4.54901
28	3190.314	0	4.56078
29	3215.730	0	4.59712
30	3226.763	0	4.61289
31	3280.830	0	4.69018
32	3299.933	0	4.71749
33	3335.695	0	4.76861

	MW displacement	MW velocity
	(amu(1/2)*Bohr)	(amu(1/2)*Bohr/sec)
Mode 1	0.0000000000D+00	0.1210270779D+14
Mode 2	-0.7353620267D+00	-0.9683048655D+13
Mode 3	-0.6070826540D+00	-0.1609322727D+14
Mode 4	0.5228022140D+00	-0.1571118510D+14
Mode 5	0.9550450222D+00	0.1182099689D+14
Mode 6	-0.2418820156D+00	0.3732420595D+14
Mode 7	0.3653776929D+00	-0.3094197298D+14
Mode 8	0.4486799750D+00	-0.1455002689D+14
Mode 9	0.3443888119D-01	-0.5151165782D+14

Mode 10	-0.2704537203D+00	-0.4135106691D+14
Mode 11	0.6029481991D-01	-0.5683092132D+14
Mode 12	-0.3799978903D+00	-0.1100824580D+14
Mode 13	0.1637909529D+00	0.5389539778D+14
Mode 14	0.3494749425D+00	0.4798109004D+13
Mode 15	0.6153125186D-01	-0.6395978707D+14
Mode 16	-0.5794977230D-01	-0.6590490576D+14
Mode 17	0.2070766339D+00	0.5353947955D+14
Mode 18	-0.2905597103D+00	-0.2877841049D+14
Mode 19	-0.6940007327D-01	-0.7084436342D+14
Mode 20	0.3053929946D+00	0.7965583848D+13
Mode 21	0.9089750757D-01	0.7266857244D+14
Mode 22	-0.3551401819D-02	-0.7975666570D+14
Mode 23	0.1332603963D+00	-0.7061032002D+14
Mode 24	-0.2799579879D+00	-0.1036487284D+14
Mode 25	-0.5453217057D-01	0.7937024205D+14
Mode 26	0.3292201921D-01	-0.1143016086D+15
Mode 27	-0.1935239644D+00	-0.1176373639D+14
Mode 28	0.1295671683D+00	0.8698419792D+14
Mode 29	-0.1932421590D+00	0.6003261409D+13
Mode 30	0.1348581721D+00	-0.8405816077D+14
Mode 31	-0.8147888830D-02	0.1182800043D+15
Mode 32	-0.1591144764D+00	-0.6568906639D+14
Mode 33	-0.1882281093D+00	-0.1619605591D+14

Summary of normal mode sampling:

Translational Energy = 0.7811337470D-04 Hartree

Vibrational Energy = 0.1098928961D+00 Hartree

MW distance from initial geometry = 0.1276637175D+01 Bohr

Start point information

Time (fs) 0.000000

EKin = 0.0537419; EPot = -193.8103973; ETot = -193.7566555 A.U.

Angular momentum (instantaneous)

JX = -0.2104889637D+01 JY = -0.2195766145D+01 JZ = 0.2968549585D+00

Jtot = 0.3056153172D+01 H-BAR; J (Quantum Number) = 0.2596784173D+01

Total energy -1.937567D+02 A.U.

Total angular momentum 3.056153D+00 h-bar

Cartesian coordinates: (bohr)

I= 1 X= 6.518968485946D-01 Y= -1.093291454403D-01 Z= 1.220017122067D-01

I= 2 X= -2.584418515160D+00 Y= 1.348043164317D-01 Z= -1.436586603681D+00

I= 3 X= -1.859649879926D+00 Y= -3.559372903857D-01 Z= 1.432789308388D+00

I= 4 X= 1.567062193888D+00 Y= 2.469380566296D+00 Z= -7.548441104482D-02

I= 5 X= 2.319729039573D+00 Y= -2.137341127842D+00 Z= -1.506260061990D-02

I= 6 X= -3.077415232681D+00 Y= 1.680373091565D+00 Z= -2.106255335934D+00

I= 7 X= -3.016107024091D+00 Y= -1.599151434276D+00 Z= -2.552695689817D+00

I= 8 X= -2.492545975615D+00 Y= -2.277387353571D+00 Z= 1.691479749160D+00

I= 9 X= -2.574459772802D+00 Y= 1.158451094420D+00 Z= 2.763974752888D+00

I= 10 X= 2.991490000650D-01 Y= 4.233087660490D+00 Z= 8.309256370417D-01

I= 11 X= 3.484579125897D+00 Y= 2.949144343918D+00 Z= -3.402925663054D-01

I= 12 X= 2.048939840521D+00 Y= -4.331451555350D+00 Z= 4.700808043890D-01

I= 13 X= 4.201239641361D+00 Y= -1.831846714931D+00 Z= -
1.086529335948D+00

MW cartesian velocity: (sqrt(amu)*bohr/sec)

I= 1 X= -7.460043842132D+12 Y= 1.864565939059D+13 Z=
1.043133167883D+13

I= 2 X= 9.720667203631D+12 Y= 6.482859072557D+13 Z= -
1.154163844192D+12

I= 3 X= -1.624024652551D+13 Y= -1.069745419645D+13 Z=
4.486975082005D+13

I= 4 X= 3.371307916424D+13 Y= 1.378960674516D+12 Z= -
3.826069631580D+12

I= 5 X= 3.147633012750D+13 Y= -4.655405228437D+13 Z=
4.682935466913D+12

I= 6 X= -7.399301394830D+13 Y= -5.130866767639D+13 Z= -
9.203606512390D+13

I= 7 X= 3.927487030861D+12 Y= 3.581987940327D+12 Z=
2.964633499041D+12

I= 8 X= -8.913783058137D+13 Y= -1.398962748137D+14 Z=
3.556512164535D+13

I= 9 X= 8.901925926018D+12 Y= 5.619450820178D+13 Z= -
3.028380079055D+13

I= 10 X= -1.362350621553D+14 Y= 2.570862156713D+13 Z= -
1.451647993389D+13

I= 11 X= 1.466453508115D+13 Y= -5.063133289576D+13 Z= -
1.820467045856D+13

I= 12 X= -7.572084607513D+12 Y= 5.734436191237D+13 Z= -
2.010802800868D+13

I= 13 X= 1.027381582394D+14 Y= 3.763601898319D+12 Z= -
5.317827009310D+13

TRJ-TRJ-TRJ-TRJ-TRJ-TRJ-TRJ-TRJ-TRJ-TRJ-TRJ-TRJ-TRJ-TRJ-TRJ-
TRJ

Input orientation:

Center Atomic Atomic Coordinates (Angstroms)
Number Number Type X Y Z

1	6	0	0.344969	-0.057854	0.064561
2	6	0	-1.367615	0.071335	-0.760209
3	6	0	-0.984084	-0.188354	0.758199
4	6	0	0.829254	1.306740	-0.039945
5	6	0	1.227548	-1.131032	-0.007971
6	1	0	-1.628498	0.889215	-1.114582
7	1	0	-1.596055	-0.846234	-1.350828
8	1	0	-1.318999	-1.205141	0.895093
9	1	0	-1.362345	0.613026	1.462632
10	1	0	0.158303	2.240054	0.439707
11	1	0	1.843960	1.560620	-0.180075
12	1	0	1.084252	-2.292105	0.248756
13	1	0	2.223200	-0.969372	-0.574967

Symmetry turned off by external request.

Stoichiometry C5H8

Framework group C1[X(C5H8)]

Deg. of freedom 33

Full point group C1

Rotational constants (GHZ): 6.8821763 4.9909682 3.7698857

Standard basis: 3-21G (6D, 7F)

Integral buffers will be 131072 words long.

Raffenetti 2 integral format.

Two-electron integral symmetry is turned off.

61 basis functions, 99 primitive gaussians, 61 cartesian basis functions

19 alpha electrons 19 beta electrons

nuclear repulsion energy 162.5400584210 Hartrees.

NAtoms= 13 NActive= 13 NUniq= 13 SFac= 7.50D-01 NAtFMM= 80
 NAOKFM=F Big=F

One-electron integrals computed using PRISM.

NBasis= 61 RedAO= T NBF= 61

NBsUse= 61 1.00D-06 NBFU= 61

SCF N**3 symmetry information disabled.

Harris functional with IExCor= 1009 diagonalized for initial guess.

ExpMin= 1.83D-01 ExpMax= 1.72D+02 ExpMxC= 1.72D+02 IAcc=1 IRadAn=
1 AccDes= 1.00D-06

HarFok: IExCor=1009 AccDes= 1.00D-06 IRadAn= 1 IDoV=1

ScaDFX= 1.000000 1.000000 1.000000 1.000000

<S**2> of initial guess= 1.0000

Requested convergence on RMS density matrix=1.00D-08 within 128 cycles.

Requested convergence on MAX density matrix=1.00D-06.

Requested convergence on energy=1.00D-06.

No special actions if energy rises.

Keep R1 and R2 integrals in memory in canonical form, NReq= 5395914.

Integral accuracy reduced to 1.0D-05 until final iterations.

Initial convergence to 1.0D-05 achieved. Increase integral accuracy.

SCF Done: E(UPBE+HF-PBE) = -193.799688015 A.U. after 23 cycles

Conv = 0.9698D-08 -V/T = 2.0097

S**2 = 0.9691

Annihilation of the first spin contaminant:

S**2 before annihilation 0.9691, after 0.1251

QCSCF skips out because SCF is already converged.

ExpMin= 1.83D-01 ExpMax= 1.72D+02 ExpMxC= 1.72D+02 IAcc=1 IRadAn=
1 AccDes= 1.00D-06

HarFok: IExCor= 205 AccDes= 1.00D-06 IRadAn= 1 IDoV=1

ScaDFX= 1.000000 1.000000 1.000000 1.000000

Range of M.O.s used for correlation: 6 61

NBasis= 61 NAE= 19 NBE= 19 NFC= 5 NFV= 0

NROrb= 56 NOA= 14 NOB= 14 NVA= 42 NVB= 42

Symmetrizing basis deriv contribution to polar:

IMax=3 JMax=2 DiffMx= 0.00D+00

G2DrvN: will do 14 centers at a time, making 1 passes doing MaxLOS=1.

FoFDir/FoFCou used for L=0 through L=1.

DoAtom=TTTTTTTTTTTTTT

Differentiating once with respect to electric field.

with respect to dipole field.

Differentiating once with respect to nuclear coordinates.

Store integrals in memory, NReq= 4381253.

There are 42 degrees of freedom in the 1st order CPHF.

39 vectors were produced by pass 0.

AX will form 39 AO Fock derivatives at one time.

39 vectors were produced by pass 1.

39 vectors were produced by pass 2.

39 vectors were produced by pass 3.

39 vectors were produced by pass 4.

39 vectors were produced by pass 5.

14 vectors were produced by pass 6.

3 vectors were produced by pass 7.

Inv2: IOpt= 1 Iter= 1 AM= 4.90D-15 Conv= 1.00D-12.

Inverted reduced A of dimension 251 with in-core refinement.

Isotropic polarizability for W= 0.000000 56.84 Bohr**3.

End of Minotr Frequency-dependent properties file 721 does not exist.

Center	Atomic	Forces (Hartrees/Bohr)		
Number	Number	X	Y	Z
1	6	-0.006964301	-0.003519281	0.022964636
2	6	0.053972544	-0.181467657	0.084776838

3	6	-0.042434281	0.026973270	-0.042662680
4	6	-0.050971873	0.063559049	0.028059554
5	6	0.040571464	-0.052436377	-0.027470558
6	1	-0.040259371	0.158712080	-0.061886319
7	1	0.007743837	0.015170321	0.011222131
8	1	0.005653275	-0.006009745	0.019494170
9	1	0.015733071	-0.022377738	-0.012075306
10	1	0.032558391	-0.054030109	-0.028252743
11	1	0.022048921	0.000286602	-0.005559801
12	1	-0.006384065	0.058470269	-0.008409065
13	1	-0.031267612	-0.003330684	0.019799143

----- Cartesian Forces: Max
0.181467657 RMS 0.051427544 -----

Internal Coordinate Forces (Hartree/Bohr or radian)

Cent	Atom	N1	Length/X	N2	Alpha/Y	N3	Beta/Z	J

1	C	-0.006964(1)	-0.003519(14)	0.022965(27)				
2	C	0.053973(2)	-0.181468(15)	0.084777(28)				
3	C	-0.042434(3)	0.026973(16)	-0.042663(29)				
4	C	-0.050972(4)	0.063559(17)	0.028060(30)				
5	C	0.040571(5)	-0.052436(18)	-0.027471(31)				
6	H	-0.040259(6)	0.158712(19)	-0.061886(32)				
7	H	0.007744(7)	0.015170(20)	0.011222(33)				
8	H	0.005653(8)	-0.006010(21)	0.019494(34)				
9	H	0.015733(9)	-0.022378(22)	-0.012075(35)				
10	H	0.032558(10)	-0.054030(23)	-0.028253(36)				
11	H	0.022049(11)	0.000287(24)	-0.005560(37)				
12	H	-0.006384(12)	0.058470(25)	-0.008409(38)				
13	H	-0.031268(13)	-0.003331(26)	0.019799(39)				

Internal Forces: Max 0.181467657 RMS 0.051427544

APPENDIX B

Sample GAMESS US Output - DRC

ECHO OF THE FIRST FEW INPUT CARDS -

INPUT CARD> \$CONTRL SCFTYP=UHF RUNTYP=DRC DFTTYP=PBE0
MAXIT=100 \$END

INPUT CARD> \$SYSTEM TIMLIM=9000 MWORDS=64 MEMDDI=64 \$END

INPUT CARD> \$BASIS GBASIS=N21 NGAUSS=3 \$END

INPUT CARD> \$GUESS MIX=.TRUE. \$END

INPUT CARD> \$DRC NSTEP=10000 DELTAT=0.1000 TOTIME= 0.0000

INPUT CARD> NPRTSM=10 NMANAL=.F. NVEL=.TRUE.

INPUT CARD> VEL(1)= -0.002488387 -0.002445898 -0.002241154

INPUT CARD> 0.018151810 0.007781557 -0.001711298

INPUT CARD> -0.007557845 -0.005073861 -0.000235612

INPUT CARD> -0.010915384 0.011407942 0.001763922

INPUT CARD> 0.008678341 0.005138657 0.010901739

INPUT CARD> -0.036180495 -0.043312993 -0.036907979

INPUT CARD> -0.061709168 -0.042818869 -0.044677763

INPUT CARD> 0.151097064 0.059010316 -0.003991509

INPUT CARD> -0.069120637 -0.003908345 -0.000947233

INPUT CARD> 0.078123611 -0.128847859 -0.024997013

INPUT CARD> 0.022008054 -0.010756880 -0.045920856

INPUT CARD> -0.103209943 -0.070600272 0.052068945

INPUT CARD> -0.050884123 0.041100200 0.004432115

INPUT CARD> \$END

INPUT CARD> \$DATA

INPUT CARD> Spiropentane

INPUT CARD> C1

INPUT CARD> C 6.0 0.4526347 -0.0285118 0.1108249

INPUT CARD>C 6.0 -1.2943614 0.0526918 -0.7002992
INPUT CARD>C 6.0 -1.0257676 -0.1938047 0.7362450
INPUT CARD>C 6.0 0.7917109 1.3987261 0.0073953
INPUT CARD>C 6.0 1.1321697 -1.2341860 -0.0826813
INPUT CARD>H 1.0 -1.7292838 1.0270942 -1.0442086
INPUT CARD>H 1.0 -1.2377274 -0.9792471 -1.3461346
INPUT CARD>H 1.0 -1.3044675 -1.2624314 0.9035486
INPUT CARD>H 1.0 -1.1873970 0.5545061 1.3153673
INPUT CARD>H 1.0 0.0107006 2.1301465 -0.1724958
INPUT CARD>H 1.0 1.7485830 1.8047201 -0.3289327
INPUT CARD>H 1.0 0.8337904 -2.1654422 0.0965990
INPUT CARD>H 1.0 2.1944203 -1.0488051 -0.2748994
INPUT CARD> \$END

64000000 WORDS OF MEMORY AVAILABLE

BASIS OPTIONS

GBASIS=N21 IGAUSS= 3 POLAR=NONE
NDFUNC= 0 NFFUNC= 0 DIFFSP= F
NPFUNC= 0 DIFFS= F BASNAM=

RUN TITLE

Spiropentane

THE POINT GROUP OF THE MOLECULE IS C1

THE ORDER OF THE PRINCIPAL AXIS IS 0

ATOM	ATOMIC		COORDINATES (BOHR)		
	CHARGE	X	Y	Z	
C	6.0	0.8553555555	-0.0538794894	0.2094286936	
C	6.0	-2.4459883751	0.0995730638	-1.3233735974	
C	6.0	-1.9384196911	-0.3662377781	1.3913013098	
C	6.0	1.4961166625	2.6432090609	0.0139750906	
C	6.0	2.1394905046	-2.3322733579	-0.1562450013	
H	1.0	-3.2678725370	1.9409266016	-1.9732681280	
H	1.0	-2.3389656335	-1.8505086933	-2.5438255366	
H	1.0	-2.4650861349	-2.3856494243	1.7074592706	
H	1.0	-2.2438549686	1.0478645875	2.4856837702	
H	1.0	0.0202212019	4.0253931987	-0.3259697960	
H	1.0	3.3043427368	3.4104264735	-0.6215926714	
H	1.0	1.5756353872	-4.0920924002	0.1825456407	
H	1.0	4.1468530689	-1.9819542535	-0.5194845402	

INTERNUCLEAR DISTANCES (ANGS.)

	1 C	2 C	3 C	4 C	5 C
1 C	0.0000000	1.9278256 *	1.6137365 *	1.4706048 *	1.3974487 *
2 C	1.9278256 *	0.0000000	1.4820804 *	2.5815378 *	2.8152370 *
3 C	1.6137365 *	1.4820804 *	0.0000000	2.5240056 *	2.5317439 *
4 C	1.4706048 *	2.5815378 *	2.5240056 *	0.0000000	2.6563607 *
5 C	1.3974487 *	2.8152370 *	2.5317439 *	2.6563607 *	0.0000000
6 H	2.6849906 *	1.1211116 *	2.2705823 *	2.7567001 *	3.7717157
7 H	2.4256860 *	1.2186914 *	2.2356546 *	3.4066728	2.6977250 *
8 H	2.2887500 *	2.0741212 *	1.1169723 *	3.5041138	2.6288112 *

9 H	2.1167277 *	2.0799448 *	0.9599353 *	2.5180084 *	3.2456662
10 H	2.2215720 *	2.5094982 *	2.7020040 *	1.0850409 *	3.5474629
11 H	2.2877080 *	3.5308677	3.5813023	1.0924980 *	3.1105555
12 H	2.1707035 *	3.1755622	2.7846826 *	3.5655327	0.9941880 *
13 H	2.0551396 *	3.6831859	3.4818169	2.8350825 *	1.0953037 *

6 H	7 H	8 H	9 H	10 H
-----	-----	-----	-----	------

1 C	2.6849906 *	2.4256860 *	2.2887500 *	2.1167277 *	2.2215720 *
2 C	1.1211116 *	1.2186914 *	2.0741212 *	2.0799448 *	2.5094982 *
3 C	2.2705823 *	2.2356546 *	1.1169723 *	0.9599353 *	2.7020040 *
4 C	2.7567001 *	3.4066728	3.5041138	2.5180084 *	1.0850409 *
5 C	3.7717157	2.6977250 *	2.6288112 *	3.2456662	3.5474629
6 H	0.0000000	2.0876284 *	3.0358120	2.4666940 *	2.2369965 *
7 H	2.0876284 *	0.0000000	2.2684184 *	3.0722182	3.5502576
8 H	3.0358120	2.2684184 *	0.0000000	1.8666982 *	3.7943542
9 H	2.4666940 *	3.0722182	1.8666982 *	0.0000000	2.4762506 *
10 H	2.2369965 *	3.5502576	3.7943542	2.4762506 *	0.0000000
11 H	3.6348149	4.2075198	4.4997273	3.5898100	1.7749958 *
12 H	4.2500682	2.7892158 *	2.4573854 *	3.6012100	4.3820054
13 H	4.5051802	3.5961119	3.6981876	4.0664780	3.8580891

11 H	12 H	13 H
------	------	------

1 C	2.2877080 *	2.1707035 *	2.0551396 *
2 C	3.5308677	3.1755622	3.6831859
3 C	3.5813023	2.7846826 *	3.4818169
4 C	1.0924980 *	3.5655327	2.8350825 *
5 C	3.1105555	0.9941880 *	1.0953037 *

6 H	3.6348149	4.2500682	4.5051802
7 H	4.2075198	2.7892158 *	3.5961119
8 H	4.4997273	2.4573854 *	3.6981876
9 H	3.5898100	3.6012100	4.0664780
10 H	1.7749958 *	4.3820054	3.8580891
11 H	0.0000000	4.0963534	2.8886496 *
12 H	4.0963534	0.0000000	1.7989450 *
13 H	2.8886496 *	1.7989450 *	0.0000000

* ... LESS THAN 3.000

ATOMIC BASIS SET

THE CONTRACTED PRIMITIVE FUNCTIONS HAVE BEEN UNNORMALIZED
 THE CONTRACTED BASIS FUNCTIONS ARE NOW NORMALIZED TO UNITY

	SHELL TYPE	PRIMITIVE	EXPONENT	CONTRACTION
--	------------	-----------	----------	-------------

C

1	S	1	172.2560000	0.061766907377	
1	S	2	25.9109000	0.358794042852	
1	S	3	5.5333500	0.700713083689	
2	L	4	3.6649800	-0.395895162119	0.236459946619
2	L	5	0.7705450	1.215834355681	0.860618805716
3	L	6	0.1958570	1.000000000000	1.000000000000

C

4	S	7	172.2560000	0.061766907377	
4	S	8	25.9109000	0.358794042852	
4	S	9	5.5333500	0.700713083689	
5	L	10	3.6649800	-0.395895162119	0.236459946619
5	L	11	0.7705450	1.215834355681	0.860618805716
6	L	12	0.1958570	1.000000000000	1.000000000000

C

7	S	13	172.2560000	0.061766907377	
7	S	14	25.9109000	0.358794042852	
7	S	15	5.5333500	0.700713083689	
8	L	16	3.6649800	-0.395895162119	0.236459946619
8	L	17	0.7705450	1.215834355681	0.860618805716
9	L	18	0.1958570	1.000000000000	1.000000000000

C

10	S	19	172.2560000	0.061766907377	
10	S	20	25.9109000	0.358794042852	
10	S	21	5.5333500	0.700713083689	
11	L	22	3.6649800	-0.395895162119	0.236459946619
11	L	23	0.7705450	1.215834355681	0.860618805716
12	L	24	0.1958570	1.000000000000	1.000000000000

C

13	S	25	172.2560000	0.061766907377	
13	S	26	25.9109000	0.358794042852	
13	S	27	5.5333500	0.700713083689	
14	L	28	3.6649800	-0.395895162119	0.236459946619
14	L	29	0.7705450	1.215834355681	0.860618805716
15	L	30	0.1958570	1.000000000000	1.000000000000
H					
16	S	31	5.4471780	0.156284978695	
16	S	32	0.8245472	0.904690876670	
17	S	33	0.1831916	1.000000000000	
H					
18	S	34	5.4471780	0.156284978695	
18	S	35	0.8245472	0.904690876670	
19	S	36	0.1831916	1.000000000000	
H					
20	S	37	5.4471780	0.156284978695	
20	S	38	0.8245472	0.904690876670	
21	S	39	0.1831916	1.000000000000	
H					
22	S	40	5.4471780	0.156284978695	
22	S	41	0.8245472	0.904690876670	

23 S 42 0.1831916 1.000000000000

H

24 S 43 5.4471780 0.156284978695

24 S 44 0.8245472 0.904690876670

25 S 45 0.1831916 1.000000000000

H

26 S 46 5.4471780 0.156284978695

26 S 47 0.8245472 0.904690876670

27 S 48 0.1831916 1.000000000000

H

28 S 49 5.4471780 0.156284978695

28 S 50 0.8245472 0.904690876670

29 S 51 0.1831916 1.000000000000

H

30 S 52 5.4471780 0.156284978695

30 S 53 0.8245472 0.904690876670

31 S 54 0.1831916 1.000000000000

TOTAL NUMBER OF BASIS SET SHELLS = 31

NUMBER OF CARTESIAN GAUSSIAN BASIS FUNCTIONS = 61

NUMBER OF ELECTRONS = 38

CHARGE OF MOLECULE = 0

SPIN MULTIPLICITY = 1

NUMBER OF OCCUPIED ORBITALS (ALPHA) = 19
NUMBER OF OCCUPIED ORBITALS (BETA) = 19
TOTAL NUMBER OF ATOMS = 13
THE NUCLEAR REPULSION ENERGY IS 163.6142656239

LEBEDEV GRID-BASED DFT OPTIONS

DFTTYP=PBE0

NRAD = 96 NLEB = 302

NRAD0 = 24 NLEB0 = 110

SWOFF = 5.00E-03 (PURE SCF -> DFT)

SWITCH= 3.00E-04 (COARSE -> TIGHT GRID)

THRESH= 0.00E+00 GTHRE= 1.00E+00

GRIMME'S EMPIRICAL DISPERSION CORRECTION= F

\$CONTRL OPTIONS

SCFTYP=UHF RUNTYP=DRC EXETYP=RUN
MPLEVL= 0 CITYP =NONE CCTYP =NONE VBTYP =NONE
DFTTYP=PBE0 TDDFT =NONE
MULT = 1 ICHARG= 0 NZVAR = 0 COORD =UNIQUE
PP =NONE RELWFN=NONE LOCAL =NONE NUMGRD= F
ISPHER= -1 NOSYM = 0 MAXIT = 100 UNITS =ANGS
PLTORB= F MOLPLT= F AIMPAC= F FRIEND=
NPRINT= 7 IREST = 0 GEOM =INPUT
NORMF = 0 NORMP = 0 ITOL = 20 ICUT = 9
INTTYP=BEST GRDTYP=BEST QMTTOL= 1.0E-06

\$SYSTEM OPTIONS

REPLICATED MEMORY= 64000000 WORDS (ON EVERY NODE).
DISTRIBUTED MEMDDI= 64 MILLION WORDS IN AGGREGATE,
MEMDDI DISTRIBUTED OVER 36 PROCESSORS IS 1777777
WORDS/PROCESSOR.
TOTAL MEMORY REQUESTED ON EACH PROCESSOR= 65777777 WORDS.
TIMLIM= 9000.00 MINUTES, OR 6.2 DAYS.
PARALL= T BALTP= DLB KDIAG= 0 COREFL= F
MXSEQ2= 300 MXSEQ3= 150

PROPERTIES INPUT

MOMENTS FIELD POTENTIAL DENSITY
IEMOM = 1 IEFLD = 0 IEPOT = 0 IEDEN = 0
WHERE =COMASS WHERE =NUCLEI WHERE =NUCLEI WHERE
=NUCLEI
OUTPUT=BOTH OUTPUT=BOTH OUTPUT=BOTH OUTPUT=BOTH
IEMINT= 0 IEFINT= 0 IEDINT= 0
MORB = 0
EXTRAPOLATION IN EFFECT
DIIS IN EFFECT
ORBITAL PRINTING OPTION: NPREO= 1 61 2 1

INTEGRAL TRANSFORMATION OPTIONS

NWORD = 0

CUTOFF = 1.0E-09 MPTRAN = 0

DIRTRF = F APOINTS =DUP

INTEGRAL INPUT OPTIONS

NOPK = 1 NORDER= 0 SCHWRZ= T

THE POINT GROUP IS C1 , NAXIS= 0, ORDER= 1

DIMENSIONS OF THE SYMMETRY SUBSPACES ARE

A = 61

..... DONE SETTING UP THE RUN

CPU 0: STEP CPU TIME= 0.14 TOTAL CPU TIME= 0.1 (0.0 MIN)

TOTAL WALL CLOCK TIME= 0.2 SECONDS, CPU UTILIZATION IS 58.33%

PARAMETERS FOR DRC CALCULATION

NSTEP = 10000 DELTAT = 0.1000 FS TOTIME = 0.0000 FS

NPRT = 0 NPUN = 0 NPRTSM = 10

NMANAL = F NHESTS = 0 VIBLVL = F

NFRGPR = 0

NVEL = T EKIN = .05562 HARTREE

NORMALIZED INITIAL VELOCITY VECTOR

ATOM	1	VEL=	-0.00248839	-0.00244590	-0.00224115
ATOM	2	VEL=	0.01815181	0.00778156	-0.00171130
ATOM	3	VEL=	-0.00755785	-0.00507386	-0.00023561
ATOM	4	VEL=	-0.01091538	0.01140794	0.00176392
ATOM	5	VEL=	0.00867834	0.00513866	0.01090174
ATOM	6	VEL=	-0.03618050	-0.04331299	-0.03690798
ATOM	7	VEL=	-0.06170917	-0.04281887	-0.04467776
ATOM	8	VEL=	0.15109706	0.05901032	-0.00399151
ATOM	9	VEL=	-0.06912064	-0.00390835	-0.00094723
ATOM	10	VEL=	0.07812361	-0.12884786	-0.02499701
ATOM	11	VEL=	0.02200805	-0.01075688	-0.04592086
ATOM	12	VEL=	-0.10320994	-0.07060027	0.05206895
ATOM	13	VEL=	-0.05088412	0.04110020	0.00443212

ATOMIC ISOTOPES USED DURING THIS CALCULATION ARE

1= 12.000000 2= 12.000000 3= 12.000000 4= 12.000000
5= 12.000000 6= 1.007825 7= 1.007825 8= 1.007825
9= 1.007825 10= 1.007825 11= 1.007825 12= 1.007825
13= 1.007825

1 ELECTRON INTEGRALS

..... END OF ONE-ELECTRON INTEGRALS

CPU 0: STEP CPU TIME= 0.01 TOTAL CPU TIME= 0.1 (0.0 MIN)

TOTAL WALL CLOCK TIME= 0.2 SECONDS, CPU UTILIZATION IS 60.00%

GUESS OPTIONS

GUESS =HUCKEL NORB = 0 NORDER= 0
MIX = T PRTMO = F PUNMO = F
TOLZ = 1.0E-08 TOLE = 1.0E-05
SYMDEN= F PURIFY= F

INITIAL GUESS ORBITALS GENERATED BY HUCKEL ROUTINE.

HUCKEL GUESS REQUIRES 40585 WORDS.

HOMO AND LUMO MIXED TO BREAK ALPHA-BETA SYMMETRY

SYMMETRIES FOR INITIAL GUESS ORBITALS FOLLOW. ALPHA SET(S).

19 ORBITALS ARE OCCUPIED (5 CORE ORBITALS).

6=A 7=A 8=A 9=A 10=A 11=A 12=A
13=A 14=A 15=A 16=A 17=A 18=A 19=A
20=A 21=A 22=A 23=A 24=A 25=A 26=A
27=A 28=A 29=A

SYMMETRIES FOR INITIAL GUESS ORBITALS FOLLOW. BETA SET(S).

19 ORBITALS ARE OCCUPIED (5 CORE ORBITALS).

6=A 7=A 8=A 9=A 10=A 11=A 12=A
13=A 14=A 15=A 16=A 17=A 18=A 19=A
20=A 21=A 22=A 23=A 24=A 25=A 26=A
27=A 28=A 29=A

..... END OF INITIAL ORBITAL SELECTION

CPU 0: STEP CPU TIME= 0.00 TOTAL CPU TIME= 0.1 (0.0 MIN)

TOTAL WALL CLOCK TIME= 0.3 SECONDS, CPU UTILIZATION IS 55.56%

AO INTEGRAL TECHNOLOGY

S,P,L SHELL ROTATED AXIS INTEGRALS, REPROGRAMMED BY
KAZUYA ISHIMURA (IMS) AND JOSE SIERRA (SYNSTAR).

S,P,D,L SHELL ROTATED AXIS INTEGRALS PROGRAMMED BY
KAZUYA ISHIMURA (INSTITUTE FOR MOLECULAR SCIENCE).

S,P,D,F,G SHELL TO TOTAL QUARTET ANGULAR MOMENTUM SUM 5,
ERIC PROGRAM BY GRAHAM FLETCHER (ELORET AND NASA
ADVANCED
SUPERCOMPUTING DIVISION, AMES RESEARCH CENTER).

S,P,D,F,G,L SHELL GENERAL RYS QUADRATURE PROGRAMMED BY
MICHEL DUPUIS (PACIFIC NORTHWEST NATIONAL LABORATORY).

2 ELECTRON INTEGRALS

THE -PK- OPTION IS OFF, THE INTEGRALS ARE NOT IN SUPERMATRIX
FORM.

STORING 15000 INTEGRALS/RECORD ON DISK, USING 12
BYTES/INTEGRAL.

TWO ELECTRON INTEGRAL EVALUATION REQUIRES 89852 WORDS OF
MEMORY.

SCHWARZ INEQUALITY OVERHEAD: 1886 INTEGRALS, T= 0.00

II,JST,KST,LST = 1 1 1 1	NREC =	1	INTLOC =	1
II,JST,KST,LST = 2 1 1 1	NREC =	1	INTLOC =	1
II,JST,KST,LST = 3 1 1 1	NREC =	1	INTLOC =	1
II,JST,KST,LST = 4 1 1 1	NREC =	1	INTLOC =	1
II,JST,KST,LST = 5 1 1 1	NREC =	1	INTLOC =	1
II,JST,KST,LST = 6 1 1 1	NREC =	1	INTLOC =	1731
II,JST,KST,LST = 7 1 1 1	NREC =	1	INTLOC =	1731
II,JST,KST,LST = 8 1 1 1	NREC =	1	INTLOC =	1731

II,JST,KST,LST = 9 1 1 1 NREC = 1 INTLOC = 8147
 II,JST,KST,LST = 10 1 1 1 NREC = 1 INTLOC = 8147
 II,JST,KST,LST = 11 1 1 1 NREC = 1 INTLOC =11831
 II,JST,KST,LST = 12 1 1 1 NREC = 2 INTLOC = 7551
 II,JST,KST,LST = 13 1 1 1 NREC = 2 INTLOC = 7551
 II,JST,KST,LST = 14 1 1 1 NREC = 2 INTLOC =10740
 II,JST,KST,LST = 15 1 1 1 NREC = 3 INTLOC = 2203
 II,JST,KST,LST = 16 1 1 1 NREC = 4 INTLOC =10383
 II,JST,KST,LST = 17 1 1 1 NREC = 5 INTLOC = 8151
 II,JST,KST,LST = 18 1 1 1 NREC = 6 INTLOC = 6240
 II,JST,KST,LST = 19 1 1 1 NREC = 7 INTLOC = 5953
 II,JST,KST,LST = 20 1 1 1 NREC = 8 INTLOC = 3669
 II,JST,KST,LST = 21 1 1 1 NREC = 8 INTLOC = 3669
 II,JST,KST,LST = 22 1 1 1 NREC = 9 INTLOC = 1980
 II,JST,KST,LST = 23 1 1 1 NREC = 9 INTLOC = 5154
 II,JST,KST,LST = 24 1 1 1 NREC = 9 INTLOC = 8354
 II,JST,KST,LST = 25 1 1 1 NREC = 10 INTLOC = 546
 II,JST,KST,LST = 26 1 1 1 NREC = 10 INTLOC = 546
 II,JST,KST,LST = 27 1 1 1 NREC = 10 INTLOC = 6703
 II,JST,KST,LST = 28 1 1 1 NREC = 10 INTLOC =13759
 II,JST,KST,LST = 29 1 1 1 NREC = 11 INTLOC = 2924
 II,JST,KST,LST = 30 1 1 1 NREC = 11 INTLOC = 2924
 II,JST,KST,LST = 31 1 1 1 NREC = 11 INTLOC = 2924

SCHWARZ INEQUALITY TEST SKIPPED 24785 INTEGRAL BLOCKS.

TOTAL NUMBER OF NONZERO TWO-ELECTRON INTEGRALS =
1589190

126 INTEGRAL RECORDS WERE STORED ON DISK FILE 8.

..... END OF TWO-ELECTRON INTEGRALS

CPU 0: STEP CPU TIME= 0.03 TOTAL CPU TIME= 0.2 (0.0 MIN)

TOTAL WALL CLOCK TIME= 0.3 SECONDS, CPU UTILIZATION IS 58.06%

U-PBE0 SCF CALCULATION

NUCLEAR ENERGY = 163.6142656239

MAXIT =100 NPUNCH= 2 MULT= 1

EXTRAP=T DAMP=F SHIFT=F RSTRCT=F DIIS=T SOSCF=F

DENSITY MATRIX CONVERGENCE THRESHOLD= 1.00E-05

COARSE -> FINE DFT GRID SWITCH THRESHOLD= 3.00E-04 (SWITCH IN \$DFT)

HF -> DFT SWITCH THRESHOLD= 5.00E-03 (SWOFF IN \$DFT)

MEMORY REQUIRED FOR UHF/ROHF ITERS= 514471 WORDS.

DFT CODE IS SWITCHING FROM THE FINE GRID NRAD= 96, NLEB= 302
TO THE COARSE GRID NRAD0= 24, NLEB0= 110

EXCHANGE FUNCTIONAL =PBE&HFX

CORRELATION FUNCTIONAL=PBE

DFT THRESHOLD =.106E-07

GRID CHANGE THRESHOLD =.300E-03

FOR AN EULER-MACLAURIN QUADRATURE USING 96 RADIAL POINTS:

SMALLEST GAUSSIAN PRIMITIVE EXPONENT= 0.1831915800 OF TYPE -
S-

ON ATOM NUMBER 6 HAS RADIAL NORMALIZATION= 1.000000

LARGEST GAUSSIAN PRIMITIVE EXPONENT= 172.2560000000 OF TYPE -
S-

ON ATOM NUMBER 1 HAS RADIAL NORMALIZATION= 1.000000

DFT IS SWITCHED OFF, PERFORMING PURE SCF UNTIL SWOFF
THRESHOLD IS REACHED.

ITER EX TOTAL ENERGY E CHANGE DENSITY CHANGE DIIS
ERROR

*** INITIATING DIIS PROCEDURE ***

1	0	-192.1917735021	-192.1917735021	0.578696241	0.381273195
2	1	-192.6483886921	-0.4566151901	0.141829644	0.054969308
3	2	-192.6824476772	-0.0340589851	0.058566403	0.023793025
4	3	-192.6899161495	-0.0074684723	0.045017787	0.012582021
5	4	-192.6928034505	-0.0028873009	0.018050175	0.006341955
6	5	-192.6938723869	-0.0010689364	0.040769609	0.006216747
7	6	-192.6958415574	-0.0019691705	0.036494705	0.005347644
8	7	-192.6970646557	-0.0012230984	0.022419184	0.003089764
9	8	-192.6974484526	-0.0003837968	0.005970342	0.001545089
10	9	-192.6974998325	-0.0000513799	0.005621900	0.000797646
11	10	-192.6975163549	-0.0000165225	0.001712335	0.000242217

CONVERGED TO SWOFF, SO DFT CALCULATION IS NOW SWITCHED ON.

*** INITIATING DIIS PROCEDURE ***

12	11	-193.7832608456	-1.0857444907	0.127292273	0.053654920
13	12	-193.8036450991	-0.0203842534	0.048534610	0.015512590
14	13	-193.8072275892	-0.0035824902	0.024240731	0.011041439
15	14	-193.8090480677	-0.0018204784	0.014392337	0.004126276
16	15	-193.8095163368	-0.0004682692	0.015103279	0.003642313
17	16	-193.8097761400	-0.0002598031	0.002623720	0.001136519
18	17	-193.8097894382	-0.0000132983	0.001975624	0.000476370
19	18	-193.8097948220	-0.0000053838	0.001419935	0.000444787
20	19	-193.8097974067	-0.0000025847	0.001623685	0.000218920
21	20	-193.8097994417	-0.0000020351	0.001219609	0.000097746
22	21	-193.8097999730	-0.0000005313	0.000232264	0.000025187

DFT CODE IS SWITCHING BACK TO THE FINE GRID

*** INITIATING DIIS PROCEDURE ***

23	22	-193.8091169385	0.0006830345	0.001787260	0.000875511
----	----	-----------------	--------------	-------------	-------------

24	23	-193.8091249223	-0.0000079838	0.001058667	0.000322258
25	24	-193.8091250584	-0.0000001361	0.000557700	0.000296426
26	25	-193.8091256677	-0.0000006093	0.000141186	0.000113393
27	26	-193.8091257655	-0.0000000978	0.000087920	0.000023421
28	27	-193.8091257763	-0.0000000108	0.000048090	0.000017133
29	28	-193.8091257814	-0.0000000051	0.000044770	0.000008767
30	29	-193.8091257832	-0.0000000018	0.000020268	0.000004368
31	30	-193.8091257837	-0.0000000006	0.000018923	0.000003022
32	31	-193.8091257840	-0.0000000003	0.000016575	0.000001511

ENERGY CONVERGED

TIME TO FORM FOCK OPERATORS= 1.8 SECONDS (0.1 SEC/ITER)

TIME TO SOLVE SCF EQUATIONS= 0.1 SECONDS (0.0 SEC/ITER)

FINAL U-PBE0 ENERGY IS -193.8091257840 AFTER 32 ITERATIONS

DFT EXCHANGE + CORRELATION ENERGY = -22.5170965557

TOTAL ELECTRON NUMBER = 38.0003394603

SPIN SZ = 0.000

S-SQUARED = 0.793

----- ALPHA SET -----

EIGENVECTORS

[Data Removed]

---- BETA SET ----

EIGENVECTORS

[Data Removed]

..... END OF UHF CALCULATION

CPU 0: STEP CPU TIME= 2.00 TOTAL CPU TIME= 2.2 (0.0 MIN)

TOTAL WALL CLOCK TIME= 2.6 SECONDS, CPU UTILIZATION IS 83.85%

PROPERTIES FOR THE PBE0 DFT FUNCTIONAL (UHF TYPE) DENSITY
MATRIX

ENERGY COMPONENTS

WAVEFUNCTION NORMALIZATION = 1.0000000000

ONE ELECTRON ENERGY = -583.1045961230

TWO ELECTRON ENERGY = 225.6812047151

NUCLEAR REPULSION ENERGY = 163.6142656239

TOTAL ENERGY = -193.8091257840

ELECTRON-ELECTRON POTENTIAL ENERGY = 225.6812047151

NUCLEUS-ELECTRON POTENTIAL ENERGY = -775.2440716553

NUCLEUS-NUCLEUS POTENTIAL ENERGY = 163.6142656239

TOTAL POTENTIAL ENERGY = -385.9486013163

TOTAL KINETIC ENERGY = 192.1394755323

VIRIAL RATIO (V/T) = 2.0086897825

MULLIKEN AND LOWDIN POPULATION ANALYSES

[Data Truncated]

BOND ORDER AND VALENCE ANALYSIS BOND ORDER
THRESHOLD=0.050

BOND				BOND				BOND			
ATOM PAIR	DIST	ORDER	ORDER	ATOM PAIR	DIST	ORDER	ORDER	ATOM PAIR	DIST	ORDER	ORDER
1 2	1.928	0.445		1 3	1.614	0.826		1 4	1.471	1.039	
1 5	1.397	1.412		2 3	1.482	0.938		2 4	2.582	0.129	
2 5	2.815	0.151		2 6	1.121	0.907		2 7	1.219	0.908	
3 8	1.117	0.902		3 9	0.960	0.896		4 5	2.656	0.072	
4 10	1.085	0.917		4 11	1.092	0.919		5 12	0.994	0.927	
5 13	1.095	0.928									

TOTAL BONDED FREE

ATOM	VALENCE	VALENCE	VALENCE
1 C	3.692	3.679	0.013
2 C	3.588	3.462	0.126
3 C	3.589	3.588	0.001
4 C	3.716	3.114	0.601
5 C	3.763	3.527	0.237
6 H	0.924	0.924	0.000
7 H	0.925	0.924	0.000
8 H	0.906	0.906	0.000
9 H	0.893	0.893	0.000
10 H	0.926	0.924	0.002
11 H	0.923	0.921	0.002
12 H	0.925	0.924	0.001
13 H	0.925	0.924	0.001

 ATOMIC SPIN DENSITY AT THE NUCLEUS (A.U.)

		SPIN DENS	ALPHA DENS	BETA DENS
1 C	6.0	0.0000811	46.97638	46.97630
2 C	6.0	-0.0873736	46.92075	47.00813
3 C	6.0	0.0043304	47.00810	47.00377
4 C	6.0	0.1293448	46.95007	46.82073
5 C	6.0	-0.0649188	46.84669	46.91161
6 H	1.0	0.0028018	0.17385	0.17105
7 H	1.0	0.0068481	0.15702	0.15017
8 H	1.0	0.0006308	0.17348	0.17285
9 H	1.0	-0.0009710	0.21395	0.21492
10 H	1.0	-0.0098297	0.17821	0.18804

11 H	1.0	-0.0115775	0.17408	0.18565
12 H	1.0	0.0070326	0.20674	0.19971
13 H	1.0	0.0080047	0.18394	0.17593

ELECTROSTATIC MOMENTS

POINT 1	X	Y	Z (BOHR)	CHARGE
	0.000000	0.000000	0.000000	0.00 (A.U.)
	DX	DY	DZ	/D/ (DEBYE)
	-1.619577	0.264848	-0.327445	1.673438

..... END OF PROPERTY EVALUATION

CPU 0: STEP CPU TIME= 0.01 TOTAL CPU TIME= 2.2 (0.0 MIN)

TOTAL WALL CLOCK TIME= 3.2 SECONDS, CPU UTILIZATION IS 69.09%

BEGINNING ONE ELECTRON GRADIENT...

..... END OF 1-ELECTRON GRADIENT

CPU 0: STEP CPU TIME= 0.00 TOTAL CPU TIME= 2.2 (0.0 MIN)

TOTAL WALL CLOCK TIME= 3.2 SECONDS, CPU UTILIZATION IS 68.87%

GRADIENT OF THE ENERGY

MEMORY FOR GRID POINT CONTRIBUTIONS TO THE DFT GRADIENT=
456808 WORDS.

CPU 0: STEP CPU TIME= 0.25 TOTAL CPU TIME= 2.4 (0.0 MIN)

TOTAL WALL CLOCK TIME= 3.4 SECONDS, CPU UTILIZATION IS 71.14%

THE COARSE/FINE SCHWARZ SCREENINGS SKIPPED 24785/ 15760
BLOCKS.

THE NUMBER OF GRADIENT INTEGRAL BLOCKS COMPUTED WAS 82558

..... END OF 2-ELECTRON GRADIENT

CPU 0: STEP CPU TIME= 0.04 TOTAL CPU TIME= 2.5 (0.0 MIN)

TOTAL WALL CLOCK TIME= 3.5 SECONDS, CPU UTILIZATION IS 70.45%

START OF DRC CALCULATION

TIME KINETIC POTENTIAL TOTAL
ENERGY ENERGY ENERGY
0.0000 0.05562 -193.80913 -193.75350

CARTESIAN COORDINATES (BOHR) VELOCITY (BOHR/FS)

6.0 0.85536 -0.05388 0.20943 -0.00249 -0.00245 -0.00224
6.0 -2.44599 0.09957 -1.32337 0.01815 0.00778 -0.00171
6.0 -1.93842 -0.36624 1.39130 -0.00756 -0.00507 -0.00024
6.0 1.49612 2.64321 0.01398 -0.01092 0.01141 0.00176
6.0 2.13949 -2.33227 -0.15625 0.00868 0.00514 0.01090
1.0 -3.26787 1.94093 -1.97327 -0.03618 -0.04331 -0.03691
1.0 -2.33897 -1.85051 -2.54383 -0.06171 -0.04282 -0.04468
1.0 -2.46509 -2.38565 1.70746 0.15110 0.05901 -0.00399
1.0 -2.24385 1.04786 2.48568 -0.06912 -0.00391 -0.00095
1.0 0.02022 4.02539 -0.32597 0.07812 -0.12885 -0.02500
1.0 3.30434 3.41043 -0.62159 0.02201 -0.01076 -0.04592
1.0 1.57564 -4.09209 0.18255 -0.10321 -0.07060 0.05207
1.0 4.14685 -1.98195 -0.51948 -0.05088 0.04110 0.00443

GRADIENT OF THE ENERGY

UNITS ARE HARTREE/BOHR	E'X	E'Y	E'Z
1 C	0.042228735	0.012888642	-0.010479322
2 C	-0.001254726	0.039196037	0.028963849
3 C	-0.029614540	0.103229972	0.110147854
4 C	-0.010565069	0.002280336	0.010892218
5 C	-0.056000423	-0.109651242	0.017873940
6 H	-0.013162056	0.023226049	0.002120776
7 H	0.010572025	-0.062470741	-0.024806559
8 H	-0.011293178	-0.021146413	-0.020601159
9 H	0.032341765	-0.086949050	-0.088767316
10 H	0.006435989	0.004012800	-0.007963102
11 H	-0.003599855	0.013179603	-0.005401522
12 H	0.032053508	0.070081694	-0.018875543
13 H	0.001857825	0.012122314	0.006895886

..... END OF ONE-ELECTRON INTEGRALS

CPU 0: STEP CPU TIME= 0.00 TOTAL CPU TIME= 2.5 (0.0 MIN)

TOTAL WALL CLOCK TIME= 3.5 SECONDS, CPU UTILIZATION IS 70.25%

TOTAL NUMBER OF NONZERO TWO-ELECTRON INTEGRALS =
1589421

125 INTEGRAL RECORDS WERE STORED ON DISK FILE 8.

..... END OF TWO-ELECTRON INTEGRALS

CPU 0: STEP CPU TIME= 0.17 TOTAL CPU TIME= 2.6 (0.0 MIN)

TOTAL WALL CLOCK TIME= 3.7 SECONDS, CPU UTILIZATION IS 71.62%

U-PBE0 SCF CALCULATION

DENSITY MATRIX CONVERGENCE THRESHOLD= 1.00E-05

COARSE -> FINE DFT GRID SWITCH THRESHOLD= 3.00E-04 (SWITCH IN \$DFT)

HF -> DFT SWITCH THRESHOLD= 5.00E-03 (SWOFF IN \$DFT)

DFT CODE IS SWITCHING FROM THE FINE GRID NRAD= 96, NLEB= 302
TO THE COARSE GRID NRAD0= 24, NLEB0= 110

ITER	EX	TOTAL ENERGY	E CHANGE	DENSITY CHANGE	DIIS ERROR
------	----	--------------	----------	----------------	------------

*** INITIATING DIIS PROCEDURE ***

1	0	-193.8108647006	-193.8108647006	0.002526929	0.001817773
2	1	-193.8109035351	-0.0000388345	0.001117429	0.000556916
3	2	-193.8109035182	0.0000000169	0.000680794	0.000618493
4	3	-193.8109062115	-0.0000026932	0.000153842	0.000077644

DFT CODE IS SWITCHING BACK TO THE FINE GRID

*** INITIATING DIIS PROCEDURE ***

5	4	-193.8103134508	0.0005927606	0.001847140	0.000877654
6	5	-193.8103213323	-0.0000078815	0.001010725	0.000359914
7	6	-193.8103214044	-0.0000000720	0.000588864	0.000337875
8	7	-193.8103221317	-0.0000007274	0.000148485	0.000116231
9	8	-193.8103222336	-0.0000001019	0.000062720	0.000020251
10	9	-193.8103222398	-0.0000000062	0.000030215	0.000016551
11	10	-193.8103222438	-0.0000000040	0.000030401	0.000006679
12	11	-193.8103222449	-0.0000000010	0.000012790	0.000003702
13	12	-193.8103222451	-0.0000000003	0.000010800	0.000002001
14	13	-193.8103222452	-0.0000000001	0.000009865	0.000000955

DENSITY CONVERGED

TIME TO FORM FOCK OPERATORS= 1.4 SECONDS (0.1 SEC/ITER)

TIME TO SOLVE SCF EQUATIONS= 0.1 SECONDS (0.0 SEC/ITER)

FINAL U-PBE0 ENERGY IS -193.8103222452 AFTER 14 ITERATIONS

DFT EXCHANGE + CORRELATION ENERGY = -22.5182824247

TOTAL ELECTRON NUMBER = 38.0003443003

SPIN SZ = 0.000

S-SQUARED = 0.793

..... END OF UHF CALCULATION

CPU 0: STEP CPU TIME= 1.54 TOTAL CPU TIME= 4.2 (0.1 MIN)

TOTAL WALL CLOCK TIME= 5.3 SECONDS, CPU UTILIZATION IS 79.21%

..... END OF 1-ELECTRON GRADIENT

CPU 0: STEP CPU TIME= 0.00 TOTAL CPU TIME= 4.2 (0.1 MIN)

TOTAL WALL CLOCK TIME= 5.3 SECONDS, CPU UTILIZATION IS 79.21%

MEMORY FOR GRID POINT CONTRIBUTIONS TO THE DFT GRADIENT=
456808 WORDS.

CPU 0: STEP CPU TIME= 0.25 TOTAL CPU TIME= 4.4 (0.1 MIN)

TOTAL WALL CLOCK TIME= 5.6 SECONDS, CPU UTILIZATION IS 79.86%

..... END OF 2-ELECTRON GRADIENT

CPU 0: STEP CPU TIME= 0.00 TOTAL CPU TIME= 4.4 (0.1 MIN)

TOTAL WALL CLOCK TIME= 5.6 SECONDS, CPU UTILIZATION IS 79.86%

----- RESTART INFORMATION FOR NEXT DRC RUN:

COORDINATES (IN ANGSTROM) FOR \$DATA GROUP ARE

C 6.0 0.4524942905 -0.0286438958 0.1107084696

C	6.0	-1.2934005881	0.0530954795	-0.7003957456
C	6.0	-1.0261614219	-0.1940945374	0.7362097616
C	6.0	0.7911354668	1.3993293109	0.0074863910
C	6.0	1.1326405148	-1.2338914063	-0.0821080998
H	1.0	-1.7311659919	1.0247450054	-1.0461669064
H	1.0	-1.2410189312	-0.9813592091	-1.3484377857
H	1.0	-1.2964439896	-1.2592566577	0.9033880869
H	1.0	-1.1911343142	0.5545132992	1.3155356700
H	1.0	0.0148188820	2.1233182872	-0.1737989844
H	1.0	1.7497564770	1.8041184296	-0.3313494317
H	1.0	0.8282498668	-2.1693507077	0.0994008311
H	1.0	2.1917230551	-1.0466600093	-0.2746818364

\$END

\$DRC NSTEP=?? DELTAT=0.1000 TOTIME= 0.1000

NPRTSM=10 NMANAL=.F. NPRT= 0 NPUN= 0 NVEL=.TRUE.

VEL(1)= -0.002818323282 -0.002546597928 -0.002159278268

0.018161613268 0.007475315413 -0.001937594735
-0.007326464372 -0.005880404541 -0.001096205473
-0.010832838319 0.011390125562 0.001678820282
0.009115876517 0.005995370407 0.010762088558
-0.034956042775 -0.045473687982 -0.037105272571
-0.062692672406 -0.037007281462 -0.042370034790
0.152147656530 0.060977544658 -0.002075004804
-0.072129357451 0.004180433946 0.007310697351
0.077524877694 -0.129221165532 -0.024256213955
0.022342944694 -0.011982964626 -0.045418358047
-0.106191847208 -0.077119898498 0.053824917003
-0.051056954518 0.039972473816 0.003790597929

\$END